Final Report
10 June 1975 - 14 June 1976

LOW THRESHOLD CW Nd LASER OSCILLATOR AT 1060 nm STUDY

Prepared for

Goddard Space Flight Center
Greenbelt Road
Greenbelt, Maryland 20771

NASA Project Officers: Dr. M. Fitzmaurice
Mr. J. Degnan

7 July 1976

Prepared by

THE AEROSPACE CORPORATION
Electronics Research Laboratory
P. O. Box 92957
Los Angeles, California 90009

Contract Number NAS 5-22387
Sponsored by National Aeronautics and Space Administration

Contributors to this report:

Dr. M. Birnbaum, Principal Investigator
The Aerospace Corporation
P. O. Box 92957
Los Angeles, California 90009

Dr. L. G. DeShazer, Principal Investigator
University of Southern California
Los Angeles, California 90007

Research Performed at Aerospace Corporation by:

Dr. M. Birnbaum, A. W. Tucker (Members of the Technical Staff)
C. L. Fincher (Assistant to the Technical Staff), J. W. Erler (Technician)
and J. G. Sliney, Jr.

Research Performed at University of Southern California by:

L. G. DeShazer, Associate Professor
K. M. Leung, Research Scientist
J. G. Sliney, Jr., Research Assistant
P. P. Yaney, Visiting Professor (University of Dayton)
J. A. Wunderlich, University of Southern California and Naval Weapons Center

TABLE OF CONTENTS

ABSTRACT

The spectroscopic and laser performance characteristics of Nd:YVO_4 were measured and compared to Nd:YAG. In TEM_{oo} CW operation at 1.06 μ, the Nd:YVO_4 laser exhibited a lower threshold and a higher slope efficiency than Nd:YAG. This laser shows great promise for development of a low threshold and efficient oscillator suitable for application in a high data rate laser communication system which should substantially outperform a similar Nd:YAG system.

ACKNOWLEDGEMENT

The cooperation of Mr. John Degnan, NASA contract monitor, is gratefully acknowledged. His suggestions throughout this contract period have been helpful and pertinent.

LIST OF FIGURES

FIGURES (continued) PAGE

LIST OF TABLES

TABLES (continued)

I. INTRODUCTION

One of the important frontier applications of lasers is that of high data rate spaceborne laser communication systems. Lasers of high efficiency and low thresholds are required in such diverse applications as communications, ranging and meterology.

An essential sub-system is the laser transmitter, which must be reliable, efficient and stable. In a prototype system under development by the U. S. Air Force, a mode-locked, frequency doubled Nd:YAG laser is used. New types of potassium-rubidium pump lamps have been designed for this application. With an input lamp power of 300 W, the Nd:YAG laser produces about 1 W at 1.06μ. It is highly desirable to obtain higher outputs without increasing the pump power requirements. This goal might be obtained with lasers using new Nd doped crystals.

Recently, detailed spectroscopic measurements have shown that the stimulated-emission cross-section of A-axis Nd:YVO_4 at 1.064μ was much larger than that of Nd:YAG at 1.0642μ. A simple theoretical analysis showed that a CW Nd:YVO_4 laser with thresholds a factor of 2 lower than Nd:YAG and with comparable slope efficiencies was feasible.

A major goal of this contract effort was to explore in depth the potentialities of the Nd:YVO_4 and to demonstrate experimentally its superiority to the Nd:YAG laser.

A broad range of characteristics were investigated and are described in the following chapters. With Nd:YVO_4 crystals, CW 1.06μ lasers were operated with thresholds a factor of 2 lower than Nd:YAG and with greater slope efficiencies. Thus, the first step in the development of new oscillators suitable for application in high data rate laser communication systems which surpass the present performance of the Nd:YAG laser has been successfully demonstrated.

II. PHYSICAL AND CRYSTAL CHARACTERISTICS OF $Nd:YVO_4$

A. Crystal Growth of $Nd:YVO_4$ *

Single crystals of rare earth doped YVO_4 have been grown by both flux and Czochrolski techniques.[1,2,3,4] Crystal growth studies using either technique have been somewhat limited and, consequently, the growth of these materials is poorly understood at this time. The crystals grown from fluxes are small (≈ 2 cm long by 2-3 mm in cross section) and elongated in the "c" axis direction. Crystals of this type are not appropriate for laser applications which require "a" axis rods ≈ 3 mm or larger in diameter and 30 mm or longer in length. On the other hand crystals of sufficient size and proper orientation have been grown by the Czochrolski process. Unfortunately these crystals contain many defects and as such are not adequate for laser application.

A detailed microscopic examination by Aerospace staff of state-of-the-art Czochrolski grown single crystals has revealed several light scattering defects related to lack of proper control of the crystal growth processes. An example of a major scattering defect is shown in Fig. 1. These shaped inclusions are most likely crystals of Ir derived from the crucible material and are scattered randomly throughout most of the crystals. Other material inclusions discovered in the crystals were of such small size (1-3 μm) that high quality optical micrographs could not be obtained. These will be described.

Preliminary examination of a "bad" "a" axis laser rod showed several zones of intense light scattering along the length of the rod. Microscopic examination showed a high volume of scattering centers with complex characteristics. They appeared as small round black dots with a rod shaped sharp index change around the dot aligned in random directions in the crystal. Normally one would assign apparent index changes to diffraction effects around the scattering centers. In this case there appears to be a sharp-irregular index change associated with most but not all of the scattering centers. Due to the small size of the centers one cannot clearly state whether the dot represents a solid phase or a void in the crystal. However, at this time a best guess

---

* A. B. Chase of The Aerospace Corporation

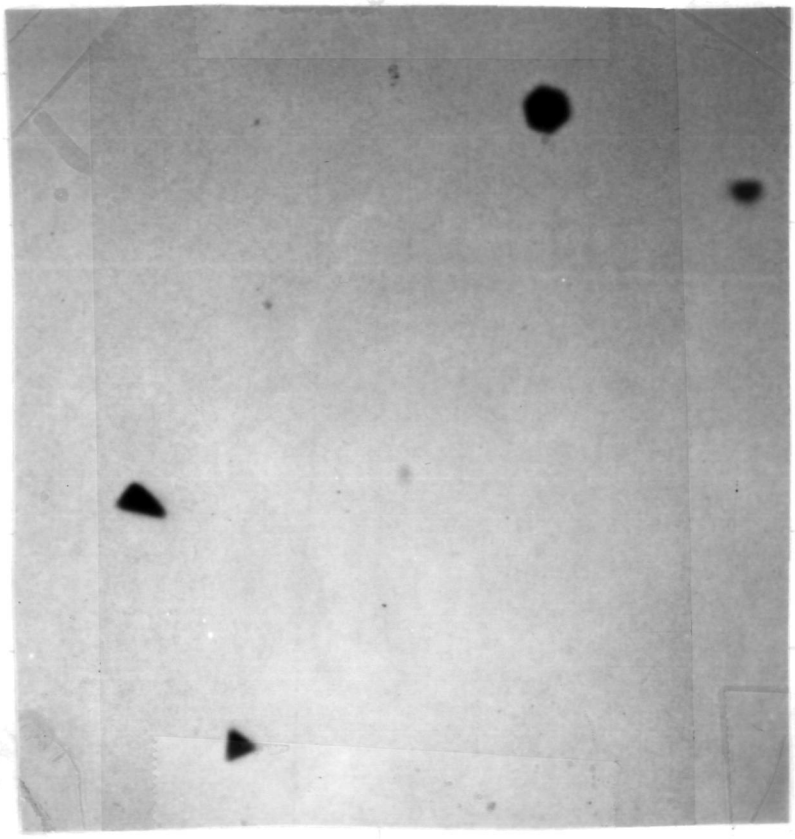

Fig. II-1 Inclusions observed in crystals of Nd:YVO_4

would be that it is a void and the index change represents a rod shaped unidentified phase associated with the void. Since their distribution was not uniform along the length of the rod, one can state that their occurrence was due to some variation of crystal growth parameters.

In order to understand the presence of the defects in the material and stipulate the means of their removal, some of the basic material properties are necessary. YVO_4 melts congruently at $1810 \pm 25^{\circ}C$ in an oxidizing atmosphere. In an inert or reducing atmosphere the melt and material loses O_2 with a corresponding increase in the melt temperature. The phase diagram for Y_2O_3 - V_2O_5 has been worked out and there are two primary phases, YVO_4 and $4Y_2O_3 \cdot V_2O_5$. The phase diagram Y_2O_3 -V_2O_5 -V_2O_3 has not been worked out at this time, but several phases are possible. In principle, the loss of O_2 from the melt does not constitute a problem, however, in practice severe problems exist.

Ir is the only useable crucible material for high temperature oxide oxide crystal growth. Specifically, an oxygen atmosphere is required for stoichiometric crystal growth and Ir is not stable at high temperatures in an oxidizing atmosphere. Ir oxidizes to IrO_2 which is soluable in the melt, becomes reduced and precipitates in the crystal, thereby causing the triangular plate scattering centers in the YVO_4 crystals. If, on the other hand, a reducing atmosphere is used, V_2O_5 loses O_2 and a lower valence state VO melt species is produced. If this species is in excess, then another Y_2O_3-VO phase is produced and will be incorporated in the crystal. The other observed defect is probably of this type. This represents the current state-of-the-art in crystal growth of YVO_4 single crystals. Some of each crystal rod is of adequate quality (i.e. does not contain inclusions) indicating that at least for some O_2 pressure good crystal growth can take place. These effects would, of course, be eliminated if a crucible could be found that would not react with YVO_4 melts in an oxidizing atmosphere. The difficulty of obtaining suitable crucibles suggests utilization of other methods.

The technique that most readily provides the required conditions is known as skull melting where the material itself is its own crucible.[5] The

use of this technique requires a different heating source than currently used. If applied to the growth of YVO_4 then high quality crystals free from scattering centers should be readily available.

B. Crystallographic properties of YVO_4^+

The crystal structure of YVO_4 is isomorphic to zircon,[6] having space-group symmetry D_{4h}^{19} *. Figure II-1 shows this tetragonal crystal structure and illustrates the unit cell. The Y^{3+} site symmetry in which the Nd^{3+} ions are found is D_{2d}. The Y^{3+} ion is at the center of a tetrahedron formed by four nn O^{2-} ions. The reduction to D_{2d} symmetry arises from the fact that this tetrahedron is shorter along the c-axis than the corresponding dimensions perpendicular to the c-axis. In addition, this irregular tetrahedron is surrounded by four nn Y^{3+} ions and their O^{2-} tetrahedra which are located below, left and right, and above, front and back, of the site in question. This large tetrahedron is oriented 90° from the orientation of the Y-O tetrahedron at its center. The V^{5+} ions are not seen by the Y^{3+} ions in the first approximation since each V^{5+} ion, due to its small size (0.59Å) is completely shielded by a tetrahedron of O^{2-} ions. Table II-1 summarizes the crystallographic properties of YVO_4.

Table II-1

CRYSTALLOGRAPHIC PROPERTIES OF YVO_4 [6]

Symmetry	Tetragonal
Space group	D_{4h}^{19}
Lattice constants	$a_o = b_o = 7.123$ Å $c_o = 6.291$ Å
Volume of unit cell	319 Å^3
Number of molecules per unit cell	4
Y-O bond distances	2.30 Å
V-O bond distances	1.64 Å
Density	4.22 g cm^{-3}

+ K. M. Leung of the University of Southern California prepared sections B, C and D. Section E was prepared by J. G. Sliney, Jr., of the University of Southern California.

* For an explanation of space-group symmetry and the symbol, please see Refs. 7, 8, 9.

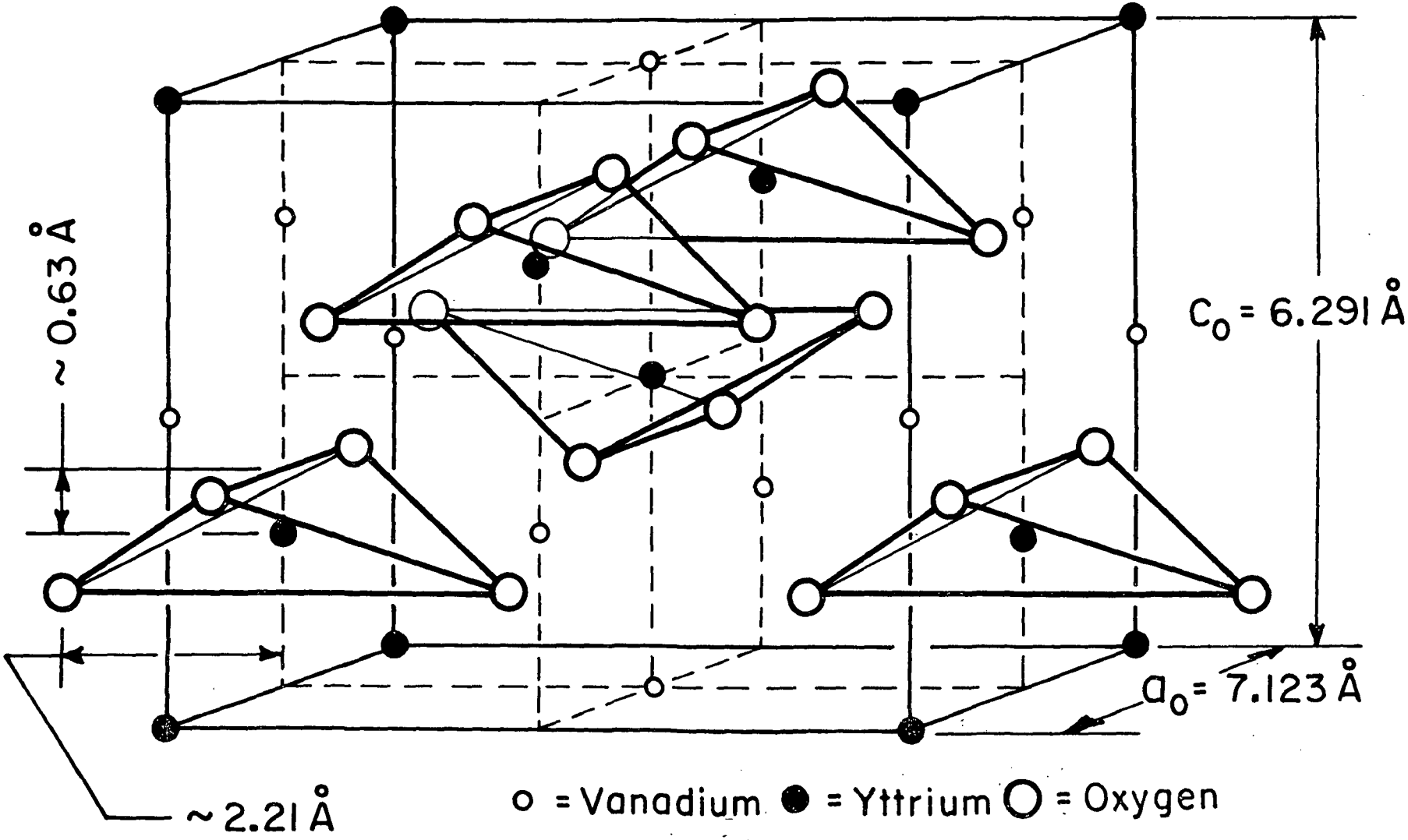

Figure II-2 The tetragonal unit cell (D_{4h}^{19}) of yttrium vanadate after Wyckoff.

[R. W. G. Wyckoff, Crystal Structure (Interscience, New York, 1963).]
The cell contains four YVO_4 molecules. Eight face-oxygen ions associated with four vanadium-oxygen tetrahedra that are located at the four off-center with four vanadium have been omitted from the cell to enhance clarity.

C. Physical properties of YVO_4

It is important to know their physical properties such as hardness, thermal conductivity, melting point, etc. in evaluating the potential value of a crystalline material as a laser crystal. YVO_4 has been available for several years in limited quantity as a single crystal laser host doped with Nd and other rare-earth ions. Most of the material parameters have been reported in the literature. In particular, YVO_4 has a moderate hardness of 480 Knoop (5 Mohs) which is equivalent to most high quality optical glasses. This hardness and a minimization of cleaving tendency allow good fabrication as a laser rod. The damage threshold of an undoped YVO_4 crystal is 1 to 2 GW/cm^2 using a single mode Q-switched pulsed ruby laser having a pulse width of 8 nsec.[10] Table II-2 lists some of the important physical properties of YVO_4 including several thermal properties. We also tabulate the properties of Nd:YAG for the purpose of comparison.

Table II-2

PHYSICAL PROPERTIES OF YVO_4 AND YAG

	YVO_4 +	YAG *
Hardness	5-6 Mohs	8-8.5 Mohs
Melting point	1810 °C	1950 °C
Thermal expansion at 300°K	$+(7.3 \pm 0.5) \times 10^{-6}$ $°C^{-1}$ normal to the c-axis	$+7.5 \times 10^{-6}$ $°C^{-1}$
Thermal conductivity at 300°K ($W\ cm^{-1}\ °K^{-1}$)	∥ c-axis 0.0523 ⊥ c-axis 0.0510	0.13
density (g/cm^3)	4.22	4.55

+ Data are taken from Refs.11 and 12.

* Data are taken from Ref. 14.

D. Optical properties of YVO_4

For an undoped YVO_4 single crystal, the transmission range is from 0.4 to 3.8 μm and is optically useful to 5 μm.[11] YVO_4 is a positive uniaxial crystal. The refractive index of YVO_4 has been measured[11] as a function of wavelength and polarization from 0.49 to 3.39 μm. Table II-3 lists the measured refractive indices at several special wavelengths. It can be seen that YVO_4 has a strong birefringence. For

Table II-3

INDICES OF REFRACTION OF YVO_4 AT SPECIAL WAVELENGTHS

Wavelength, μm	Index of Refraction	
	Ordinary (σ)	Extraordinary (π)
0.4880	2.0298	2.2712
0.5145	2.0192	2.2546
0.5890	1.9997	2.2270
0.6328	1.9915	2.2148
0.6943	1.9824	2.2021
1.065	1.958	2.168
2.00	1.93	2.13
3.39	1.91	2.11

example, $\Delta n = +0.2273$ at Na-D line and +0.210 at 1.06 μm. The fluorescence and laser action from Nd:YVO_4 can be observed in two different ways: along the optic axis (C-cut) or transverse to it (A-cut). The latter configuration was chosen throughout this work. When viewing the fluorescence and laser action transverse to the c-axis, there are two polarizations of the electric field vector: perpendicular to the c-axis (σ) and parallel to the c-axis (π). The most intense laser transitions for this uniaxial crystal is π-polarized.

Over the visible region (0.4880 to 0.6943 Å), the index change is 0.0474 for ordinary ray and 0.0691 for extraordinary ray. There are two different

results for the temperature dependence of the dispersion for Nd:YVO_4. Figure II-2 depicts the change in refractive index as a function of temperature for Nd:YVO_4 according to data taken with the prism in a liquid helium dewar and an argon laser.[11] At room temperature, dn/dT is $+3.9 \times 10^{-5}$ $^oK^{-1}$ for Nd:YVO_4. Another result determined by using Fizeau interferometry gives a different value of dn/dT for Nd:YVO_4.[12] The value of dn_o/dT near room temperature is $+(8.5 \pm 0.9) \times 10^{-6}$ $^oK^{-1}$ and that of dn_e/dT is $+(2.9 \pm 0.9) \times 10^{-6}$ $^oK^{-1}$ for Nd:YVO_4 as compared to $+7.3 \times 10^{-6}$ $^oK^{-1}$ for Nd:YAG.[13] The discrepancy of these two results in dn/dT for Nd:YVO_4 requires further study of these thermal properties in order to make a meaningful comparison with Nd:YAG.

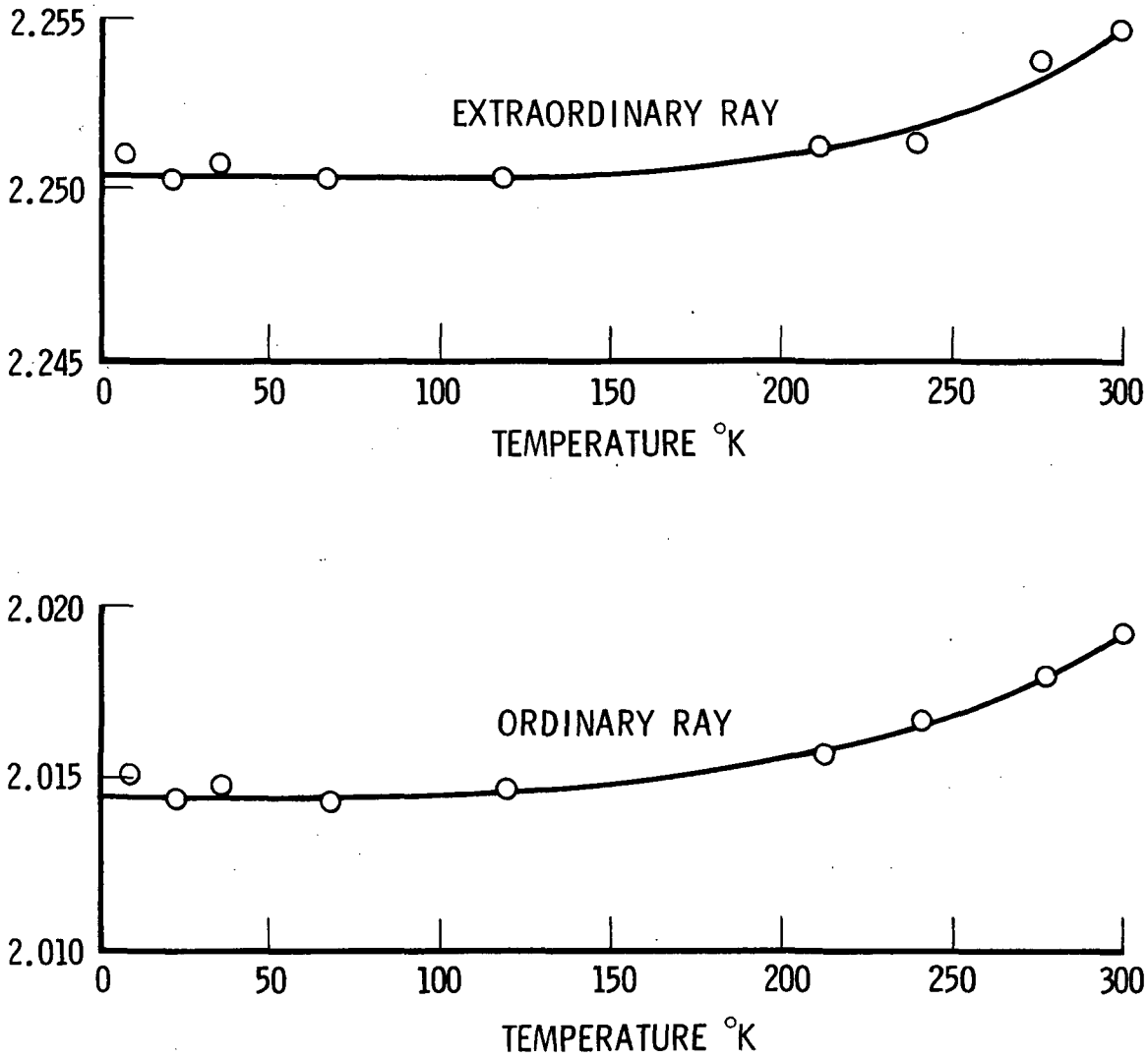

Fig. II-3 Refractive Index vs Temperature, Nd:YVO_4

E. Percent concentration of Nd^{3+} in $Nd:YVO_4$

To begin, the definitions of percent concentration used in this report need to be made clear. There are two definitions of concentration which are commonly used. They are weight percent and atomic percent. The convention used in this report is atomic percent defined as follows according to the standard usage.[14,15,16] In this usage, one atomic percent doping of Nd^{3+} means that one Nd^{3+} ion replaces one Y^{3+} ion out of one hundred Y^{3+} ions. In this case, the formula for $Nd:YVO_4$ reads:

$$Nd_{.01}Y_{.99}VO_4 .$$

More generally, one writes for any amount (x) of Nd^{3+} doping

$$Nd_x:Y_{1.00-x}VO_4.$$

The first method used to determine the concentration of Nd^{3+} ions in YVO_4 was emission spectroscopy which was performed on three samples at Pacific Spectrochemical Laboratory, Inc. The samples sent were cut from the same crystals of $Nd:YVO_4$ which were used in several different experiments including fluorescence lifetime measurements, as well as absorption and transmission measurement. The samples were cut in order of increasing concentrations (1% to 3%) in order to avoid contamination of the more lightly doped crystals. The cutting was performed using a diamond wire saw, which had previously been used to cut a crystal of glycerol. The samples cut for analysis were mounted on a glass slide using phenol salycilate. The low melting point of the latter allows one to avoid excessive heating of the crystals to be cut. After cutting, the crystals were cleaned in trichloroethylene, methanol and acetone.

The atomic percent of Nd^{3+} present in each sample was determined by emission spectroscopy performed by Pacific Spectrochemical Laboratory, Inc.[17] A sample of pure YVO_4 was provided in order to allow Pacific Spectrochemical to make a calibration using a known amount of Nd. Two

calibrations were made and the one with a scale closest to the spectra of the three samples of Nd:YVO_4 was finally used to determine the atomic percent of Nd^{3+} present in each sample. The accuracy of the measurements made was certified by Pacific Spectrochemical to be ± 7.5% on each measurement.

The results reported by Pacific Spectrochemical are given in weight percent of Nd_2O_3 which necessitates converting their data into atomic percent. The following is a sample calculation:

Sample Calculation for 1 Atomic Percent

Nd_2O_3 for Weight Percent

$Nd_2 = 2 \times 144.\underline{24} = 288.\underline{48}$

$O_3 = 3 \times 15.\underline{9994} = (+)\ 47.\underline{9982}$

$336.\underline{4782} \cong 336.\underline{48}$

Ratio $\frac{Nd_2}{Nd_2O_3}$ = 85.73% Nd by weight

$Nd_{0.01}Y_{0.99}VO_4$ for Atomic Percent

$Nd_{0.01} = 0.01 \times 144.22 = 1.4427$

$Y_{0.99} = 0.99 \times 88.92 = 88.0308$

$V = 1 \times 50.95 = 50.9500$

$O_4 = 4 \times 16 = +64.0000$

204.4235

Combining atomic percent with weight percent formula gives:

$$\frac{Nd_{0.01}}{Nd_{0.01}Y_{0.99}VO_4} = \frac{1.4427}{204.4235}$$

$$= 0.706 \text{ wt.\%}$$

This gives the conversion factors:

1 at.% = 0.706 wt.%
1.416 at% = 1 wt.%

The conversion factor for Nd:YVO_4 is calculated to be 1.416. In addition, it needs to be pointed out that Pacific Spectrochemical reported the weight percent of Nd_2O_3, which was used for calibration and is standard procedure as reported by Belt [18] and others. [19, 20] Consequently, one needs a further conversion factor which has been calculated to be 0.8573. Taking all these conversion factors into account, one arrives at the values listed in the table below which includes a comparison with the amounts put in the melt by Union Carbide which grew the crystals.

Table II-4

Union Carbide Nd at.% (in melt)		Pacific Spectrochemical Nd_2O_3 wt.% (in crystal)	at.%	Expected at.%	Adjusted PSL Values
Sample E	~0.5	0.25	0.303	---	---
D	1	0.34	0.412	.43	.412
C	2	0.59	0.716	.86	.788
B	3	1.30	1.58	1.29	1.42

In addition to the emission spectroscopy data on the Nd concentrations provided by Pacific Spectrochemical, absorption spectroscopy measurements were made on the same crystals by J.G. Sliney and K.M. Leung using a Cary 17 spectrophotometer. This absorption data provided a method for determining the concentrations relative to one another. If one knows the thickness of the crystals and the absorptivity (optical density), then one can measure the ratios of the concentrations and compare them with the values obtained by the emission method. Because the depth of the absorption "valleys" is proportional to the absorptivity, the depth of several well defined absorption lines was measured and compared for various concentrations and thicknesses. The 5304 Å line in the visible and the 7424 Å line in the infrared both in π polarization were chosen as being the best candidates, because they were well resolved and were not strongly absorbed or weakly absorbed lines. The 5304 Å line was used by Pressley et al. [21] The ratios of the concentrations are given in Table II-5.

Table II-5

ABSORPTION SPECTROSCOPY DATA

Samples	Ratio of Concentrations	5304 Å/π	7431 Å/π
D = 1 at.% (in melt)	C/D	1.90	1.95
C = 2	B/D	3.22	3.39
B = 3	B/C	1.70	1.77

In the 2nd Quarterly Progress Report, P.P. Yaney [22] reported a ratio of 2.05 ± 0.2 using infrared absorption data on crystals of nominal 1 and 2% concentrations, but the data on the 1% crystal was not obtained on the Cary 17. All the data taken by J.G. Sliney and K.M. Leung was obtained using a Cary 17 spectrophotometer. Table II-6 summarizes all the data to date starting with Union Carbides at.% (in the melt).

Table II-6

Ratio of Concentrations	Union Carbide	PSL Emission Spectroscopy	Sliney-Leung Absorption Spectroscopy 5304 Å/π	Sliney-Leung Absorption Spectroscopy 7431 Å/π	Adjusted PSL Values
C/D	2	1.74 ± .26	1.90 ± .38†	1.95 ± .39†	1.91
B/D	3	3.84 ± .58	3.22 ± .65†	3.39 ± .68*	3.45
B/C	1.5	2.21 ± .33	1.70 ± .34†	1.77 ± .35	1.80
$\frac{\text{D medium}}{\text{D thin}}$	1‡	---	0.91	0.62	---
$\frac{\text{C medium}}{\text{C thin}}$	1‡	---	1.19	0.45	---
$\frac{\text{B medium}}{\text{B thin}}$	1‡	---	0.93	0.92	---

† These ratios were obtained using data from the three thin (L ~ 1 mm) crystals.
‡ Expected ratio assuming uniform crystal growth.
* These ratios were obtained using data from the three medium (L ~ 3 mm) crystals.

Tables II-4 and II-6 list Adjusted PSL Values. These were obtained by taking the 1% crystal concentration listed by PSL to be within a few percent of the actual value. The reasoning that supports this choice is based on the knowledge that the 0.412 at.% reported by PSL falls within a few percent of 0.43 at.% which is the percent one would expect from a well-grown crystal. The 0.43 at.% is known to hold true for Nd:YVO_4 crystals from other data. Specifically, emission spectroscopy data was obtained on a total of eight YVO_4 crystals doped with varying amounts of Nd (0.5% - 3%). From the analysis [23] of this data, which included not only the Nd concentration, but also significant levels of impurities, the segregation coefficient [24] was determined to be 0.43.

Using the 0.412 at.% PSL data as most accurate, it is obvious that the 0.716 at.% PSL data is too low in both the C/D and B/C ratios using absorption spectroscopy. Similarly, the 1.58 at.% PSL data is too high in the B/D and B/C ratios. Raising the 0.716 at.% PSL value by approximately one half the difference between it and the expected value, as well as lowering the 1.58 at.% PSL value by about the same amount, leads to the Adjusted PSL Values for the ratios of the concentrations. It should be noted that these Adjusted PSL ratios lie within the accuracy of the ratios obtained by absorption spectroscopy. The justification for computing the Adjusted PSL Values was based on two factors. First of all, the segregation coefficient was known from the analysis of the eight Nd:YVO_4 crystals. Secondly, the absorption data was taken over a larger volume of the sample than the emission spectroscopy data. Both factors were taken into account in order to compute the Adjusted PSL Values.

In conclusion, it should be noted that the general convention used to designate concentration in this report is simply 0.5, 1, 2 and 3% which is to be taken to mean 0.5, 1, 2 and 3 at.% in the melt as grown by Union Carbide. Any exceptions to this general convention will be noted.

References: Chapter II

1. D. Elwell and H. J. Scheel, Crystal Growth from High Temperature Solutions (Academic Press, N. Y., 1975).

2. R. Feigelson, J. Am. Ceram. Soc. 51, 538 (1968).

3. J. J. Rubin and L. G. Van Uitert, J. Appl. Phys. 37, 2920 (1966).

4. A. B. Chase, "Exploratory Flux Growth" in Solid State Materials: Preparation and Properties, Vol. 1 (Marcel Dekker, N. Y., 1971).

5. J. F. Wenikus and A. F. Armington, "Skull Melting of Zirconia" in Conference Program Abstracts of Third American Conference on Crystal Growth, Stanford Univ., July 13-17, 1975, pp. 198-9.

6. E. Broch, Z. Physik Chem. 20B, 345 (1933).

7. A. Schoenflies, Krystallsysteme und Krystallstructur(Leipzig, 1891).

8. R. S. Federov, Z. Krist., 20, 28 (1892).

9. For example, see
T. Janssen, Crystallographic Groups (American Elsevier Publishing Company, Inc. New York, 1973); and
J. M. Robertson, Organic Molecules and Crystals (Cornell Univ. Press, Ithaca, N. Y., 1953).

10. K. M. Leung and L. G. DeShazer, "Surface defects on crystals of TiO_2 and YVO_4 studied by laser-induced damage effects," in Laser Induced Damage in Optical Materials: 1974, edited by A. J. Glass and A. H. Guenther, NBS Special Publication 414, 193-199 (1974).

11. H. G. McKnight and L. R. Rothrock, "Research and Development Work for the Growth of Single Crystal Yttrium Orthovanadate," Final Technical Report, U. S. Army ECOM Contract No. DAAB0772-C-0022 (April 1973).

12. R. J. Pressley, P. V. Goedertier, and H. Weakleim, "MBT-70 Laser Materials Research and Exploratory Development," RCA Lab., Princeton, N. J., Final Technical Report (Oct. 1969).

13. J. D. Foster and L. M. Osterink, Appl. Opt. 7, 2428 (1968).

14. R. F. Belt, Laser Focus, pp. 44-47 (Apr. 1970).

15. R. J. Pressley, P. V. Goedertire and H. Weakliem, "MBT-70 Laser Materials Research and Exploratory Development," Contract No. DAAK02-69-C-0040, p. 7.

16. J. K. Guha, "Spectroscopy and Laser Properties of Neodymium in Yttrium Aluminum Garnet and Yttrium Orthoaluminate," dissertation, University of Southern California (1973); (University Microfilm, Inc., Ann Arbor, Michigan) pp. 39-41.

17. Report No. 67123, Pacific Spectrochemical Laboratory, Inc. (Los Angeles, California), (March 1976).

18. R. F. Belt, Laser Focus, pp. 51-52 (Aug. 1973).

19. See pp. 4, 7 in Ref. 15.

20. See pp. 39-41 in Ref. 16.

21. See p. 12 in Ref. 15.

22. "Low Threshold CW Nd Laser Oscillator at 1060 nm Study," 2nd Quarterly Report, The Aerospace Corp. (6 Feb. 1976), Contract No. NAS 5-22387, National Aeronautics and Space Administration, p. 4.

23. A. B. Chase, the Aerospace Corporation, private communication.

24. R. A. Laudise, The Growth of Single Crystals (Prentice-Hall, Englewood Cliffs, N. J., 1970).

III. LASER DESIGN SPECTROSCOPY

A. Introduction *

One of the main objectives of this program is to determine the spectroscopic parameters of Nd:YVO_4 required for the analysis of the laser feasibility tests and for the design of lamp-pumped lasers. Most of the standard spectroscopy has been completed under a U.S. Army Contract and is described in report ECOM-74-0104-F.

In this work, the polarized fluorescence and absorption spectra for Nd:YVO_4 at ~85°K and ~300°K were obtained using a 1-meter Czerny-Turner grating spectrograph. These spectra provide us the necessary data to determine the energy level scheme of the states directly involved in the 1.06 μm laser action. Measurement of the fluorescence lifetime of the upper laser level, $^4F_{3/2}$ of Nd:YVO_4 has been carried out as a function of the concentration of Nd ions (nominally 1, 2, and 3 %), and as a function of temperature for 1 % Nd sample. This information may help us to understand whether the non-radiative relaxation processes will play an important role in quenching fluorescence in Nd:YVO_4 and to determine the optimum concentrations for efficient laser action. Absorption and transmission traces covering the spectral range from 0.3 to 0.9 μm have also been obtained on a Cary 17 spectrophotometer for a number of Nd:YVO_4 crystals of various Nd^{3+} concentrations (nominally 1, 2, and 3 %) and thicknesses ranging from 1 mm to 5 mm. Fast scans were used to obtain compressed spectra and slow scans to obtain expanded spectra. Based on the expanded absorption spectra of a 2% Nd^{3+} in YVO_4 thin sample, Yaney has determined a spectral map of Nd:YVO_4 pump bands and the corresponding spectroscopic parameters necessary for the design of lamp-pumped CW Nd:YVO_4 lasers. The results of these laser design spectroscopic studies and analysis are presented in the following sections.

---

* P. P. Yaney of the University of Dayton and K. M. Leung of the University of Southern California prepared sections A and B. P. P. Yaney also prepared section D.

B. Spectroscopic studies

The optical spectrum of Nd^{3+} in single crystal YVO_4 has been investigated by several groups of researchers.[1, 2, 3, 4] A general illustration of energy levels for Nd ions in YVO_4 is given in Fig. III-1 which shows a 4-level laser system. In this work, we are interested in details on both the laser transitions at 1.06 μm and the spectral map of the pump bands.

The crystal-field splitting in D_{2d} symmetry for the states of interest are given below using group theoretical arguments [5]

$$^4F_{3/2} \rightarrow \Gamma_6 + \Gamma_7$$

$$^4I_{9/2} \rightarrow 2\Gamma_6 + 3\Gamma_7$$

$$^4I_{11/2} \rightarrow 3\Gamma_6 + 3\Gamma_7$$

The selection rules governing the transitions are summarized in Table III-1. Thus, we see that the $^4I_{9/2} \rightarrow {}^4F_{3/2}$ transition group can have ten σ and five π transitions.

Table III-1

ELECTRIC DIPOLE SELECTION RULES IN D_{2d} SYMMETRY[a]

	$\Gamma_6(1/2)$	$\Gamma_7(3/2)$
$\Gamma_6(1/2)$	σ	πσ
$\Gamma_7(3/2)$	πσ	σ

a. The quantities in parentheses are the crystal field quantum numbers $|\mu|$.

Figures III-2 and III-4 show the absorption and fluorescence spectra for the $^4I_{9/2} \rightarrow {}^4F_{3/2}$ transitions at room temperatures. Because of the large thickness of the sample used to obtain these spectra, the high-cross-section transition completely absorbs the incident light thereby causing this line to become flat-topped. The large thickness was used to insure

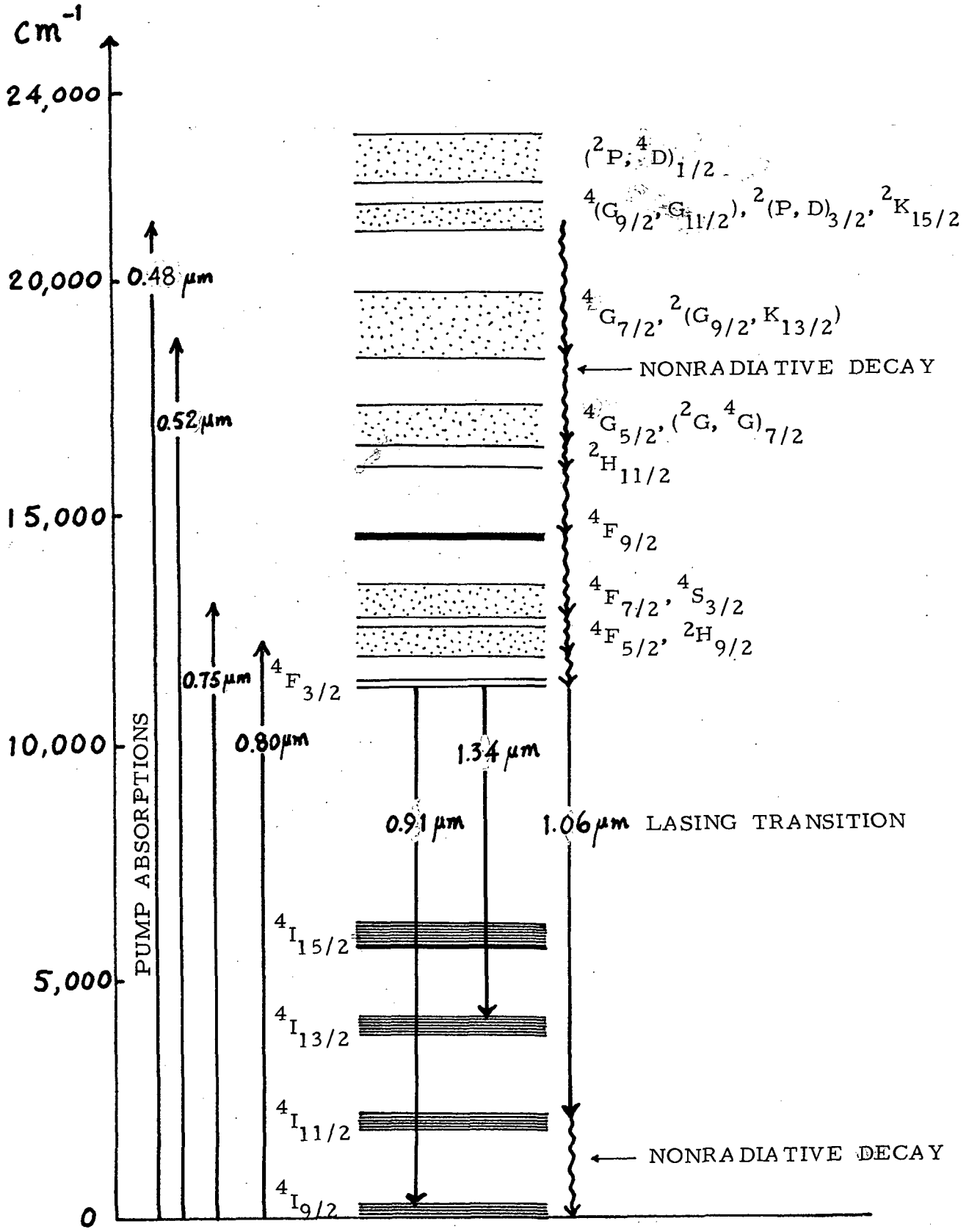

Figure III-1. Energy Levels and Laser Transitions of Nd Ion in YVO_4

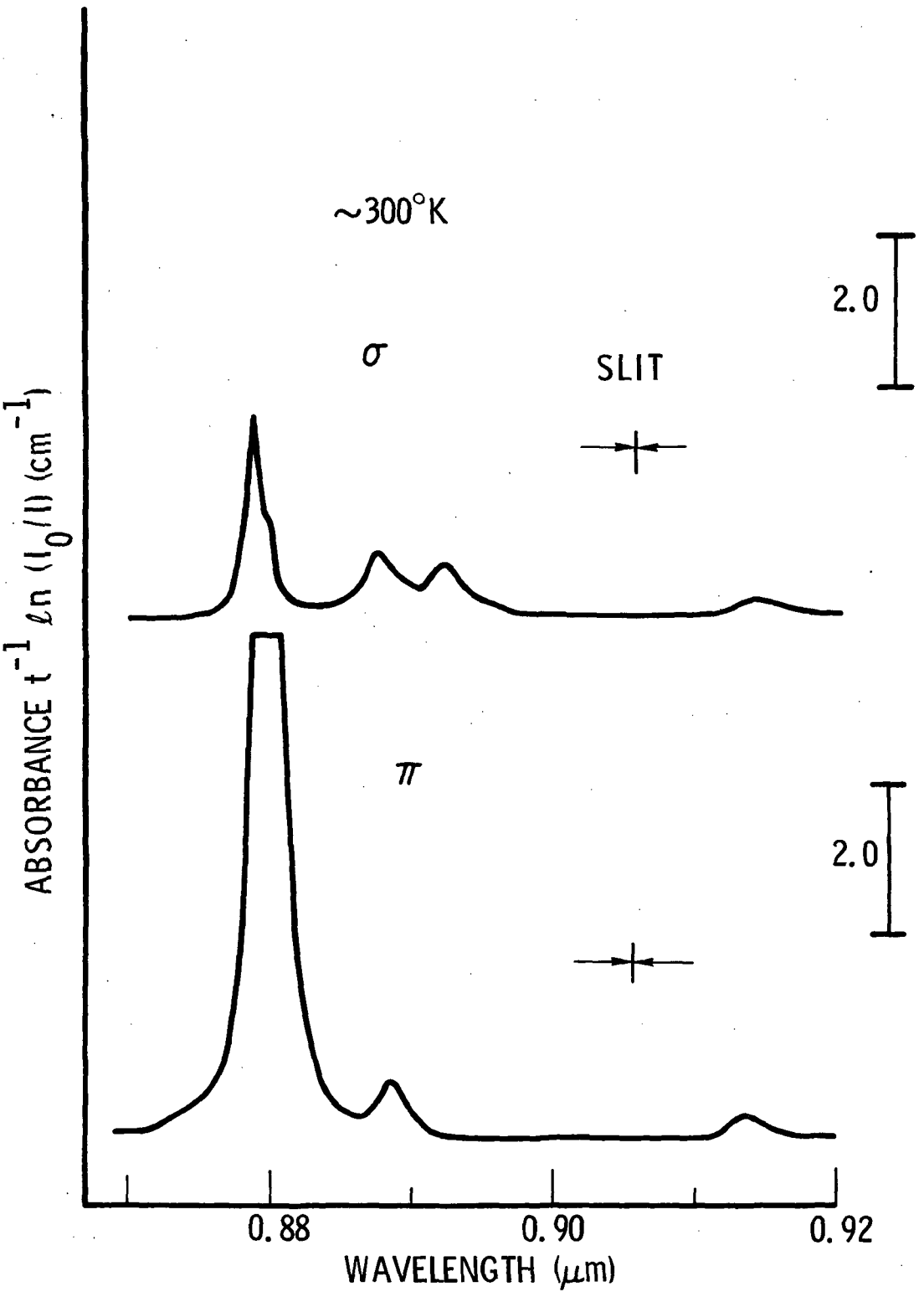

Figure III-2 Absorption lines of Nd:YVO_4 in the 0.9 μ region.

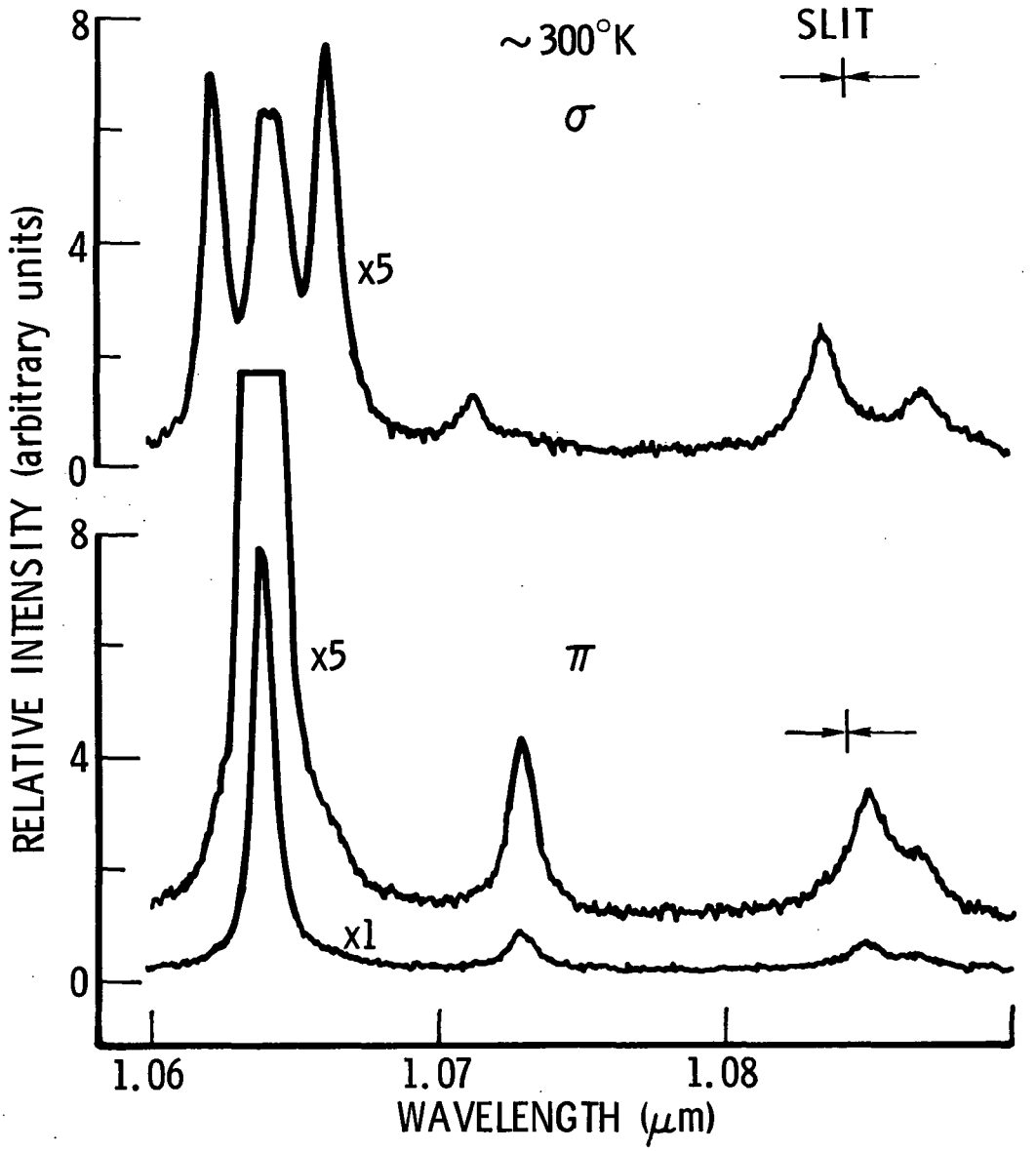

Figure III-3 Fluorescence of Nd:YVO_4 in the 1.06 μ region.

that all pertinent electronic transitions were found. Clearly, there are lines missing which are permitted by the selection rules. The absence of allowed transitions and the unusual concentration of line strength into one transition in π polarization within a given line group can be shown via the Judd-Ofelt theory[6] to be a consequence of the symmetry of the site and ion placements in the unit cell which cause the $A^7_{\pm 6}$ odd-parity crystal-field coefficient to be dominant. The fluorescence spectra at room temperature for the $^4F_{3/2} \rightarrow {}^4I_{11/2}$ transitions are given in Fig. III-3. From Table III-1, there should be 12 σ lines and 6 π lines. Only the low temperature σ spectrum shows the required 12 lines. In the π spectrum we have only four lines. The strong π line appears in σ polarization as the second of the four strong lines, counting from the short wavelength end. We shall identify the third line of this group as being one of the missing π lines. This line can be seen on the long-wavelength side of the strong π line only as an asymmetry in the lower half of the strong π line.

The energy level scheme based on the studies summarized above is given in Fig. III-5 for room temperature. Also shown are the observed transitions. The experimental frequencies of these transitions taken at room temperature are presented in Table III-2. The line widths and peak cross sections of the $^4F_{3/2} \xrightarrow{\pi\sigma} {}^4I_{11/2}$ transitions at room temperature were also measured. These results are given in Table III-3. The strengths were determined by comparing the fluorescence intensities to the intensity of the $^4I_{9/2}(e) \rightarrow {}^4F_{3/2}(b)$ resonance line. The laser transition $^4F_{3/2}(a) \rightarrow {}^4I_{11/2}(a)$ is at 10 640.9 $\pm$ 0.2 Å and is predominantly π polarized. For convenience, we have included a diagram to display the energy levels for the ^4I term in Fig. III-6.

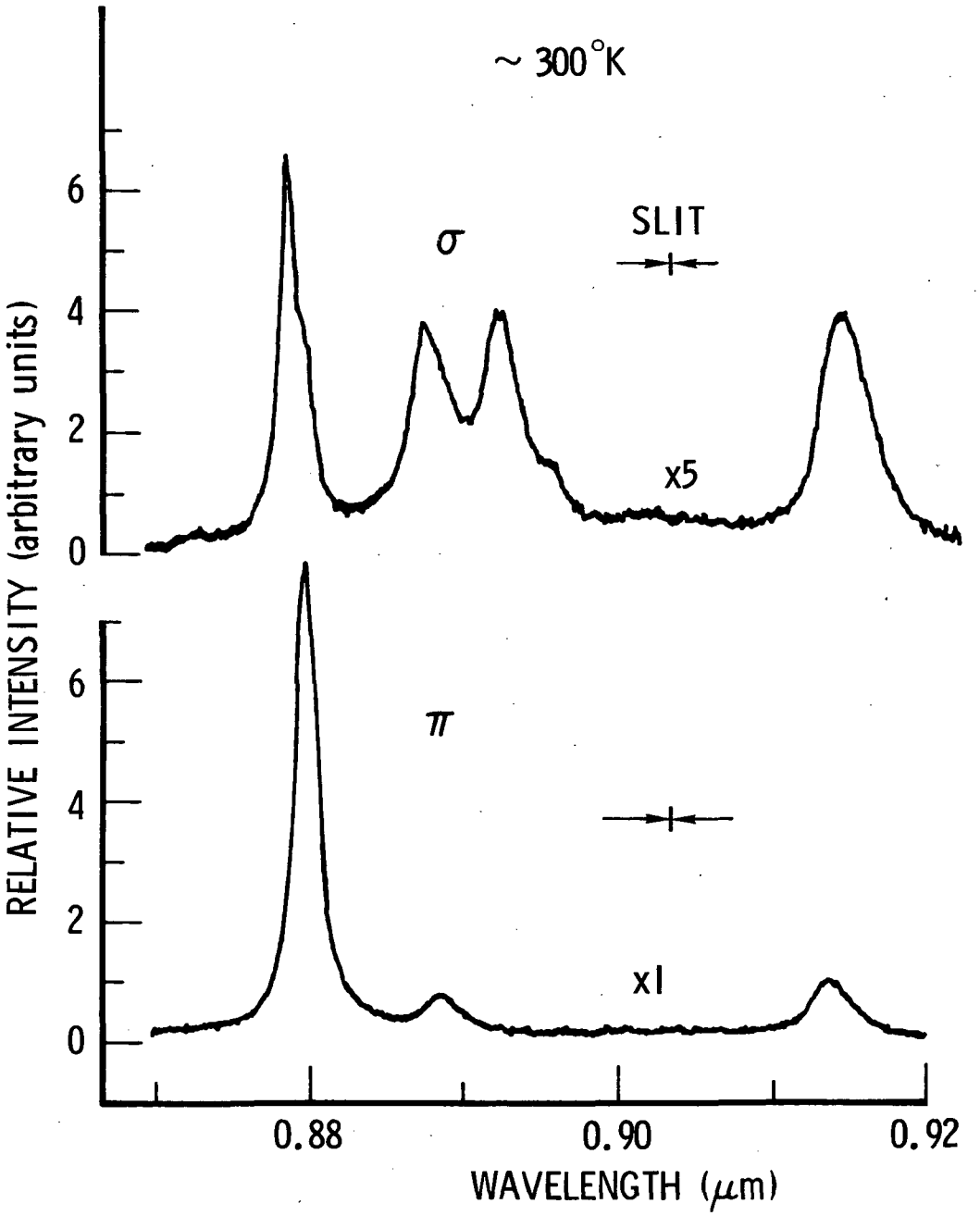

Figure III-4 Fluorescence of Nd:YVO_4 in the 0.9μ region.

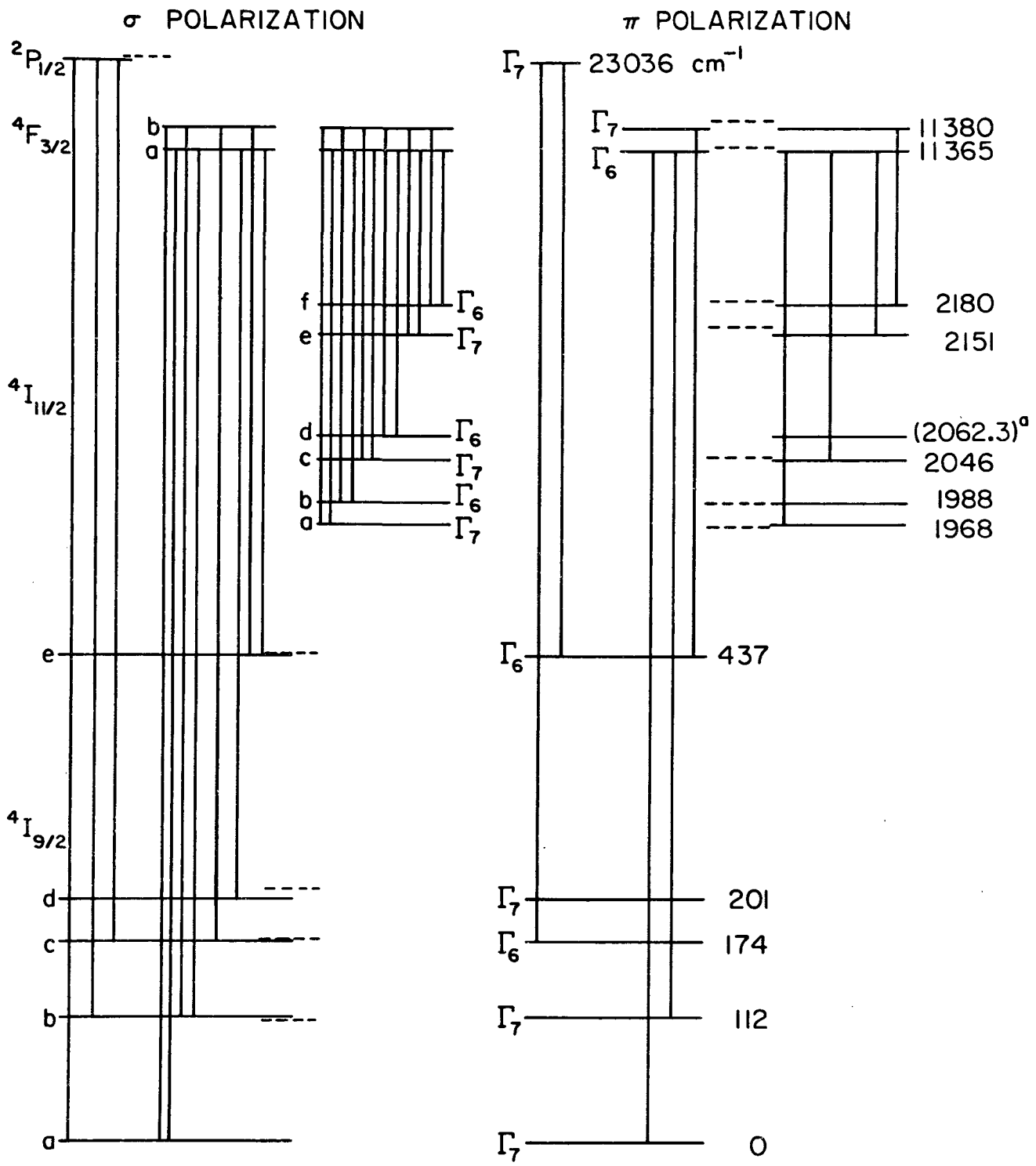

Figure III-5 Classification of the energy levels of Nd in YVO_4.

Table III-2

OBSERVED TRANSITIONS OF ~1 ATOMIC % Nd^{3+} IN YVO_4 AT ROOM TEMPERATURE[a]

Transition	Polarization[b]	$\nu_{air}(cm^{-1})$
$^4F_{3/2} \leftrightarrow {}^4I_{9/2}$		
a - a	σ, π	11 365.4
a - b	σ, π	11 253.2
a - c	-	n/o
a - d	σ	~11 164
a - e	σ	10 929[c]
b - a	σ, (π)	11 379.6
b - b	σ	11 267[c]
b - c	σ	11 205.5
b - d	-	n/o
b - e	σ, π	10 943
$^4F_{3/2} \rightarrow {}^4I_{11/2}$		
a - a	σ, π	9 397.7
a - b	σ, (π)	9 377.5
a - c	σ, π	9 319.1
a - d	σ	n/o
a - e	σ, π	9 214.8
a - f	σ	9 185.9[c]
b - a	σ, (π)	9 411.9
b - b	σ, π[d]	9 391.6[c]
b - c	σ	9 333.7
b - d	σ, π[d]	n/o
b - e	σ	9 228.8
b - f	σ, π	9 200.0

Values to 0.1 cm^{-1} are accurate to ±0.5 cm^{-1} or better.
All other values are to ±1 cm^{-1}.

a. See Figures 2-4 for traces of spectra. n/o means "not observed".
b. The σ transitions which appear weakly in π polarization are denoted by (π).
c. These values had to be deduced from other values because of interference from neighboring lines.
d. This polarization was not resolved.

Table III-3. Parameters for $^4F_{3/2} \rightarrow {}^4I_{11/2}$ Transitions of Nd:YVO_4 at Room Temperature.[a]

Transition	Frequency[b] (cm^{-1})	Linewidth[c] (cm^{-1})	Peak Cross-section (x 10^{-19} cm^2)[c] Along c-axis	Along a-axis σ	Along a-axis π
b → a	9411.9	7.8	13	7.0	--[d]
a → a	9397.7	6.9	~12	~6.4	30
b → b	9391.6	6.5	~ 9	~4.9	--[d]
a → b	9377.5	7.7	17	9.4	--[d]
b → c	9333.7	12.8	2.4	1.6	n/o
a → c	9319.1	9.7	weak	weak	3.0
b → d	(9323.5)	--	n/o	n/o	n/o
a → d	(9306.2)	--	n/o	n/o	n/o
b → e	9228.8	11.6	7.2	4.2	n/o
a → e	9214.8	9.1	weak	weak	3.0
b → f	9200.0	15.2	6.6	2.0	weak
a → f	9185.9	--	weak	weak	n/o

a. See Figure III-3 for traces of spectra. n/o means not observed. See Table III-2.

b. Frequencies in parentheses are ~85°K values.

c. These data were obtained from a sample having a Nd weight percentage of 0.91%. Cross section values to ±20%.

d. These lines are too obscured by a → a line for measurement.

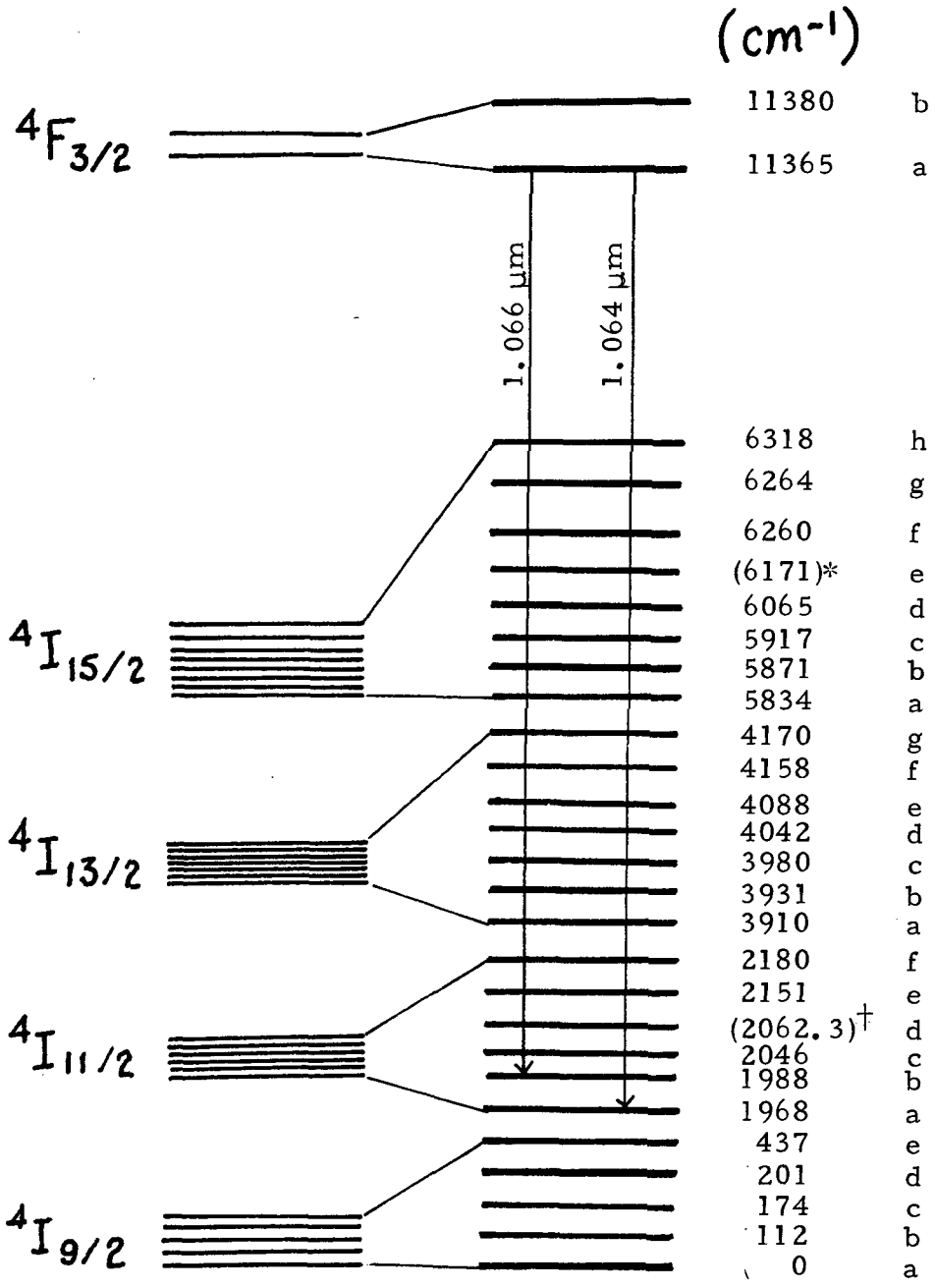

Figure III-6. Energy Level Diagram of the Five Lowest Multiplets of Nd^{3+} in YVO_4. The 1.06 μm Laser Transitions are Indicated.

* theoretical value

† ~85°K value

C. FLUORESCENCE PROPERTIES [+]

1. Introduction

Due to a variety of results in lifetime measurements, [1, 2, 7, 8] it is evident that a systematic study of the fluorescence lifetime as a function of temperature is needed for Nd:YVO_4. In this work, measurement of the fluorescence lifetime of the upper laser level, $^4F_{3/2}$ of Nd:YVO_4 has been obtained as a function of the concentration of Nd ions (nominally 0.5, 1, 2 and 3 %) and also as a function of temperature for 1% sample. In the following sections, the experimental apparatus and procedures will be described and significant results will be presented.

2. The experimental apparatus

The fluorescence lifetime measurements were made using the experimental arrangement shown in Fig. III-7. The output of a pulsed Argon ion laser (0.5145 μm, 4 μsec FWHM and ~20 W peak power) was used to excite the fluorescence from the Nd:YVO_4 crystals (concentrations of nominally 0.5, 1, 2 and 3 % Nd^{3+}). The laser power input to the crystal was monitored by a photodiode (ITT model 4018, biplanar diode) and the fluorescence signal was detected by a photomultiplier (RCA model 7201, S1 surface). The signal from the photodiode was displayed on one channel of a dual beam oscilloscope (Tektronix model 555) whose traces were triggered by the photodiode's signal. The other trace displayed the fluorescence decay signal.

The output of the Argon laser was horizontally polarized; the crystal's c-axis was oriented in the vertical direction, providing minimum absorption of the pump light. The lens, L_1 (focal length 25 cm), was used to spread out the laser spot size on the face of the crystal; the beam area was measured to be 0.5 cm^2. The filter, F_1 (various Kodak neutral density filters), allowed control over the input laser power to the crystal. The

---

[+] J. G. Sliney, Jr. of the University of Southern California and the Aerospace Corporation.

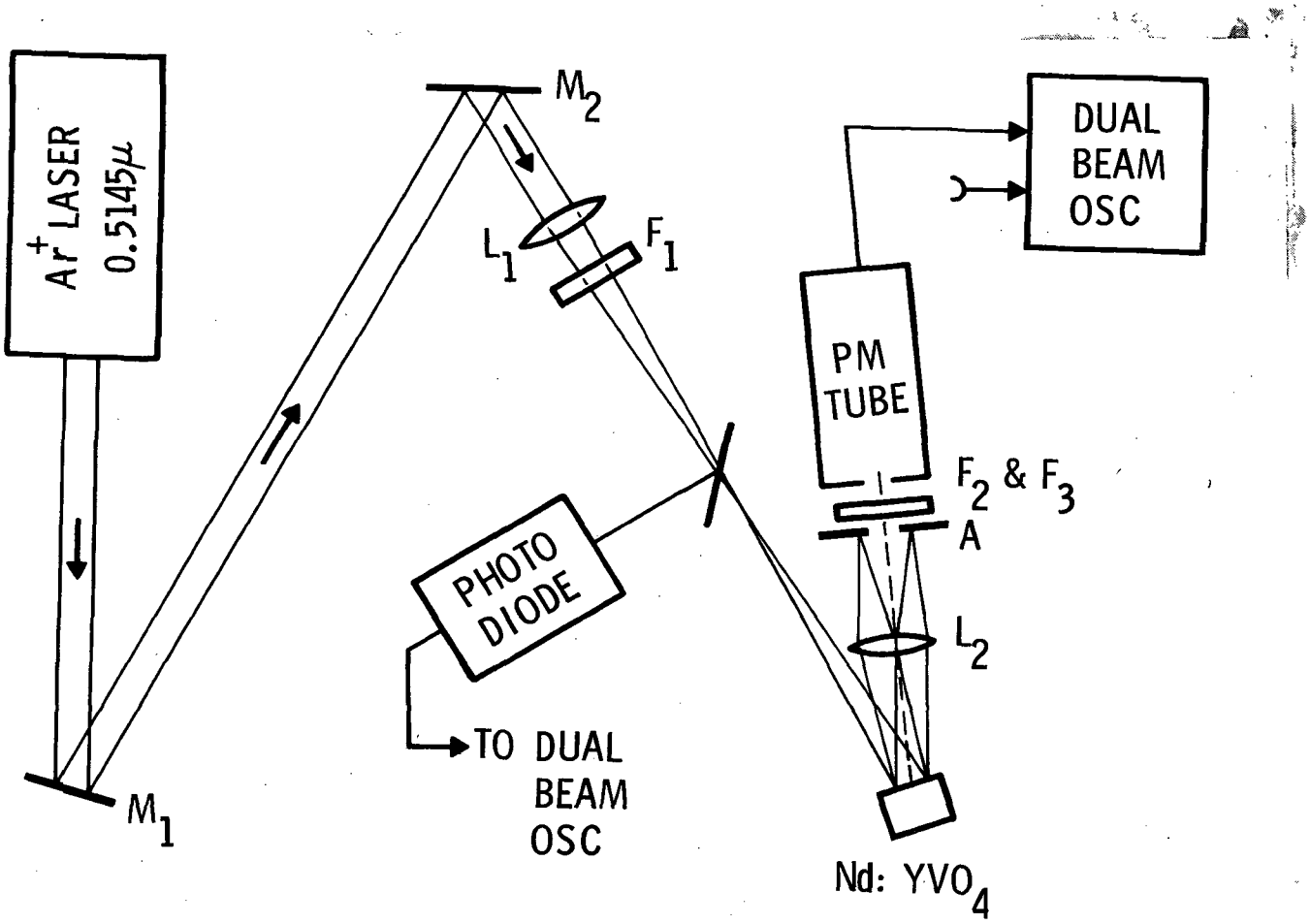

Figure III-7. Diagram of Experimental Apparatus

laser pulse was monitored by a photodiode (ITT model 4018). The lens, L_2 (focal length 8.9 cm) was used to collect the fluorescence from the crystal and focus it onto the photomultiplier tube (RCA model 7102). Before striking the photomultiplier, the fluorescence radiation passes through two filters, F_2 and F_3. The former is a narrow band-pass filter at 1.06 μm (Baird Atomic, model B2NIR, 54% transmission at 1.06 μm and 270 Å bandwidth). The latter filter was a sharp cut off red filter (Corning CS 2-59, 80% transmission at 1.06 μm and negligible transmission below 0.61 μm). The aperture, A, which eliminated the directly reflected laser light,

was connected to a housing around the photomultiplier so that stray light could not leak around the filters.

The output of the photomultiplier, which was biased at ~1 KV, was fed into a high-gain differential amplifier (Tektronix plug-in model 1A7A). The differential amplifier had a scale ranging from 10 μV/cm to 10 V/cm and a variable bandwidth with settings ranging from 100 Hz to 1 MHz. The usual bandwidth setting used was 30 KHz; the vertical scale settings used were typically 20, 50, and 100 μV/cm. The output of the photodiode, which was biased at ~1 KV, was fed into a fast-rise calibrated preamp (Tektronix plug-in model type L) in the oscilloscope. Typical traces are displayed in Fig. III-8. Multiple exposures were made on various time bases.

3. Crystals

The crystals of Nd:YVO_4 used in these experiments were taken to be nominally 0.5, 1, 2 and 3 % Nd^{3+} in YVO_4 as specified by Union Carbide. Two groups of crystals were used. The first group to be tested had been cut and their faces polished flat and parallel, so that they were suitable for laser operation. The 1% and 2% crystals of this group were anti-reflection coated for 1.06 μm, but the 3% crystal was not. The 2% and 3% crystals lacked a polished face at right angles to the faces polished flat and parallel, so that the right angle geometry as described by Garbuny[9] could not be used. The geometry used for all the crystals tested in both groups was that shown in Fig. III-7, which can be described as "nearly head-on geometry".

The second group of crystals were labelled spectroscopic crystals, because their surfaces had not been ground and polished flat and parallel but only polished. These crystals were not anti-reflection coated for 1.06 μm. All the lifetimes reported here were obtained using the spectroscopic crystals with the addition of the 2% and 3% crystals which were from the first group.

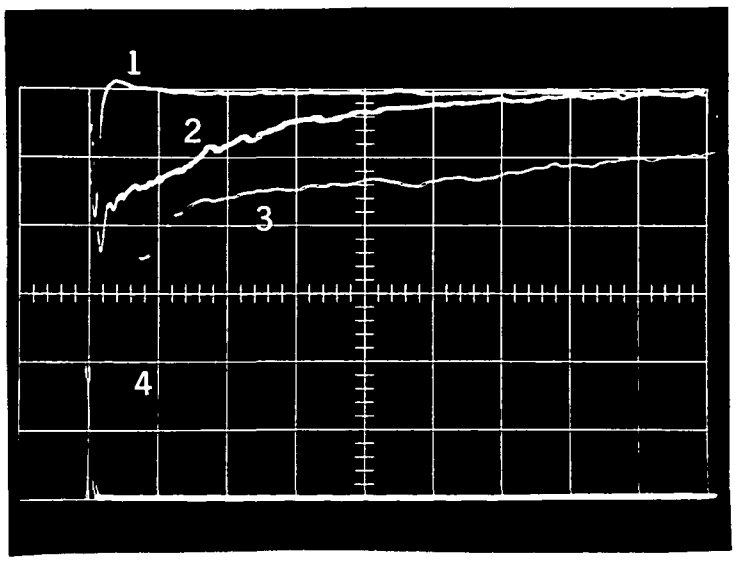

50 μsec/cm traces 1 and 2
10 μsec/cm trace 3

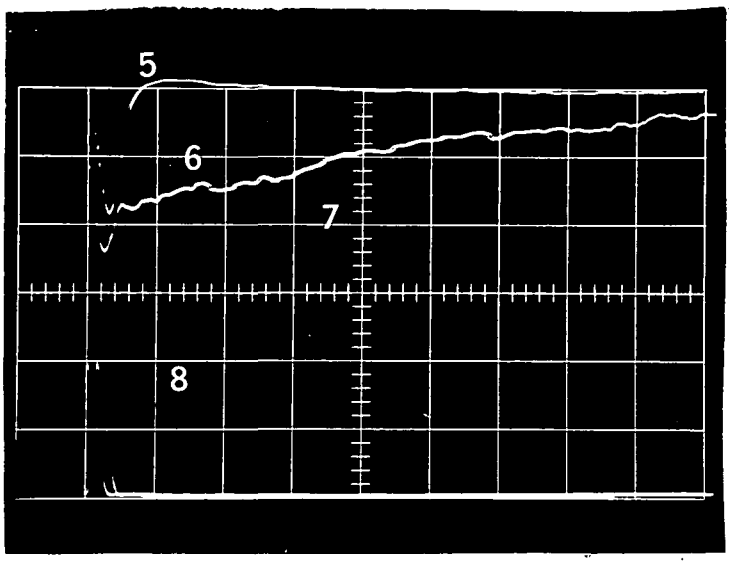

20 μsec/cm traces 5 and 6
5 μsec/cm trace 7

Figure III-8 Typical Oscilloscope Traces

In the upper photo trace 1 is the background from the electronics used in the experiment. The fluorescence decay is displayed in trace 2 and trace 3. The traces labeled 4 are the laser pulses. In the lower photo, trace 5 is the background. The fluorescence decay is displayed in trace 6 and trace 7. The traces labeled 8 are laser pulses.

All the crystals used in these experiments were grown by Union Carbide using the Czochralski Method. Previous work by Pressley et al.[2] was with material grown by three different methods. The 1% spectroscopic crystal was cut from the same boule as the specimen used in the 1% thin (~1 mm) crystal for the absorption measurements.

4. Temperature measurements

The fluorescence lifetime of the 1% spectroscopic crystal as a function of temperature was measured from 90°K to 465°K. For temperatures below room temperature, liquid nitrogen was used to cool the cold finger. Both the crystal and the thermocouple were affixed to a copper block using a silicone heat-sink compound (G C Electronics, type DC-Z9) to provide good thermal contact. The crystal was enclosed in a vacuum tight stainless steel housing, which had circular windows (2.5 cm in diameter). The collection lens, L_2, in Fig. III-7 was 5 cm in diameter and 8.9 cm from the crystal. The solid angle of light collected was measured to be 2.5×10^{-1} steradians.

The other end of the cold finger was immersed in a dewar of liquid nitrogen. The typical temperature recorded by the copper-constantan thermocouple after equilibrating for approximately one hour was 90°K. The thermocouple was connected to a cold junction compensator (West Instruments Corp., model AC-II Autocomp). The voltage was read on a microvoltmeter (Hewlett-Packard, model 425A DC Micro Volt-Ammeter).

For the temperatures above 300°K, the dewar was removed and heating coils were wrapped around the copper conduction tube. Temperature measurements were made with a copper-constantan thermocouple. Its calibration curve was checked during the experiments by immersing the thermocouple in liquid nitrogen and in a solution of ethyl alcohol and dry ice. For temperatures above 300°K a thermometer was used. The

values measured corresponded to within a degree (°K) with those values listed on the thermocouple's calibration chart.

5. Experimental procedures

The data was reduced manually from the photographs and plotted on semilog paper over several lifetimes. In each case, at least two photographs with different time bases (20 μsec/cm and 50 μsec/cm) were used to provide data for the semilog plots. Figure III-9 shows a semilog plot of the 1% Nd:YVO_4 lifetime data.

In our calibration procedure we measured the fluorescence lifetime at 1.06 μm of a Nd:YAG laser crystal (nominally 1% Nd) at room temperature. We found its fluorescence lifetime to be 233 ±7 μsec, which agrees with the values published in the literature. [10, 11]

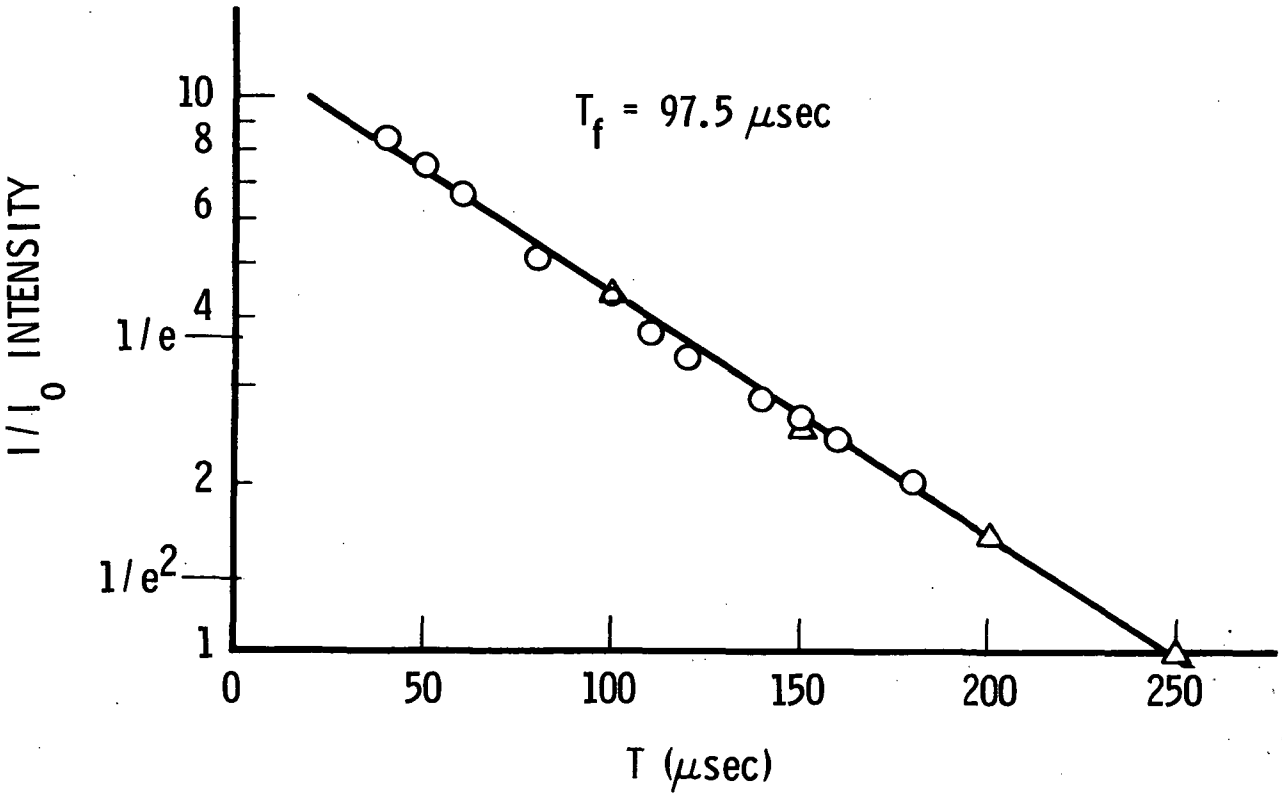

Figure III-9. Semilog Plot of the Normalized Intensity of 1% Nd:YVO_4 as a Function of Time

An electronic boxcar was not used in this initial work, because the signal to noise ratio was good and hence a manual data reduction was judged to be adequate. A considerable number of photographs were taken; random selection of photographs taken under similar conditions yielded almost identical results when the data was reduced.

Two methods of determining the uncertainty were used. The first was the method of standard deviation, which yielded an uncertainty of ±3.8 μsec for the 20 μsec/cm time base photographs and ±6.6 μsec for the 50 μsec/cm time base. The second method was the geometrical method. The two worst lines were drawn through the data points on the semilog plots and the differences averaged. This method yielded an uncertainty of ± 8 μsec for the 20 μsec/cm time base and ±8.5 μsec for the 50 μsec/cm. In order to provide a conservative error estimate for the lifetime measurements, an average value was obtained from the σ, based upon the usual statistical treatment of the data and the larger uncertainties obtained from the geometrical method. The uncertainty was computed to be ±7 μsec.

6. Results

The lifetime as a function of temperature is given in Table III-4. The graph of the lifetime as a function of temperature is given in Fig. III-10. The fluorescence lifetime of the 1% Nd^{3+} sample was measured at various temperatures ranging from 90°K to 465°K.

Table III-4

FLUORESCENCE LIFETIMES AT 1.06 μm for 1% Nd^{3+}

Temperature (°K)	90	180	300	377	453
τ_f (μsec)	95	99.7	97.5	107.5	87.1

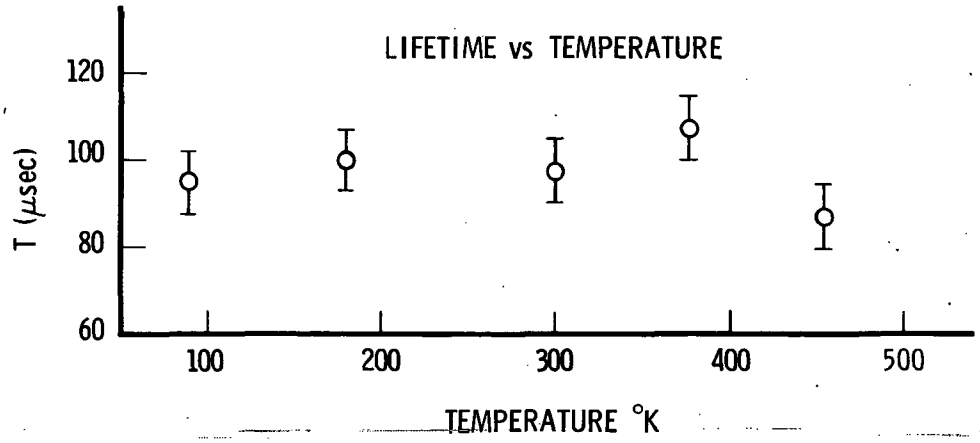

Figure III-10. Fluorescence Lifetime of 1% Nd:YVO_4 as a Function of Temperature

Measurements of the fluorescence lifetimes of Nd:YVO_4 at 1.06 μm were made at room temperature, 300°K, for 0.5%, 1%, 2% and 3% concentrations of Nd^{3+} in YVO_4. The lifetimes for the four different concentrations are given in Table III-5. The graph of the lifetime of Nd:YVO_4 as a function of concentration is shown in Fig. III-11.

Table III-5

Nd:YVO_4 FLUORESCENCE LIFETIMES AT 1.06 μm

at. % Nd^{3+}	0.5%	1%	2%	3%
τ_f (μsec)	106 ±7	97.5 ±7	74.2 ±7	56.9 ±7

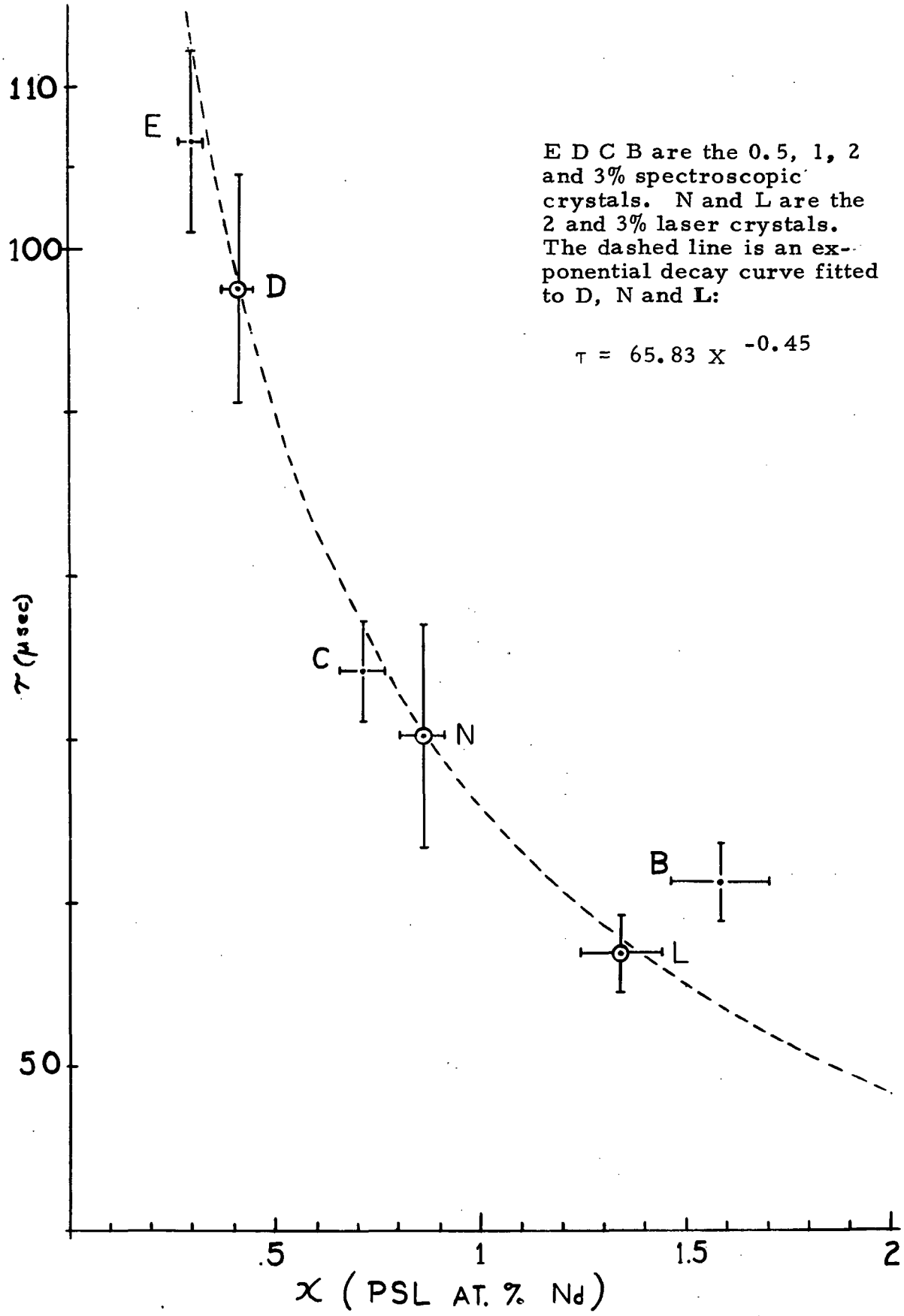

Figure III-11. Fluorescence Lifetime of Nd:YVO_4 as a Function of Neodymium Ion Concentration.

7. Discussion

We have obtained data on the fluorescence lifetime of Nd:YVO_4 at 1.06 μm as a function of temperature and as a function of concentration. Our data agrees generally with Pressley's[2] data which exhibited a shortening of lifetime with increasing concentration. However, our data on the temperature dependence differs from that of Bagdasarov et al.[1] who reported that the lifetime shortened with a decrease in temperature. We found no change in the lifetime from 300°K to 90°K.

Two processes that shorten lifetimes are non-radiative transitions and stimulated emission. Since non-radiative transitions do not play a role at 90°K, stimulated emission is the process that we think may be responsible for shortening the lifetime at low temperature.

The following results are given in support of the conclusion that stimulated emission may be the process responsible for the shortened lifetimes observed by Bagdasarov et al.[1] In the first place, stimulated emission at 1.06 μm has been observed by Tucker[12] at room temperature in one of the Nd:YVO_4 laser crystals in an experiment whose geometry was similar to ours. Secondly, Pressley, et al.[2] reported a linewidth narrowing at lower temperatures (9 Å at 300°K and 1 Å at 90°K). Thirdly, we observed that, when the laser beam area was expanded from a tight focus to ~0.5 cm^2 on the 1% crystal's face, the fluorescence lifetime lengthened to the present value of 97.5 ± 7 μsec. This lifetime was independent of laser input peak power over the range from 2.75 W to 7.25 W.

8. Conclusions

The fluorescence lifetime measurements of Nd:YVO_4 herein reported represent by far the most thorough study of this important parameter. By study of a variety of crystals of different concentrations over a wide temperature range we have greatly enlarged the state of our knowledge. We have shown that over the temperature range of 90 to 377°K, the fluorescence

lifetime of the $^4F_{3/2}$ level remains constant at approximately 100 μsec and decreases somewhat to 87 μsec at 453°K - the highest temperature at which lifetime measurements were obtained. These results have several important implications for utilization of Nd:YVO_4 as a laser material. The independence of the lifetime with temperature provides a strong indication that the fluorescence efficiency of the $^4F_{3/2}$ level approaches unity. In many applications, the laser crystal requires cooling to maintain the crystal at an operating temperature and in some cases, with only air cooling, the laser crystal will be operated at temperatures in the neighborhood of 300°C and higher. The Nd:YVO_4 offers a clearly advantageous situation with regard to possible operation above room temperature.

On the scientific side, the detailed measurements presented here clarify the ambiguous measurements of earlier investigations; particularly with regard to observation of shortened lifetimes at low temperature.

The lifetime results as a function of concentration show the expected trend. Over the concentration range of 0.3 to 1.6 PSL at.% Nd, the lifetime decreases from 105 to 60 μsec at room temperature. This can be attributed to concentration quenching - namely, non-radiative relaxation by transfer of excitation to neighboring Nd^{3+} ions. The observed decrease in lifetime has been curve fitted to a decaying exponential which is of the form $\chi^{-1/2}$ where χ is the concentration in atomic percent Nd.

D. The design of a lamp-pumped CW Nd:YVO_4 laser

1. Introduction

In order to design a solid state laser it is necessary to know to what degree the pump light penetrates the outer portion of the rod and reaches the lasing volume. The fraction of the pump light that arrives at the lasing volume is a function of the radius of the rod and the concentration of the ion responsible for the light absorption. The fraction of the pump light which is absorbed in a thickness d due to an absorbing ion of concentration n_o averaged over wavelength λ can be represented by the expression

$$\bar{\alpha}(d, n_o) = \frac{\int H_\lambda \alpha_\lambda (d, n_o)\, d\lambda}{\int H_\lambda\, d\lambda} , \qquad (1)$$

where H_λ is the spectral irradiance incident on the sample due to the lamp and α_λ is the spectral absorptivity of the sample. The absorptivity is related to the transmissivity τ_λ by the relation

$$\alpha_\lambda = 1 - \tau_\lambda , \qquad (2)$$

where, in the absence of non-absorptive scattering,

$$\tau_\lambda = e^{-A_\lambda d} , \qquad (3)$$

and A_λ is the absorption coefficient. In other words, we are not concerned here with the light that does not enter the medium (i.e., the light that is reflected from the rod surface), nor with excitation of the lasing volume that may occur by indirect schemes.

Generally, the functions H_λ and α_λ for a given lamp and rod, respectively, are very complex, consisting of both broad bands and superimposed strong, sharp lines. For this reason, a determination of $\bar{\alpha}$ should be done experimentally using the lamp of interest, where the main difficulty would be to properly account for or to eliminate the reflected light. This situation is probably more critical for uni-axial materials such as YVO_4 which

produce highly polarized spectra. In these circumstances the optimum combination of pump cavity configuration, rod orientation, and rod geometry is not obvious and may be complicated functions of not only d and n_o, but also of lamp input power (or energy).

In order to obtain a rough idea of the behavior of $\bar{\alpha}$, Eq. (1) can be approximated by assuming H_λ is constant over the wavelength band of interest. This gives

$$\bar{\alpha}(d, n_o) \approx (\Delta\lambda)^{-1} \int \alpha_\lambda (d, n_o)\, d\lambda ,$$

or, from Eq. (2),

$$\approx (\Delta\lambda)^{-1} \int [1 - \tau_\lambda (d, n_o)]\, d\lambda , \tag{4}$$

where $\Delta\lambda$ is the bandwidth over which there is significant absorption. In a transmission measurement situation, the quantity measured is transmittance $\tau_{\lambda m}$ which is related to τ_λ by the expression[13]

$$\tau_{\lambda m} = \frac{(1 - \rho_\lambda^{\,2})\, \tau_\lambda}{1 - \rho_\lambda^{\,2} \tau_\lambda^{\,2}} , \tag{5}$$

where ρ_λ is the spectral reflectivity of the sample. If $\rho_\lambda \lesssim 0.2$, then Eq. (5) can be approximated to give (within 4%)

$$\tau_\lambda \approx \tau_{\lambda m} (1 - \rho_\lambda^{\,2})^{-1} . \tag{6}$$

This is a reasonable approximation since ρ_λ for the materials of interest is a very slowly varying function in the wavelength regions of interest and $\rho_\lambda = 0.2$ corresponds to a refractive index of about 2.5. Since YVO_4 is a positive uniaxial crystal and the extraordinary (π polarization) index is 2.34 at 4000 Å,[3] Eq. (6) can be used. Assuming the transmission measurement is made using a double-beam spectrophotometer such as the Cary 17, τ_λ can best be found by balancing the instrument against a pure

(i.e., undoped), optical-quality sample of the host material, YVO_4 in this case, located in the reference beam. Otherwise, either the instrument can be balanced for each absorption band, or the transmission scale can be renormalized for each band. In any case, since the absorption occurs in relatively narrow bands of lines, it is somewhat simpler to integrate $1 - \tau_\lambda$, as given in Eq. (4), rather than τ_λ.

In evaluating Eq. (4), there is the problem of determining $\Delta\lambda$ for each band. This is clearly a matter of judgement since the bands are all different requiring slightly different approaches for arriving at $\Delta\lambda$. Actually, this circumstance is not a point of great significance since we are ultimately interested only in how $\bar{\alpha}$ varies with changes in the values of d and n_o. That is, we can specify $\Delta\lambda$ for each band for a specific pair of values of d and n_o and use these bandwidths for all combinations of d and n_o. Clearly, from Eqs. (1) and (2), we can also obtain the averaged transmissivity $\bar{\tau}$ from

$$\bar{\tau} = 1 - \bar{\alpha}. \tag{7}$$

2. Spectral analysis of a 2 % Nd in YVO_4 crystal

Instead of using the straight-forward, but cumbersome method of obtaining and integrating transmission traces of a number of samples varying in concentration and thickness, Yaney has chosen to measure carefully one sample having particular values of thickness (d) and concentration (n_o). The sample used was the thin (L = 0.103 cm) 2% Nd in YVO_4 crystal.* Expanded traces of the absorbance D_λ (optical density) were obtained using a Cary 17. The results of these studies are presented in Table III-6.

A close examination of Table III-6 shows large differences in the peak-absorption-coefficient, A_p, values for the two polarizations within a given band. These differences can be roughly characterized by calculating an

---

* Please refer to Chapter II, Section E for an explanation of the definition of concentration.

Table III-6. Wavelengths λ (in air) and Absorption Coefficients, A_p, of Peaks and Shoulders in the Absorption Bands of 2 % Nd^{3+} in YVO_4 Observed in π and σ Polarizations at Room Temperature. The State Identities Are Tentative.

State	π		σ	
	λ(Å)[1]	$A_p(cm^{-1})$[2]	λ(Å)[1]	$A_p(cm^{-1})$[2]
$^4F_{3/2}$	9138	0.7	9144	0.6
	8887	1.6	8957	0.9, sh
	8799	37.3	8924	1.6
	8745	0.9, sh	8877	2.0
	8716	0.2, sh	8787	5.6
$^4F_{5/2}$, $^2H_{9/2}$	8355	0.7, bd	8357	1.8
	8214	1.8, sh	8293	0.3
	8191	2.9, i	8198	3.4, i
	8127	14.0, i	8164	6.3
	8085	37.1	8135	3.7, i
	8057	17.4, sh	8086	17.2
	8019	6.3, sh	8065	10.7, i
	7990	2.9, sh	8003	1.3
$^4F_{7/2}$, $^4S_{3/2}$	7748	1.3, bd	7885	0.6, bd
	7621	4.9, i	7763	0.3, bd
	7593	8.5, i	7678	1.6
	7572	10.3	7601	3.1, i
	7525	11.2, i	7558	11.4, i
	7506	11.8, i	7525	10.1, i
	7498	12.3, i	7506	8.3, sh
	7492	11.8, i	7467	5.6, i
	7431	17.2	7427	10.3
$^4F_{9/2}$	6938	0.4, sh	6906	0.4, bd
	6894	0.7, bd	6841	0.4, bd
	6844	1.3, bd	6792	0.4, bd
$^2H_{11/2}$	6263	0.4	--	--

Table III-6. continued

State	π		σ	
	λ(Å)[1]	$A_p(cm^{-1})$[2]	λ(Å)[1]	$A_p(cm^{-1})$[2]
$^4G_{5/2}, (^2G, ^4G)_{7/2}$	6046	0.3, sh	6103	5.8
	6017	8.5, i	6049	3.1, bd
	5984	43.8	6018	3.4, sh
	5958	35.8, i	6007	4.2, sh
	5944	38.7, i	5983	14.8
	5932	32.2, sh	5958	15.6, i
	5892	11.2, i	5942	16.3, i
	5867	12.3, i	5933	16.3, i
	5833	14.8, i	5894	32.6
	5769	1.1, sh	5871	8.3, i
			5854	7.2, i
			5847	6.7, sh
			5834	3.8, sh
			5809	5.8, i
			5796	17.2
$^4G_{7/2}$,	5435	1.6	5460	0.1, ?
$^2(G_{9/2}, K_{13/2})$	5411	5.4	5449	0.1, ?
	5386	0.9, sh	5408	0.3, bd
	5357	0.7	5383	1.8, i
	5335	2.0	5375	2.0, i
	5328	1.6, sh	5367	2.5, sh
	5304	4.5	5362	3.1
	5291	1.3, sh	5353	2.2, sh
	5279	1.3, i	5335	6.9, i
	5260	2.2, sh	5327	14.1
	5250	5.1, i	5310	1.6, sh
	5226	4.5, i	5303	1.3, sh
	5219	3.4, sh	5286	6.7
	5204	5.1, i	5260	1.8
	5174	3.1, i	5252	2.0, i
	5119	3.4, bd	5249	2.0, i
	5099	2.2, sh	5234	3.6, sh
	5074	0.9, sh	5229	5.1, i
			5222	4.5, i
			5218	4.9, i
			5206	2.0, i
			5179	1.3, bd
			5164	1.1, i, bd
			5144	1.6, v bd
			5115	0.9, sh

Table III-6. continued

State	π		σ	
	λ(Å)[1]	$A_p(cm^{-1})$[2]	λ(Å)[1]	$A_p(cm^{-1})$[2]
$^4(G_{9/2}, G_{11/2})$, $^2(P, D)_{3/2}$, $^2K_{15/2}$	4852	0.7	4908	0.7
	4825	1.3, sh	4898	0.4
	4820	1.8	4858	0.2, sh
	4809	0.7, sh	4839	0.4, i
	4791	0.4	4825	0.7, i
	4761	5.1	4817	0.4, sh
	4716	1.6, i	4809	0.4, sh
	4675	0.9, bd	4799	0.4, i
	4628	0.7	4793	0.4, i
			4761	0.7
			4738	0.4
			4708	0.4, sh
			4684	0.4, i, bd
			4676	0.4, i, bd
			4657	0.7, i
			4651	0.7, i
			4635	0.7, bd
$(^2P, ^4D)_{1/2}$	4528	0.1, ?	4341	4.7
	4424	0.2	4361	0.2
	4374	2.9	4374	0.4
$^2D_{5/2}$	4256	0.1	--	--
	4238	0.4		
$^2(P, D)_{3/2}$	3851	0.1	3854	0.4
	3831	0.9, i	3842	0.1
	3813	3.6, i	3834	0.2, bd
	3805	2.0, sh	3820	1.8, i
	3796	2.2, sh	3817	1.9, i
			3814	1.7, i
			3805	1.3, i
			3801	1.6, i
			3795	3.8, 8
			3790	4.1, i
			3785	1.5, sh

Table III-6. continued

State	π		σ	
	λ(Å)[1]	$A_p(cm^{-1})$[2]	λ(Å)[1]	$A_p(cm^{-1})$[2]
$^4D_{3/2}, ^2D_{5/2}$	3679	1.3	3679	0.2, i
	3674	0.7, i	3674	0.2, i
	3666	0.7	3666	0.4, i
	3661	0.4, sh	3661	0.7, sh
	3644	6.5	3648	2.2, i
	3626	14.1	3638	2.3, sh
	3602	9.4	3635	2.5, i
	3588	4.5, i	3623	5.8, i
	3572	10.7	3612	3.6, sh
			3600	5.4, i
			3572	6.5, i
			3562	5.1, i
			3548	14.8
			3522	0.2

[1] Wavelength accuracy $\approx \pm 1$ Å.

[2] Absorption coefficient values were measured with ± 0.1 cm^{-1} precision; however, estimated accuracy gives $\lesssim \pm 5\%$ additional uncertainty with the stronger features being the more accurately measured cases. Symbols: i - interference from a neighboring line or feature making A_p simply the total strength at the wavelength of the peak; sh - shoulder corresponding to an incompletely formed peak on the side of a neighboring feature; bd - broad; v bd - very broad; ? - indicates questionable existence. Double dash entry indicates that features were too weak to be measured.

average wavelength $\bar{\lambda}$ obtained by averaging the wavelengths of peaks weighted by the peak optical density D_p as given below.

$$\bar{\lambda} \equiv \frac{\Sigma_i D_{pi} \lambda_i}{\Sigma_i D_{pi}} , \tag{8}$$

where the sums are taken over all the peaks of the line group. The results of these calculations are given in Table III-7. As an example of the influence of polarization on $\bar{\lambda}$, we note that $\bar{\lambda}$ for the band located near 8800Å changes by 52Å if the polarization of the incident light is rotated by 90°.

Optical density data allows a determination of the oscillator strength f which is given by the expression [14]

$$f = \frac{mc^2}{\pi e^2 (n_i - n_f)} \int A_\nu \, d\nu \tag{9}$$

where n_i and n_f are the initial and final state population densities (in cm^{-3}); (the statistical weights of the levels in Nd:YVO_4 are equal); ν is the wavenumber (in cm^{-1}); e, the electronic charge; m, the electronic mass and c, the velocity of light. If the bandwidth over which the integration in Eq. (9) is taken is sufficiently small, then Eq. (9) can be approximated by

$$f \approx \ell_D \bar{\lambda}^{-2} \int D_\lambda \, d\lambda , \tag{10}$$

where $\bar{\lambda}$ is given by Eq. (8), $\tau_\lambda = 10^{-D_\lambda}$, and

$$\ell_D \equiv \frac{mc^2 \ell n \, 10}{\pi e^2 (n_i - n_f) d} . \tag{11}$$

We wish to calculate an overall oscillator strength for each band of absorption lines. However, because the $^4I_{9/2}$ ground state consists of levels at

0, 112, 174, 201, and 437 cm^{-1}, [15, 16] there is some question as to an appropriate value for n_i. For these measurements n_f is negligible. From the usual Boltzmann distribution, the populations of the above levels at 300°K are 40, 23, 17, 15, and 5% of n_o, respectively. Neglecting transitions from the 437 cm^{-1} level due to its small population, and averaging the remaining populations gives $n_i \approx 0.24\, n_o$. The value of n_o can be found from the expression $n_o = n_c x / (a_o b_o c_o)$ where n_c is the number of metal atoms of the host for which an impurity atom can substitute in a unit cell of dimension $a_o \times b_o \times c_o$ and x is the fractional atomic concentration of the impurity. For YVO_4, $a_o = b_o = 7.123$ Å, $c_o = 6.291$ Å, and $n_c = 4$ [17]; thus with $x = 0.02$, we find $n_o = 2.51 \times 10^{20}$ cm^{-3}. For $d = 0.103$ cm, we obtain from Eq. (11) $\ell_D = 41.9$ Å. The integrals for Eq. (10) were obtained by integrating the area under each band of lines using a planimeter. The resulting values obtained for $\int D_\lambda d\lambda$ and f are given in Table III-7.

We can estimate $\bar{\alpha}$ from the values of $\int D_\lambda d\lambda$ in Table III-7 where, from Eq. (4), we have that

$$\bar{\alpha} \approx (\Delta\lambda)^{-1} \int [1 - 10^{-D\lambda}]\, d\lambda,$$

which can be further approximated to

$$\bar{\alpha} \approx 1 - 10^{-\bar{D}} \equiv \bar{\alpha}_D = 1 - \bar{\tau}_D, \tag{12}$$

where

$$\bar{D} = (\Delta\lambda)^{-1} \int D_\lambda d\lambda. \tag{13}$$

Basically, we arrived at Eq. (12) by replacing each band of lines by a rectangular band of height $\bar{D}$ and width $\Delta\lambda$. As it was previously pointed out in this report, any approach which does not account for the actual spectrum of the lamp is already an approximate one, at best. Thus, this

Table III-7

Spectroscopic Parameters of 2 at.% Nd^{3+} in YVO_4

Optical-density-weighted average wavelengths $\bar{\lambda}$, integrated optical densities $\int D_\lambda d\lambda$, oscillator strengths f, effective bandwidths $\Delta\lambda$, average optical densities $\bar{D}$, and average absorptivities in the "rectangular" approximation $\bar{\alpha}_D$ of the absorption bands of 2 at.% Nd^{3+} in YVO_4 observed in π and σ polarizations at room temperature for a sample thickness of 0.103 cm.[1]

State	$\bar{\lambda}$ (Å)[2]		$\bar{\nu}$ (cm^{-1})[2]		$\int D_\lambda d\lambda$ ($D\times$Å)[3]		$f(10^{-6})$[4]		$\Delta\lambda$(Å)		$\bar{D}$		$\bar{\alpha}_D$	
	π	σ	π	σ	π	σ	π	σ	π	σ	π	σ	π	σ
$^4D_{3/2}, {}^2D_{5/2}$	3611	3558	27693	28106	22.4	25.6	72	85	72	78	0.31	0.33	0.51	0.53
$^2(P, D)_{3/2}$	3809	3803	26254	26295	4.09	3.78	12	11	36	27	0.11	0.14	0.22	0.28
$^2D_{5/2}$	4242	--	23574	--	~0.1	--	~0.3	--	--	--	--	--	--	--
$(^2P, {}^4D)_{1/2}$	4378	4344	22841	23020	1.41	1.34	3.1	3.0	11	6.4	0.13	0.21	0.26	0.38
$^4(G_{9/2}, G_{11/2})$, $^2(P, D)_{3/2}, {}^2K_{15/2}$	4766	4761	20982	21004	9.56	5.01	18	9.3	160	190	0.060	0.026	0.13	0.06
$^4G_{7/2}$, $^2(G_{9/2}, K_{13/2})$	5258	5284	19019	18925	31.7	30.2	48	45	220	190	0.14	0.16	0.28	0.31
$^4G_{5/2}, (^2G, {}^4G)_{7/2}$	5940	5913	16835	16912	232.9	166.4	277	199	160	220	1.46	0.76	0.96	0.83
$^2H_{11/2}$	6263	--	15967	--	0.27	--	0.25	--	--	--	--	--	--	--
$^4F_{9/2}$	6875	6846	14545	14607	4.47	2.49	4.0	2.2	135	150	0.033	0.017	0.07	0.04
$^4F_{7/2}, {}^4S_{3/2}$	7517	7518	13303	13301	77.2	61.0	57	45	165	155	0.47	0.39	0.66	0.59
$^4F_{5/2}, {}^2H_{9/2}$	8087	8114	12366	12324	111.3	51.0	71	32	93	135	1.20	0.38	0.94	0.58
$^4F_{3/2}$	8807	8859	11355	11288	45.1	11.6	24	6.2	27	85	1.67	0.14	0.98	0.28

[1] See text and Table III-6 for details. Double dash entry indicates that features were too weak to be measured.
[2] See Eq. (8) in text and Table III-6. $\bar{\nu} = 1/\bar{\lambda}$
[3] Accuracy of area measurements $\approx \pm 0.1$ D×Å plus ±1%. D is optical density unit.
[4] Values calculated on the basis of 2 at.% in the melt as grown by Union Carbide (see Chapter II, Section E).

"rectangular" approximation is really within the bounds of the approximation that H_λ in Eq. (1) is constant for each band, - also a "rectangular" approximation. The choice of an effective bandwidth $\Delta\lambda$ is clearly important in this approximation. Generally, the values of $\Delta\lambda$, given in Table III-7 were arrived at by summing the widths of the dominant features and lines in each band where the widths were measured at about the half-maximum values. Thus, most values of $\Delta\lambda$ in Table III-7 are not actual widths but are the widths of the "compressed" bands, that is, mimimum widths that would occur if the dominant lines and features were placed as close as possible to each other within each band. The values obtained for $\bar{D}$ and $\bar{\alpha}_D$ from Eqs. (12) and (13) are given in Table III-7. We note that $\bar{\alpha}_D$ for the strong bands at 8807, 8087 and 5940Å in π polarization are nearly unity for this sample.

This approach to $\bar{\alpha}$ provides a means for characterizing the dependence of $\bar{\tau}_D$ on n_o and d for each band. Using Eqs. (10) and (13), $\bar{D}$ is given by

$$\bar{D} = \frac{f\bar{\lambda}^2}{\ell_D \Delta\lambda} \tag{14}$$

Since ℓ_D is inversely proportional to the product $n_o d$, Eq. (14) can be rewritten

$$\bar{D}_r = \frac{f\bar{\lambda}^2}{\ell_D \Delta\lambda}\, r = \bar{D}r, \tag{15}$$

where r is the ratio of any particular value of $n_o d$ or xd to the value for which ℓ_D is calculated. For each band, f, $\bar{\lambda}$, and $\Delta\lambda$ are constant; thus, we can plot for each band $\log \bar{\tau}_D$ versus r from the expression

$$\log \bar{\tau}_D = -\bar{D}r, \tag{16}$$

obtained from Eqs. (12) and (15). These plots for the strong bands are presented in Fig. III-12 and were obtained using the values of $\overline{D}$ given in Table III-7. Clearly, the $\overline{\tau}_D$ values obtained from Fig. III-12 should be compared to the values of $\overline{\tau}$ obtained from direct integration of transmissivity traces as described by Eqs. (4), (6) and (7) to strengthen our confidence in this approach. Nevertheless, we anticipate that the plots in Fig. III-12 provide a reasonable picture of the relative behavior of the various absorption bands for wider ranges of values of Nd^{3+} concentration and depth of penetration of incident radiation than can be easily obtained by any other approach. In order to show the validity of Eq. (15), transmissivity data [18] was obtained for a number of Nd:YVO_4 crystals as a function of Nd ion concentration and thickness.

The values of r for the three Nd:YVO_4 crystals from which transmissivity data have been obtained are as follows:

Table III- 8

	1%	2%	3%
	L = 0.116 cm	L = 0.103 cm	L = 0.072 cm
r =	0.563	1	1.05

Since the absorbance can be found directly from the measured values of the transmissivity, one can calculate it and compare it with the value obtained by the product of r and the absorbance obtained for the 2% thin crystal using transmissivity data. The following examples using the 752 nm/π band illustrate the procedure.

$$\overline{D}_{1\%} = -\log \overline{\tau}$$
$$\overline{D}_{1\%} = 0.0651 \quad \Big| \quad \overline{D}_{3\%} = 0.119$$
$$\overline{D}_{1\%} = \overline{D}_{2\%} r$$
$$\overline{D}_{1\%} = 0.0698 \quad \Big| \quad \overline{D}_{3\%} = 0.130$$

The two values agree within the limits of the accuracy of the transmissivity measurements. The values of the following bands, 881, 809, 594, 477 and 438 nm/π, were calculated [18] in the same fashion and good agreement was obtained for both the 1% and 3% absorbances.

3. Determination of pump power absorbed in Nd:YVO_4 laser rods

In order to apply Fig. III-12 to the design of a CW laser, we note that the choice of resonant cavity fixes the diameter of the lasing volume d_ℓ and that the minimum diameter of the laser rod is determined by rod-fabrication limitations. Generally, it is more efficient for the pump light to be mostly absorbed on the first pass through the laser rod since much of the transmitted light will be lost due to multiple reflections off of the cavity walls and the rod surface. Thus, making the laser rod diameter d_r small requires a large ion concentration x; however, because of ion-lattice interactions and other processes, it is common that the fluorescence lifetime τ_f of the laser transition decreases for $x \geq 1\%$. (In fact, this shortening of τ_f at 1.06 μm was observed in Nd:YVO_4. See Section C of this chapter.) A decrease in τ_f increases the threshold power requirement of the laser thereby placing a limit on the size of x. Also, the optical quality of a laser rod generally begins to deteriorate when $x > 1\%$. Therefore, we will specify a design value for the product xd for a given lamp and a given average transmissivity $\bar{\tau}_D$, which, from the above considerations, will permit us to obtain values for d_r and x.

A reasonable target value for $\bar{\tau}_D$ is 20% ($\bar{\alpha}_D$ = 80%) for a single pass through the rod diameter. From Eq. (16), as seen in Fig. III-12, intercepts between the plots and the 20% line for bands (a) through (d) with the exception of $(a)_\sigma$ give values for r between 0.42 and 1.84. A design value for r can be obtained from an average over these values weighted by the strengths and wavelengths of the bands, f and $\bar{\lambda}$, respectively, given in Table III-7 and by the approximate radiance N (or irradiance H) of the lamp in these bands. The inclusion of $\bar{\lambda}$ comes from the fact that the pump power at threshold (for a given population inversion) is inversely proportional to the pump light wavelength. In addition, we must account for the polarization dependence of the bands. To do this, we assume the laser rod is cylindrical in shape and is irradiated uniformly around the cylindrical axis with unpolarized light of radiant intensity $\mathcal{I}$. In other words, the light is focused

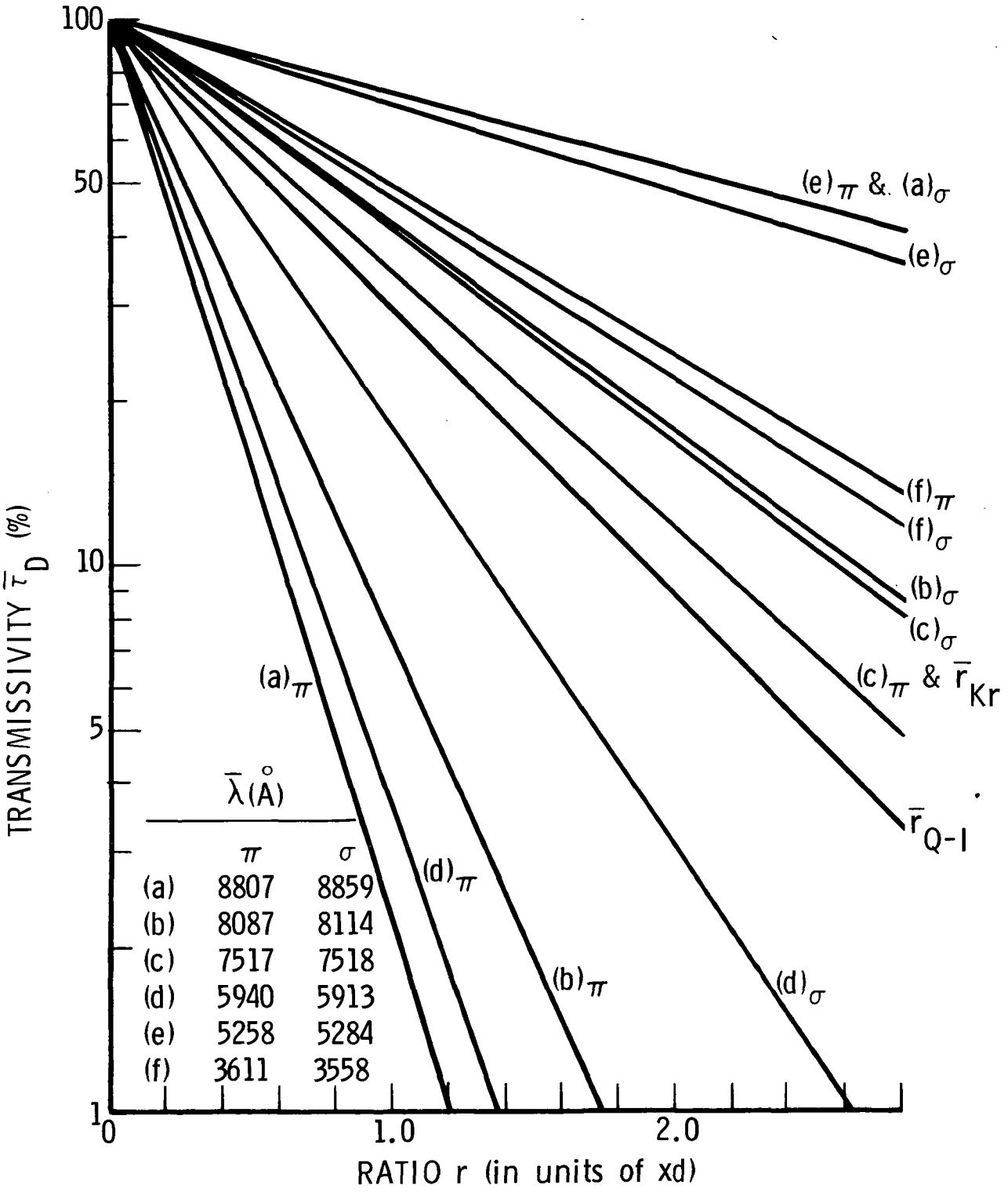

Figure III-12 The average transmissivity for π and σ polarizations of the strong absorption bands centered at $\bar{\lambda}$ of $Y_{1-x}Nd_xVO_4$ obtained using the "rectangular" approximation on the bands as a function of x and the depth of penetration of the incident radiation d. At r = 1.0, x = 2% and d = 0.103 cm. The lines labeled $\bar{r}_{Kr}$ and $\bar{r}_{Q-I}$ are the average values obtained for r using Eq. (17) for a krypton lamp and a quartz-iodine tungsten-filament lamp, respectively. See Tables III-7 and III-9 and text.

on the rod axis as would occur in a long elliptical-cylindrical pumping cavity with an ideal line source. The 1.06 μm laser transition occurs in π polarization; therefore, the c-axis is perpendicular to the cylindrical axis of the rod. The radiant power of the light polarized parallel to the rod axis integrated around the rod is $P_{\parallel}^{\sigma} \approx 2\pi k \ell$, and induces σ transitions. The light polarized perpendicular to the rod axis induces both π and σ transitions. Integrating this light around the rod gives $P_{\perp}^{\sigma} = P_{\perp}^{\pi} \approx \pi k \ell$, where k is constant. Thus, the σ bands must be weighted by a factor of about 3 over the π bands for this configuration. A design or average value of r can be found from

$$\bar{r} = \frac{\sum_i r_i w_i}{\sum_i w_i} \tag{17}$$

where $w_i = p_i f_i \bar{\lambda}_i N_i$ (or $w_i = p_i f_i \bar{\lambda}_i H_i$) with $p_i = 1$ or 3 for the π or σ bands, respectively, and the summation is taken over the π and σ bands of interest.

Among the lamps commonly used for CW pumping of neodymium solid-state lasers are the krypton plasma lamp and the quartz-iodine tungsten-filament lamp. Values of the radiance N_i for a continuous krypton lamp were obtained by integrating the spectral radiance trace[19] over the bands of interest (i.e., over Δλ in Table III-7). The areas of the line spectra of the lamp were weighted by the ratio of the actual approximate optical density of the absorption band at the wavelength of the line to the average optical density $\bar{D}$ of the band given in Table III-7. A small allowance for the spectral width of the instrument was included. The results of these approximate measurements of N_i, the values of r_i from Fig. III-12, and the weighting factors w_i for the krypton lamp are presented in Table III-9. Clearly, the σ bands dominate the contributions to the summations in Eq. (17). We obtain from Table III-9 and Eq. (17) $\bar{r} \doteq 1.48$ for this case.

Since xd = 2% × 0.103 cm at r = 1, then $\overline{xd}$ = 0.31% cm. Thus, for a rod having d_r = 3 mm, a concentration of about 1% is obtained. We note from Fig. III-12 at $r \approx 0.5\bar{r}$ which, for a given concentration, corresponds to the center line of the rod, three of the five "strongest" bands (i.e., the bands having the largest w's), have values of $\bar{\tau}_D$ close to 50%. This is a reasonable situation.

The calculation of w_i in Eq. (17) for the quartz-iodine lamp is somewhat simpler since the lamp spectrum is smooth. Using tabulated values for spectral irradiance H_λ of a 1000-watt lamp operated at a correlated color temperature of 3063°K,[19] values of H_i were obtained by calculating $\Delta\lambda H_\lambda$ at $\bar{\lambda}$ for each of the bands of interest. These values plus the corresponding weighting factors for this case are also given in Table III-9. Again, applying Eq. (17) we obtain $\bar{r}$ = 1.32 which gives $\bar{x}d$ = 0.27% cm. For a rod with d_r = 3 mm, a concentration of 0.9% is recommended by this approach. This is 10% lower than that recommended above for krypton lamp pumping. The reason for this shift is quite evident from Table III-9. Recognizing that the weighting factors, w, in Table III-9 indicate, for the given lamp, the relative contributions of the bands to the pumping of the Nd^{3+} ion, then it is clear that the krypton lamp pumping bands (b) and (c) at ~8100 and ~7500 Å, respectively, dominate the contributions thereby causing $\bar{r}$ to favor the higher values of r associated with these bands. With quartz-iodine lamp pumping, on the other hand, band (d) at ~5900 Å is dominant with significant contributions from bands (b) and (c); thus, the value of $\bar{r}$ is shifted down towards the small values of r obtained for band (d).

Within this admittedly oversimplified view of this problem, the values of $\bar{r}$ obtained above for the two lamps are "universal" values in that they define a plot of $\bar{\tau}_D$ versus r for each lamp from which any value of τ_D can be used to find the corresponding values of r and xd. These plots are

Table III-9. Ratio Parameter r (at $\bar{\tau}_D$ = 20%) Versus Radiances N (or Irradiances H) and the Corresponding Weighting Factors w, of Two Different Lamps for the Absorption Bands of Nd:YVO_4 in π and σ Polarizations

Band[1]	r[1]	Krypton Lamp		Quartz-Iodine Lamp	
		N[2] $\left(\frac{mW}{mm^2 \cdot sr}\right)$	w[3] $\left(\frac{\mu m \cdot \mu W}{mm^2 \cdot sr}\right)$	H[4] $\left(\frac{\mu W}{cm^2}\right)$	w[3] $\left(\frac{\mu m \cdot nW}{cm^2}\right)$
$(a)_\pi$	0.42	0.4	0.008	68	1.4
$(a)_\sigma$	5.00	0.6	0.01	216	3.6
$(b)_\pi$	0.58	52	3.0	229	13.1
$(b)_\sigma$	1.84	79	6.1	333	25.9
$(c)_\pi$	1.49	51	2.2	382	16.4
$(c)_\sigma$	1.79	34	3.4	359	36.4
$(d)_\pi$	0.48	2.9	0.5	227	37.4
$(d)_\sigma$	0.92	5.1	1.8	308	108.7
$(e)_\pi$	5.00	2.8	0.07	207	5.2
$(e)_\sigma$	4.37	2.5	0.2	86	6.1

[1] See Fig. III-12 and text. The values for $\bar{D}$ in Eq. (16) are given in Table III-7.

[2] See Ref. 19 and text. Lamp was operated at 35 A and 65 V. It had a 5 cm arc length, 5.5 mm bore diameter, and 2 atm. gas pressure.

[3] $w = pf\bar{\lambda}N$ or $pf\bar{\lambda}H$ where f and $\bar{\lambda}$ are given in Table III-8. See text concerning the polarization weighting factors p.

[4] See Ref. 19 and text. Lamp was a GE type DXW rated at 1000 W. It was operated at 8.00 A and H_λ was measured at 50 cm. The correlated color temperature was 3063°K.

also shown in Fig. III-12. For example, with the krypton lamp and $\bar{\tau}_D = 10\%$, $r = 2.11$ corresponding to $xd = 0.44\%$ cm. In general, once determinations of d_ℓ and minimum laser-rod diameter that can be conveniently (or dependably) fabricated have been made, a trial value for d_r can be specified. The Nd ion concentration is then obtained from $x = xd/d_r$. If τ_f is significantly reduced at this value of x, then the largest permissible value of x is used to calculate d_r.

References: Chapter III

1. Kh. S. Bagdasarov, G.A. Bogomolova, A.A. Kaminskii and V.I. Popov, Dokl, Akad. Nauk SSSR 180, 1347 (1968) [Soc. Phys. Dokl. 13, 516 (1968)].

2. R.J. Pressley, P.V. Goedertier, and H. Weakliem, "MBT-70 Laser Materials Research and Exploratory Development," RCA Lab., Princeton, New Jersey, Report (October 1969).

3. M. Bass, L.G. DeShazer and U. Ranon, Technical Report ECOM-74-0104-1 (October 1974), U.S. Army Electronics Command, Fort Monmouth, New Jersey.

4. N. Karayianis, C. A. Morrison and D.E. Wortman, J. Chem. Phys. 62, 4125 (1975).

5. For example, see
M. Hamermesh, Group Theory, (Addison Wesley, Reading, Mass., 1962), and
C. Herzfeld and P. Meijer,"Group Theory and Crystal Field Theory" in Solid State Physics, Vol. 12, Eds. F. Seitz and D. Turnbull, (Academic Press, New York, 1961).

6. B.R. Judd, Phys. Rev. 127, 750 (1962); G.S. Ofelt, J. Chem. Phys. 37, 511 (1962).

7. J.R. O'Connor, Appl. Phys. Lett. 9, 407 (1966).

8. J.P. Anthes, "Search for Non-Exponential Fluorescence Decay of Neodymium Ions in Laser Glass," dissertation, University of Southern California (1974); (University Microfilm, Inc., Ann Arbor, Michigan).

9. M. Garbuny, Optical Physics, (Academic Press, New York, 1965) pp. 110-113.

10. T. Kushida, H.M. Marcos and J.E. Geusic, Phys. Rev. 167, 289 (1968).

11. M. Birnbaum and J.A. Gelbwachs, J. Appl. Phys. 43, 2335 (1972).

12. A.W. Tucker, The Aerospace Corporation, private communication.

13. P.W. Kruse, L.D. McLaughlin and R.B. McQuistan, Elements of Infrared Technology, (J. Wiley & Sons, New York, 1962) p. 139.

IV. LASER PERFORMANCE OF Nd:YVO_4 AT 1060 nm*

A. Introduction

Lasers of high efficiency and low thresholds are required in diverse applications, such as communications, ranging, and meteorology. The Nd:YAG laser has represented the state-of-the-art in most applications requiring low threshold and efficient lasers. O'Connor [1] had observed almost 10 years ago that Nd:YVO_4 possessed a larger stimulated emission cross section at 1.06 μ than Nd:YAG and obtained low-threshold laser operation at 90°K. Recently, detailed spectroscopic measurements quantified O'Connor's observations by showing that the stimulated emission cross section of a-axis Nd:YVO_4 at 1.0634μ was 4.6 times greater than that of Nd:YAG at 1.0642μ. [2]

The superiority of Nd:YVO_4 lasers at 1.06μ over Nd:YAG is demonstrated here by a comparison of the laser characteristics of small spectroscopic samples of Nd:YVO_4 with a high optical quality Nd:YAG laser rod. The comparisons were affected by end-pumping with cw and pulsed argon ion lasers at 514.5 nm, with emphasis on cw performance. Development of Nd:YVO_4 lasers is hindered by the lack of large (3 ×30 mm) laser grade crystals. However, difficulties in vanadate crystal growth have been identified and large laser-grade crystals may soon be available.[3]

Assessment of the performance characteristics of Nd:YVO_4 lasers requires knowledge of the gain and loss coefficients of this material, and the doping level which optimizes laser performance. The determination of the parameters required for analysis of laser performance is described below.

B. Determination of Laser Parameters

The equations describing the laser performance can be derived from consideration of the laser threshold condition:

$$R_1' \; R_2' \; \exp \; 2L \, (n_u \, \sigma - \Delta) \; = \; 1 \qquad (1)$$

*A. W. Tucker and M. Birnbaum at Electronics Research Laboratory, The Aerospace Corporation

where the symbols stand for the following: R_1' and R_2' are the corrected mirror reflectivities, (see explanation which follows); L, the length of the laser sample; n_u, the density of Nd^{3+} ions in the upper state of the laser transition; σ, the peak stimulated emission cross section; Δ, the total losses per cm (exclusive of transmission losses by the mirrors) which include, for example, diffraction losses, excited state absorption, and scattering losses. The rod ends were plane parallel and carefully aligned with the plane, dielectric coated, end mirrors. In laser operation, the Fabry-Perot condition for maximum reflectivity $R' = [r^{1/2} + R^{1/2}]^2 / [1 + (rR)^{1/2}]^2$ should be a good approximation with r, the Fresnel reflectivity of the crystal and R, the mirror reflectivity.[4]

In cw operation, the upper level population is related to the pump power according to equation (4)*:

$$n_u = \frac{\eta f_B P_a \tau}{h\nu_p V} \qquad (4)^*$$

where n_u is the population per cm^3 of the upper laser level, η, the quantum efficiency, namely, the fractional number of Nd^{3+} in the $^4F_{3/2}$ level per absorbed photon; f_B, the fractional population in the upper laser sublevel of the $^4F_{3/2}$ state; P_a, the pump power absorbed by the laser crystal; τ, the fluorescence lifetime of the $^4F_{3/2}$ level; $h\nu_p$, the energy per pump photon and V, the volume pumped. Substitution of (4)* into (1) yields:

$$2L\sigma \frac{\eta f_B P_T \tau}{h\nu_p V} = 2L\Delta - \ell n\, R_1' R_2' \qquad (6)^*$$

where $P_T = P_a$ at threshold.

The advantages of our method, namely, the accessibility of the quantities in equation (6)* to direct measurement have been described earlier.[5]

---

* Repeated Equation (2) and (3) from Page IV-14 and IV-15. Equation numbers correspond to page IV-14 and IV-15.

A number of auxilliary measurements are required to estimate P_a. This is illustrated in Fig. IV-1.

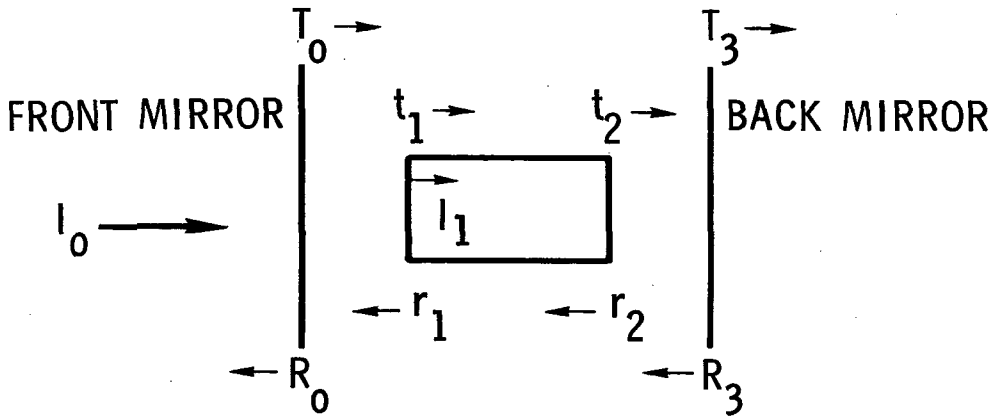

The fraction of the incident power, I_o, absorbed by the crystal is $A = 1\text{-}e^{-\alpha L}$ where α is the absorption coefficient and L the pathlength through the crystal. A correction must be applied to account for the reflection of the incident beam from the various surfaces, and must be considered in estimating P_a. Methods of measurement of reflectivities and other parameters are described in the following sections.

1. Measurement of P_a Absorbed Pump Power

The reflection and absorption coefficients of the samples were determined at the pump wavelength of 514.5 nm. The YVO_4 crystals are birefringent and consequently, the optical coefficients depend upon the orientation of the plane of polarization, for example, whether the pump beam polarization is along the a-axis or c-axis of the crystal. Maximum absorption of the 514.5 nm pump beam occurs when the polarization is parallel to the c-axis for an a-axis rod. All measurements in Section IV-C refer to the arrangement with the pump light polarization parallel to the YVO_4 crystal c-axis rods.

A diagram of the experimental arrangement for measurement of absorbed pump power is shown in Fig. IV-2. A polarized cw argon ion laser at 514.5 nm

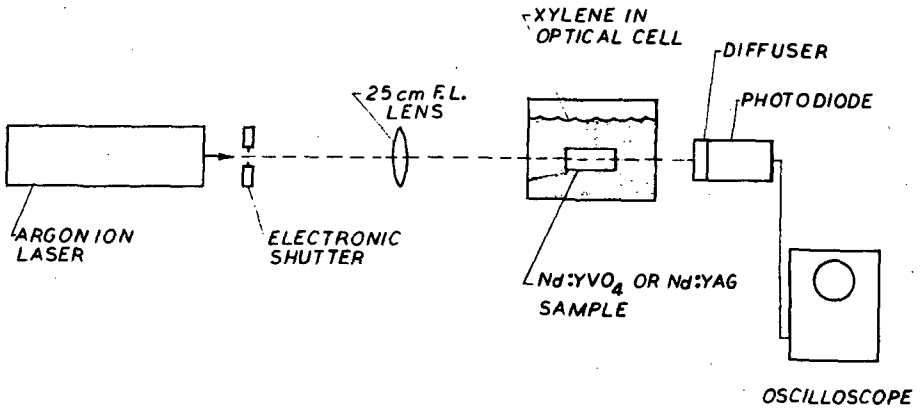

Fig. IV-2 Absorption of Nd:YVO_4 and Nd:YAG Samples at 514.5 nm.

was adjusted for operation at 100 mW. The beam was chopped with an electronic shutter at a 10 pulse per second repetition rate which provides 2 ms pulses for a 2% duty cycle, thereby reducing the heat load. The beam (polarized parallel to c-axis) was focused into the sample with a 25 cm focal length lens. To reduce effects of surface reflections, the crystal was immersed in xylene (index of refraction, 1.505). Although the index match was not exact, the surface reflections were less than 2%, which results in a small correction to the directly measured values. The ratio of the power detected with the sample in xylene and with the sample removed, provided the fraction of pump light absorbed by the sample. Measurements for pump polarizations parallel to the c-axis and the a-axis were obtained; the values are listed in Table IV-1. Values in Table IV-1 were not corrected for the

small index mismatch. Since the measurements were performed with an 514.5 nm argon ion laser, we would also need to account for the possibility that the crystal acts as an etalon. How closely the resonance condition is fulfilled is generally unknown. However, these measurements can be used until greater accuracy is required. The c-axis of the crystals was determined by first obtaining laser action and then measuring the polarization direction of the 1060 nm output beam which is parallel to the c-axis. For each sample, absorption measurements were obtained by directing the beam at 3 different positions on the sample. Ten measurements were obtained at each position. The standard deviation of an entry of Table IV-1 is estimated to be $\pm$ 0.25%.

TABLE IV-1

SUMMARY OF ABSORPTION MEASUREMENTS

SAMPLE[a]	Orientation of C-Axis with respect to Polarization of 5145 Å Pump	Absorption, A (%)	Sample Length (cm)	Absorption Coefficient α (cm^{-1})
1% YVO_4	E // C	44.4	.483	1.215
	E ⊥ C	42.1		1.131
2% YVO_4	E // C	76.3	.749	1.922
	E ⊥ C	74.4		1.819
3% YVO_4	E // C	89.8	.795	2.871
	E ⊥ C	88.9		2.765
1% YAG # 1	N/A	54.4	1.275	.616
1% YAG # 2	N/A	42.8	0.955	.585

[a] The 1% YVO_4, 2% YVO_4 and 1% YAG #1 were AR coated at 1060 nm; the 3% YVO_4 and 1% YAG #2 were not.

In the first progress report under this contract, we showed that in the case of the 1% Nd:YVO_4 crystal, losses at 1060 nm were approximately 16% per cm. These losses were ascribed mainly to scattering from inclusions of 1 - 3 microns which cause mainly small angle scattering. In our geometry (Fig. IV-2) this scattered light would be seen by our photodetector. Consequently, small angle scattering does not affect our measurement of the transmitted light and, consequently, does not result in a fictitious absorption.

For the Laser Performance tests in Section IV-C, a Lexel 504 power meter was used to measure the pump power absorbed at 514.5 nm by measuring the input, output, and reflected pump power from the Nd:YVO_4 laser. In addition, an ITT F4018 bi-planar photodiode with an S-1 photo-sensitive surface was used to monitor the 514.5 nm input power. A 5% difference was noted using the two techniques. An EMI 9684QB photomultiplier with an S-1 photo-sensitive surface was used to monitor the output power at 1060 nm. These three detectors were calibrated at 514.5 nm and 1060 nm, respectively, with a TRG ballistic thermopile. The nominal accuracy of these calibrations was approximately $\pm 2\%$, $\pm 2\%$ and $\pm 10\%$ for the Lexel 504, ITT F4018, and the EMI 9684QB, respectively. The Lexel 504 and ITT F4018 were calibrated using a commercial argon ion laser while the EMI 9684QB photomultiplier was calibrated at 1064 nm with a "noisy" commercial Nd:YAG laser.

2. Reflectivity of Crystal Surfaces at 514.5 nm

In determination of the laser parameters, values of the reflectivity of the crystals at both the pump and the laser wavelengths are required. A diagram of the experimental arrangement is shown in Fig. IV-3. Many features of the measurement procedure were similar to those employed in absorption measurements and refers in particular to the output power and duty cycle of the argon ion laser.

The pump laser was placed 1.7 m from the crystal and focused onto the crystal surface with a 1 m focal length lens placed 112 cm from the crystal surface. The crystals were oriented with the c-axis of the crystal parallel to the pump beam polarization and were tilted for a one-degree deflection of the reflected beam (plane of incidence normal to polarization direction of incident beam). Reflections from the rear surface were suppressed by immersion in xylene as shown in Fig. IV-3.

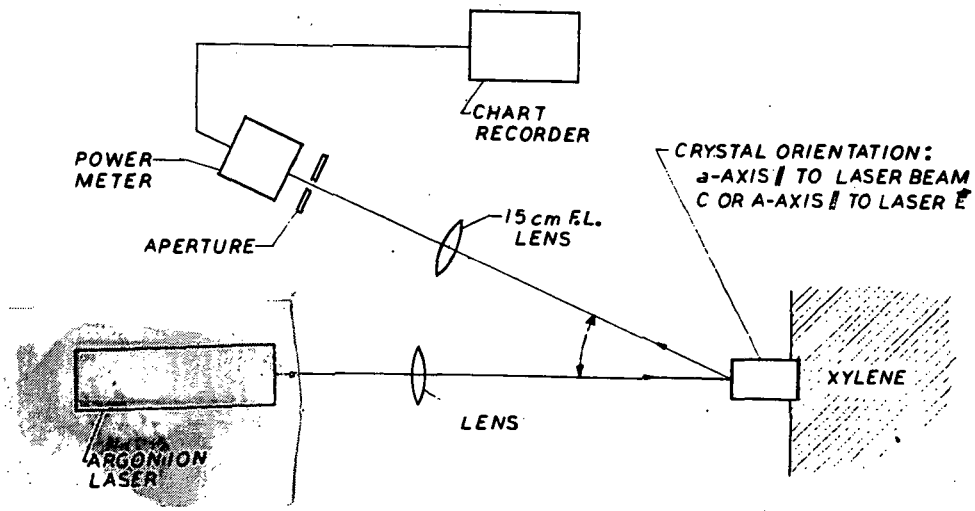

Fig. IV-3 Single Surface Reflection of Nd:YVO_4 and Nd:YAG Samples at 514.5 nm.

Normal incidence reflectivity (approximately) was obtained by measurement of reflected light in the arrangement of Fig. IV-3. Following this, the crystal was removed and the light reflected from a reference mirror (100% reflectivity) in the same position was measured. The ratio of these values yielded the surface reflectivity of the crystal. For completeness, reflectivities for polarization parallel to the a-axis were also measured. For each sample, the reflectance at 3 different positions on the sample was obtained. The values were based upon 10 measurements at each position. The estimated standard deviation was $\pm$ 0.4%. These results are summarized in Table IV-2.

TABLE IV-2

SUMMARY OF MEASUREMENTS OF REFLECTION COEFFICIENTS AT 514.5 nm

SAMPLE[a]	Orientation of C-Axis With Respect to Polarization of 5145 Å Pump	Measured Reflectance, r_c (%)	Calculated Reflectance from Refractive Index (%)
1% YVO_4	E // C	15.6%	
	E // A	13.8%	
2% YVO_4	E // C	15.3%	
	E // A	12.7%	
3% YVO_4	E // C	14.6%	14.9%
	E // A	12.3%	11.4%
1% YAG #1	N/A	9.1%	
1% YAG #2	N/A	8.0%	8.6%

[a] The 1% YVO_4, 2% YVO_4 and 1% YAG #1 were AR coated at 1060 nm; the 3% YVO_4 and 1% YAG #2 were not.

3. Reflectivity of Crystals at 1060 nm

In order to evaluate laser performance, knowledge of crystal reflectivity at the laser wavelength is required. It is generally simpler, however, to eliminate these reflections by AR (anti-reflection) coatings. Such coatings were applied to the 1% and 2% of Nd:YVO_4 samples at USC. The AR coatings were nominally <1% at 1060 nm when first applied. The effectiveness of the coatings diminished with use and the passage of time.

The experimental arrangement is shown in Fig. IV-4 and is similar to that of Fig. IV-3 except that a cw polarized Nd:YAG laser (25 mW at 1064 nm) was used as a source with the output beam polarized parallel to the c-axis of the crystals. The laser samples were fabricated with plane parallel ends and consequently could function as etalons. The reflections from the rear surface of the non-AR coated samples can be suppressed by immersing the rear surface in an index-matching liquid such as xylene. However, xylene is inadequate in that there is still a weak reflection from the rear surface resulting from the incomplete index match. A correction can be made to take this into account. The samples with AR coated surfaces were measured both with back surfaces immersed in xylene and with back surfaces in contact with air.

Two techniques were used to measure the surface reflectance of the crystals. In the first method, the reflection of the crystals (both AR and non-AR coated samples) with the back surface immersed in xylene was measured and compared with the reflectance of a nominally total reflector at the same position. A correction was applied to the measurement to account for the index mismatch. In the second technique, the back surface (both AR and non-AR coated samples) was not immersed in xylene and a correction was applied to the non-AR coated samples only. The reflected power was monitored using a chart recorder and averaged over a 5-minute period to an accuracy of about $\pm 2\%$. Agreement was obtained within experimental error.

The results of these measurements are summarized in Table IV-3. The crystal AR coatings appear quite effective in suppressing surface reflections at 1060 nm (except for the 2% YVO_4 crystal). Nevertheless, the laser crystals, fabricated with plane parallel faces, functions as an etalon and can exhibit a substantial effect depending upon how closely a resonance is approached.

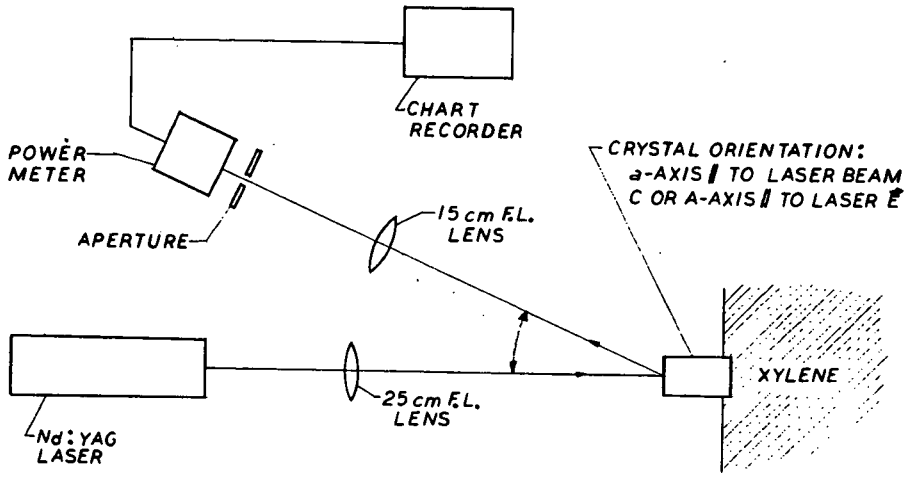

Fig. IV-4 Surface Reflectivity of Nd:YVO_4 and Nd:YAG Samples at 1.064 μm.

TABLE IV-3

SUMMARY OF SURFACE REFLECTIVITY OF CRYSTALS AT 1060 nm

SAMPLE[a]	Measured Reflectance, r_c (%)	Index of Refraction at 1.06μ of Pure Material
1% YVO_4	0.6	E // C 2.168
2% YVO_4	1.6	E // A 1.958
3% YVO_4	13.1	
1% YAG #1	0.06	
1% YAG #2	8.9	1.8186

[a] The 1% YVO_4, 2% YVO_4 and 1% YAG #1 were AR coated at 1060 nm; the 3% YVO_4 and 1% YAG #2 were not.

4. Optical Isolator

Although the technique of laser pumping has proved most effective in determining the laser parameters of new materials, a difficulty was encountered in application of the method. Optimum adjustment of the crystal laser under test proved troublesome because of optical coupling (feedback) between the pump laser (Argon ion) and the test laser (Nd:YVO_4). This problem could be circumvented by use of an optical isolator which functions in a manner analogous to the familiar microwave isolator. However, optical isolators are not generally commercially available.

An isolator, using Faraday rotation, was constructed and tested (Fig. IV-5).[6] The rotator consists of two slabs (single crystals of ZnSe) each 2.16 mm thick (AR coated for 514.5 nm) and mounted between the drilled pole pieces of a permanent magnet. Special pole pieces with a 0.7 cm gap, (shown in Fig. IV-5) produce the required 7 K gauss for a 42.3° rotation of the polarization plane of the 514.5 nm light in a single passage through the crystals. A Glan-Thomson prism (on the input side) passes the pump light from the laser but blocks the reflected signal which has been rotated 90° by two passes through the rotator. A drawback of the rotator in its present form is that about 50% of the pump light is absorbed by the ZnSe crystals. A description of the optical isolator is presented in Appendix I.

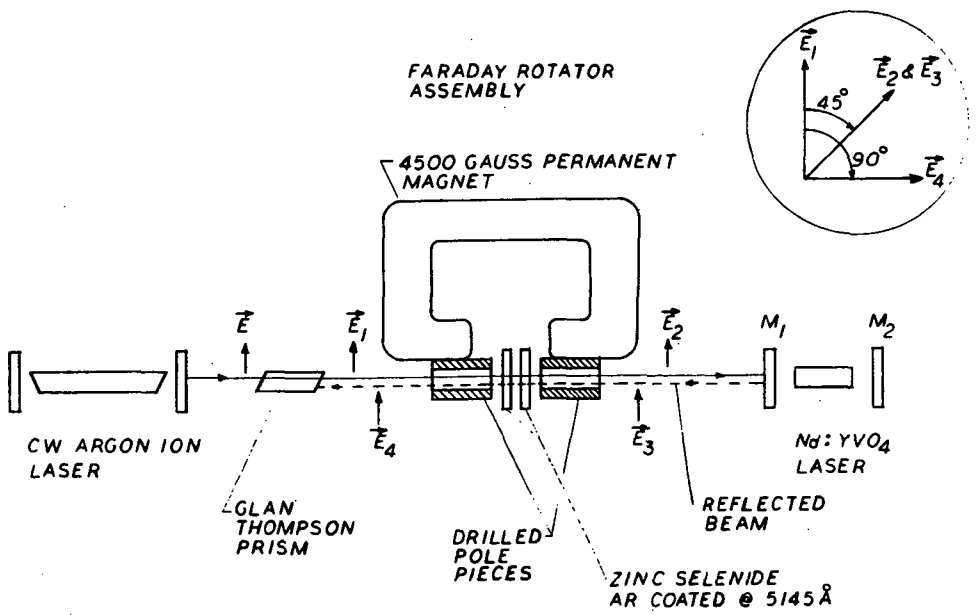

Fig. IV-5 Optical Isolator Using a ZnSe Faraday Rotator

C. Comparative Laser Performance of Nd:YVO_4 and Nd:YAG

1. Introduction

We have already demonstrated that cw laser operation can be obtained with small samples of Nd:YVO_4 and Nd:YAG. An advantage of the Nd:YVO_4 crystal (compared to Nd:YAG) is that the output, for an a-axis cylinder, is 100% plane polarized. Most communication systems use polarization modulators which require a polarized laser output.

The superiority of Nd:YVO_4 lasers at 1060 nm over Nd:YAG is demonstrated here by a comparison of the laser characteristics of small spectroscopic samples of Nd:YVO_4 with a high optical quality Nd:YAG laser rod. Development of Nd:YVO_4 lasers is hindered by the lack of large (3 x 30 mm) laser grade crystals. The comparisons were effected by end pumping with a cw argon ion laser operating at 514.5 nm. A major advantage of the laser pumping technique is that only small samples are required. This permits demonstration of feasibility and measurement of the required laser parameters without requiring an expensive and time-consuming crystal growth program. On hand samples of Nd:YVO_4 were utilized in the performance of this work.

A knowledge of the stimulated-emission cross section is essential in evaluating laser-system parameters such as maximum gain, optimum mirror reflectivity and maximum output power. The use of the laser end-pumping technique not only simplifies the measurement but affords a unique method for comparing directly the stimulated-emission cross section of Nd^{3+} at 1060 nm in a variety of different hosts.

Stimulated-emission cross sections were obtained from measurements of the laser threshold power as a function of mirror reflectivity. The equation describing the laser performance can be derived from consideration of the laser threshold condition, which states that for a fluorescence material to exhibit laser operation, the round-trip optical gain resulting from pumping, including feedback, must exceed the

---

*A. W. Tucker, J. W. Erler and M. Birnbaum at Electronics Research Laboratory, The Aerospace Corporation

round-trip losses within the cavity;

$$R_1' R_2' \exp 2L(g-\Delta) = 1 \tag{1}$$

where R_1' and R_2' represent the effective mirror reflectivities, L is the length of the laser crystal, g is the single-pass gain coefficient at threshold, Δ is the total internal losses per cm (exclusive of transmission losses by the mirrors) which include, for example, diffraction losses, excited state absorption, and scattering losses. The rod ends were plane parallel and carefully aligned with the plane, dielectric coated, end mirrors. Corrections were applied to account for end reflections of the rods in cases where the samples were not anti-reflection coated. In laser operation, the Fabry-Perot condition for maximum reflectivity should be a good approximation,

$$R' = \frac{\left[r^{1/2} + R^{1/2}\right]^2}{\left[1 + (rR)^{1/2}\right]^2} \tag{2}$$

where r is the Fresnel end reflectivity of the crystal and R, the mirror reflectivity.

For a four-level material when the population in the terminal level is negligible, the small signal gain coefficient, g_o is related to the population density of the upper laser level, n_u, by,

$$g_o = \sigma n_u \tag{3}$$

where σ is the peak stimulated emission cross section of the laser transition.

In cw operation, the upper level population density is related to the pump power absorbed according to equation (4):

$$n_u = \frac{\eta f_B \tau P_a}{h\nu_p V} \tag{4}$$

where η is the quantum efficiency, namely, the fractional number of Nd^{3+} ions in the $^4F_{3/2}$ state per absorbed photon,* $h\nu_p$ is the energy per pump photon, τ is the spontaneous radiative lifetime for transition between upper and lower laser levels, P_a is the pump power absorbed by the laser crystal,

*This quantity is close to 1 for most Nd doped laser crystals,[16] the ratio η_{YAG} to η_{YVO_4} should be unity to a close approximation.

V is the volume pumped, and f_B is the fractional number of Nd^{3+} ions in the noted laser sublevel of the $^4F_{3/2}$ state. For Nd:YAG, the laser transition originates from the upper sublevel of the $^4F_{3/2}$ state so that f_B for YAG is,

$$f_B = \frac{1}{1 + e^{hc(\Delta\nu)/KT}}$$

where h is Planck's constant, c is the velocity of light, K is Boltzman's constant, T is the Kelvin Temperature and $(\Delta\nu)$ is the level splitting in wavenumbers between the upper and lower sublevels of the $^4F_{3/2}$ state. For YAG, $(\Delta\nu) = 88\ cm^{-1}$. For Nd:$YVO_4$, the laser transition originates from the lower sublevel of the $^4F_{3/2}$ state so that f_B for YVO_4 is,

$$f_B = \frac{1}{1 + e^{-hc\Delta\bar{\nu}/KT}}$$

where $(\Delta\nu) = 14.2\ cm^{-1}$.

Combining equation (3) and (4) one obtains for the small signal gain coefficient,

$$g_o = \frac{\sigma \eta f_B \tau P_a}{h\nu_p V} \tag{5}$$

For operation at threshold, $g = g_o$. Upon substitution of equation (5) into equation (1) it follows that,

$$-\text{Ln}\, R_1' R_2' = \left(\frac{2L\sigma\eta f_B \tau}{h\nu_p V}\right) P_T - 2L\Delta \tag{6}$$

where $P_T = P_a$ at threshold.

One of the more difficult quantities to measure in a four-level laser system, such as Nd:YVO_4, is the loss factor, Δ. The main feature of our method is the directness with which the laser threshold power, P_T, can be determined. By plotting the laser threshold power as a function of $-\text{Ln}\, R_1' R_2'$, according to equation (6), the loss coefficient, Δ, is obtained from the ordinate intercept at $P_T = 0$.

The stimulated-emission cross section of the sample is determined from the slope, M, of the P_T vs. $-\mathrm{Ln}\, R_1' R_2'$ plot according to equations (7) and (8),

$$M = \frac{d\,(-\mathrm{Ln}\, R_1' R_2')}{dP_T} = \frac{\eta f_B \tau}{h\nu_P V}\, 2L\sigma \tag{7}$$

$$\sigma = M\, \frac{h\nu_P \pi d^2}{8\eta f_B \tau} \tag{8}$$

where $\frac{\pi d^2 L}{4}$ is the volume of the pumped filament.

From equation (8), an absolute determination of the cross-section requires a knowledge of the diameter of the pumped filament which is a difficult measurement to obtain with the required degree of accuracy.

Computation of the stimulated emission cross section of one sample in terms of a standard sample can be obtained more accurately since the diameter of the pumped filament is not required. All that matters is that it be the same for both samples.

The value of the stimulated emission cross section for Nd:YAG, σ_{YAG}, is well documented. The value we will accept here is that reported by Singh, Smith and Van Uitert[7] as $4.6 \times 10^{19}\,\mathrm{cm}^2$. The value of the stimulated emission cross section of Nd:YVO_4, σ_{YVO_4}, can then be determined in terms of σ_{YAG} from the ratio,*

$$\frac{\sigma_{YVO_4}}{\sigma_{YAG}} = \frac{M_{(YVO_4)}\,[\eta f_B \tau]_{(YAG)}}{M_{(YAG)}\,[\eta f_B \tau]_{(YVO_4)}} \tag{9}$$

The small signal gain coefficient, g_o, and the single pass rod gain, G_o, are valuable parameters in specifying the performance of the laser. Combining equations (7) and (4) and using the experimental value of σ_{YVO_4} determined from equation (9) we obtain the population density of each sample as a function of pump power absorbed.

*Fluorescence of Nd^{3+} in crystals has never been observed from higher lying states than the $^4F_{3/2}$. This provides very strong evidence that the pump quantum efficiency (η) is very close to unity for Nd:YAG, $NdYVO_4$ and other crystals that have been studied [ref. 7, p. 2567].

$$n_u = \frac{M P_a}{2 L \sigma_{YVO_4}} \tag{10}$$

Knowledge of atomic per cent of Nd^{+3} ions in the samples allows one to calculate the population density of Nd^{+3} ions in the ground state, n_o, from the expression;

$$n_o = \frac{Ad}{(M_{Nd} - M_Y)\frac{1}{R} M_{YVO_4}} \tag{11}$$

where A is Avogadro's number, 6.023×10^{23} molecules/mole; M_{Nd} is the atomic weight of neodymium, 144.27 gm/mole; M_Y is the atomic weight of Yttrium, 88.92 gm/mole; M_{YVO_4} is the molecular weight of YVO_4, 203.87 gm/mole; R is the atomic per cent of Nd^{+3} in the samples; and d is the density of the sample in gm/cm^3. The values of R and n_o for each sample are listed in Table IV-4.

Table IV-4

GROUND STATE POPULATION DENSITY, n_o

Crystal	Atomic Percent Nd^{+3}	n_o ($cm^{-3} \times 10^{19}$)
Nd:YVO_4-1	0.67	8.43
Nd:YVO_4-2	0.86	10.7
Nd:YVO_4-3	1.34	17.0
Nd:YAG-1	0.89	4.12

Using these values for n_o, and equation (10), the population inversion density as a function of pump power absorbed may be calculated from equation (12)

$$\left(\frac{n_u}{n_o}\right) = \frac{M P_a}{2 L \sigma_{YVO_4} n_o} \tag{12}$$

The small signal gain coefficient, g_o, can be found by combining equations (5) and (7)

$$g_o = \frac{M}{2L} P_a \qquad (13)$$

Using equations (12) and (13), g_o and $\left(\frac{n_u}{n_o}\right)$ can be calculated for several values of P_a and a plot of g_o vs. $\left(\frac{n_u}{n_o}\right)$ can be obtained for each sample.

Finally, the single pass rod gain, $\mathrm{Ln}\,G_o$, may be calculated from equation (14)

$$\mathrm{Ln}\,G_o = g_o L = \frac{M}{2} P_a \qquad (14)$$

A plot of g_o and $\mathrm{Ln}\,G_o$ vs. P_a can be obtained for each sample using equations (13) and (14) respectively.

Last quarter, the spectroscopic parameters and lifetime studies of $Nd:YVO_4$ required for analysis of the laser feasibility tests were completed. In addition, calibration of the apparatus and determination of auxiliary parameters such as reflection and absorption coefficients required for measurement of the laser characteristics of $Nd:YVO_4$ were also completed. Finally, upon final construction of the Faraday rotation optical isolator, which could be useful in precise determination of $Nd:YVO_4$ laser parameters, the laser feasibility tests were started.

This quarter, most of the effort was devoted to analyzing the laser performance of $Nd:YVO_4$ such as assessment of both the loss and gain coefficients of the material, measurements of slope efficiencies, and comparison of the stimulated emission cross section and the saturation parameter of $Nd:YVO_4$ to that of Nd:YAG. Three crystals of $Nd:YVO_4$, of different dopings of neodymium, were used in this study and were compared to data obtained with a crystal of Nd:YAG. The study was performed by pumping the crystals with a chopped cw argon ion laser beam at 514.5 nm and monitoring the 1060 nm output of the crystal laser. The losses, Δ, and the stimulated emission cross section, σ, were determined for each sample by measuring the threshold power absorbed, P_T, as a function of the mirror reflectivities, R_1 and R_2. Six output mirror reflectivities were

used in the study and the slope efficiencies for each mirror set were determined. The small signal gain coefficient, g_o, and the single pass rod gain, G_o were calculated to assist in engineering comparisons.

In a comparison of Nd:YVO_4 and Nd:YAG at 1060 nm, the superiority of the laser characteristics of Nd:YVO_4 was demonstrated (Fig. IV-12).

2. Experimental Procedure

The output and input measurements were made using the experimental arrangement shown in Figures IV-6,-7 respectively. The crystals were pumped by an argon ion laser operating at 514.5 nm. The beam was chopped with an electronic shutter which provided 2 msec square pulses at a rate of 10 pulses per second. The input beam was then focused into the crystal with a 25 cm focal length lens. The crystals were pumped along the a-axis with the c-axis oriented parallel to the polarization of the pump beam. The samples were polished to a flatness of 1/10 λ with the rod ends parallel to within 10 arc-seconds. The Nd:YAG-1, Nd:YVO_4-1, and Nd:YVO_4-2 rods were anti-reflection coated at 1060 nm while the Nd:YVO_4-3 sample was not. The resonator consisted to two plane parallel mirrors; one a total (100%R) reflector at 1060 nm, M_1 and the other a partial reflector at 1060 nm, M_2.

The input power ranged from 50 to 900 mW and was monitored by a power meter in the cw mode (shutter open) as shown in Figure 2. At the same time the input power, P_1', was set, measurement of the transmitted power, P_2', and reflected power, P_3', were made using the same power meter. Bandpass filter 2 (Corning 4-96), which has 80% transmission at 514.5 nm and negligible transmission above 680 nm, stops any 1060 nm output from interfering with these measurements. P_1', P_2' and P_3' are corrected to their appropriate values P_1, P_2, and P_3, respectively, when multiplied by the attenuation constant which corrects for filter transmission, beam splitter reflectivities, and back surface reflection losses from M_1 and M_2.

A calibrated EMI 9684 photomultiplier, with an S-1 surface, was used to measure the 1060 nm output power, P_o. The output power at

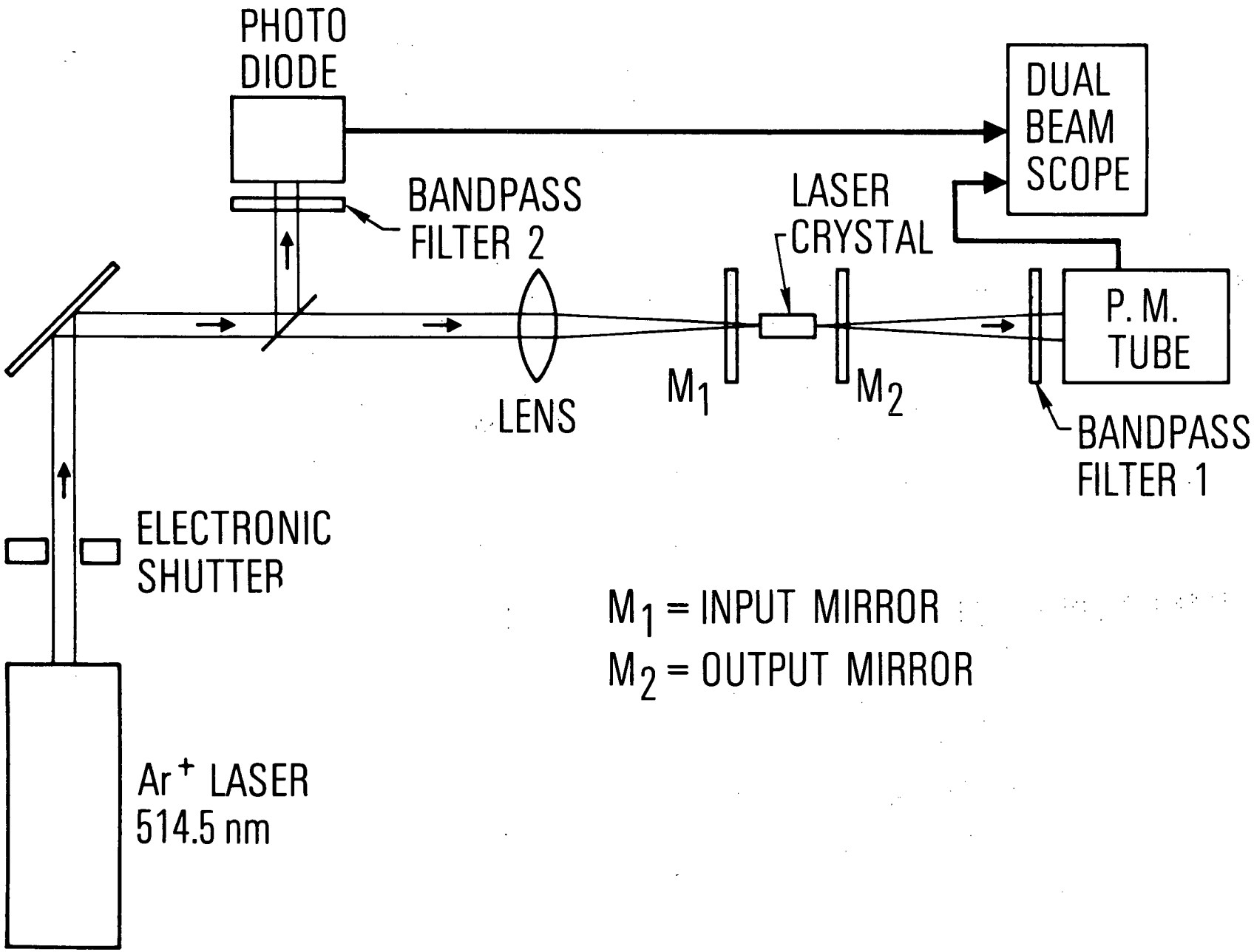

Figure IV-6 Experimental Arrangement. Input and Output Pump Power, and 1.06 μm Output Monitored.

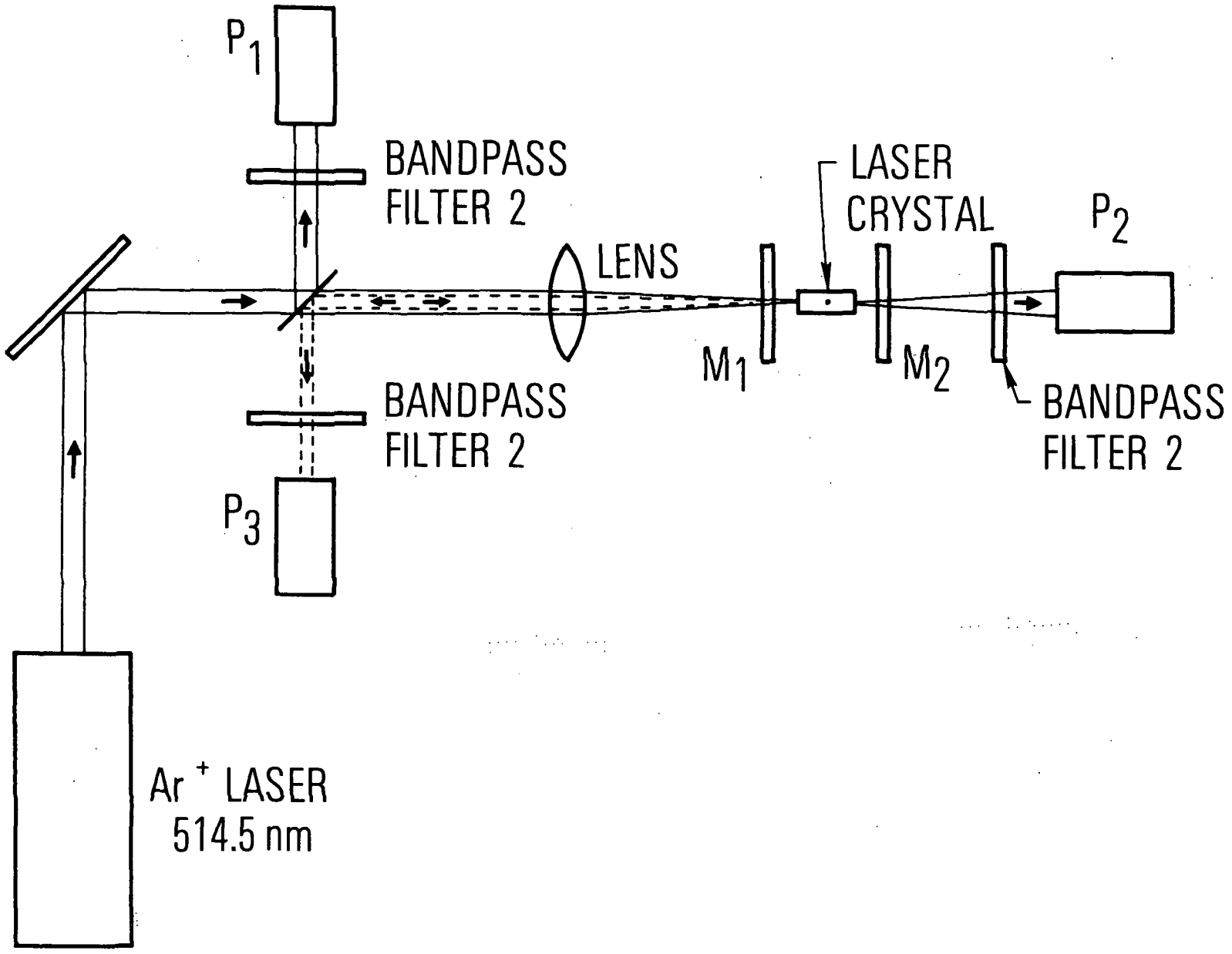

Figure IV-7 Experimental Arrangement. Input, Reflected and Output Pump Power, and 1.06 μm Output Monitored.

1060 nm was measured on a pulsed basis to reduce thermal effects in the crystal. As a check on the above cw measurements, the input power was again monitored off a beam splitter with a photodiode and observed on a dual beam oscilloscope simultaneously with the 1060 nm output pulse from the photomultiplier tube. Bandpass filter 1 (Corning 7-56), which is 70% transmitting at 1060 nm and has negligible transmission below 750 nm, stops any unwanted 514.5 nm pump power from entering the PMT. The input power was set at levels ranging from threshold to 900 mW. P_1', P_2' and P_3' were measured and a photograph of the 514.5 nm input pulse and 1060 nm output pulse on the scope was taken.

Data was obtained on three different crystals of Nd:YVO_4 and one crystal of Nd:YAG at the six different output mirror reflectivities. The three crystals of Nd:YVO_4 were doped with different amounts of neodymium as shown in Table IV-4. Nd:YVO_4-1 was run twice to check the reproducibility of the data. The fourth crystal was the Nd:YAG-1 which served as the reference sample. The mirror reflectivities used were 99, 94, 85, 78, 71, and 63 percent at 1060 nm for the output mirror and 100 percent at 1060 nm for the input mirror.

The data obtained gave P_1, P_2, P_3 and the output power, P_o, at approximately 10 power settings for each mirror. Equation (15) was used to calculate the absorbed power, P_a.

$$P_a = P_1 - (P_2 + P_3) \tag{15}$$

3. Results

Slope efficiencies were obtained for each sample at each output mirror reflectivity by plotting P_o vs. P_a. The highest slope efficiencies were obtained for the Nd:YVO_4-2 sample and this data is shown in Figure IV-8. The lines shown were determined by making a least squares fit to the data points.

Threshold powers were obtained by observing the 514.5 nm input power at which the 1060 nm output could no longer be detected. Using these thresholds a plot is made of P_T at threshold vs. $-\text{Ln } R_1' R_2'$. The loss coefficient, Δ, was obtained from the ordinate intercept at

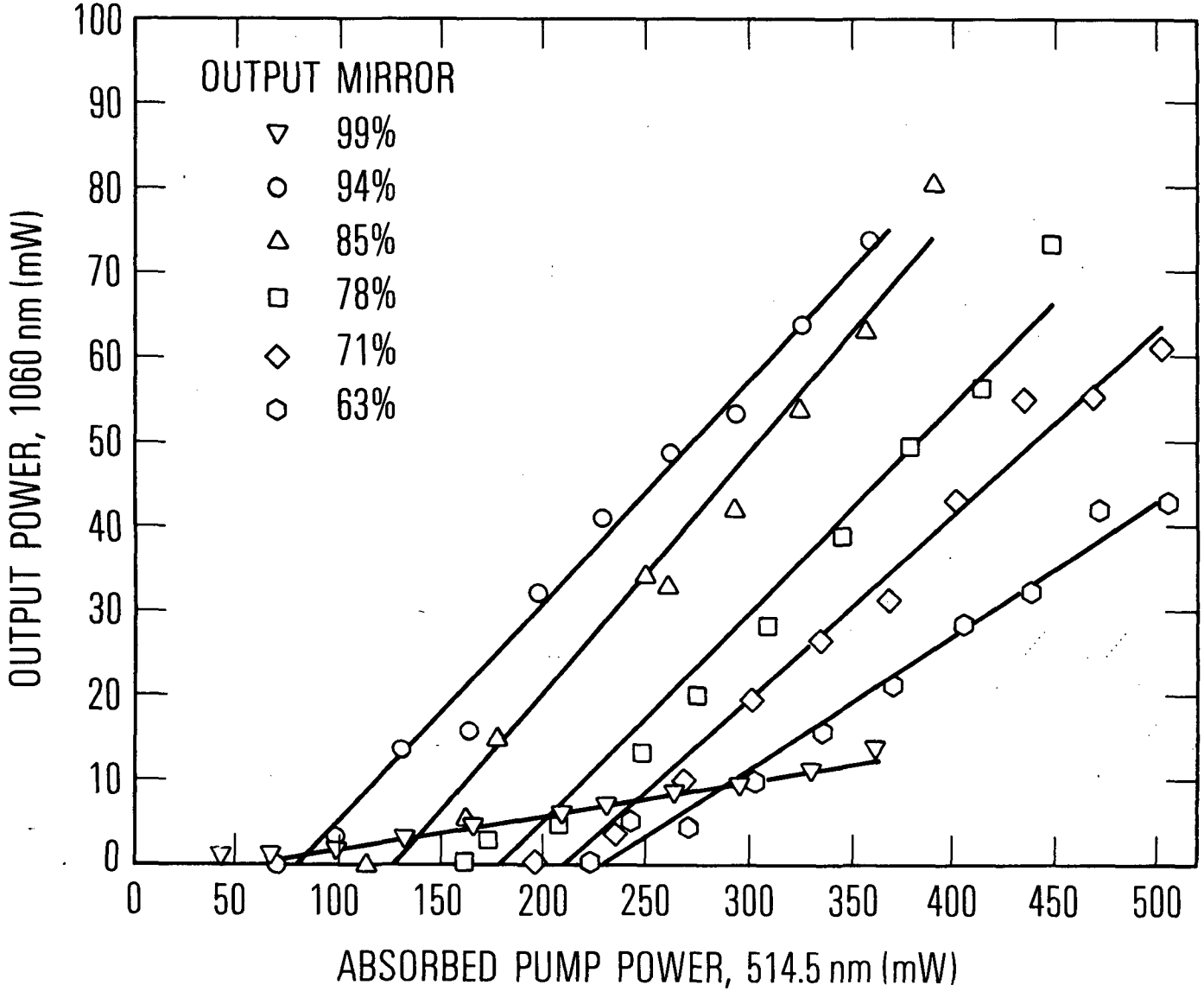

Figure IV-8 Output Versus Input for Nd:YVO_4-2 for 99, 94, 85, 78, 71, and 63% output mirror reflectivities.

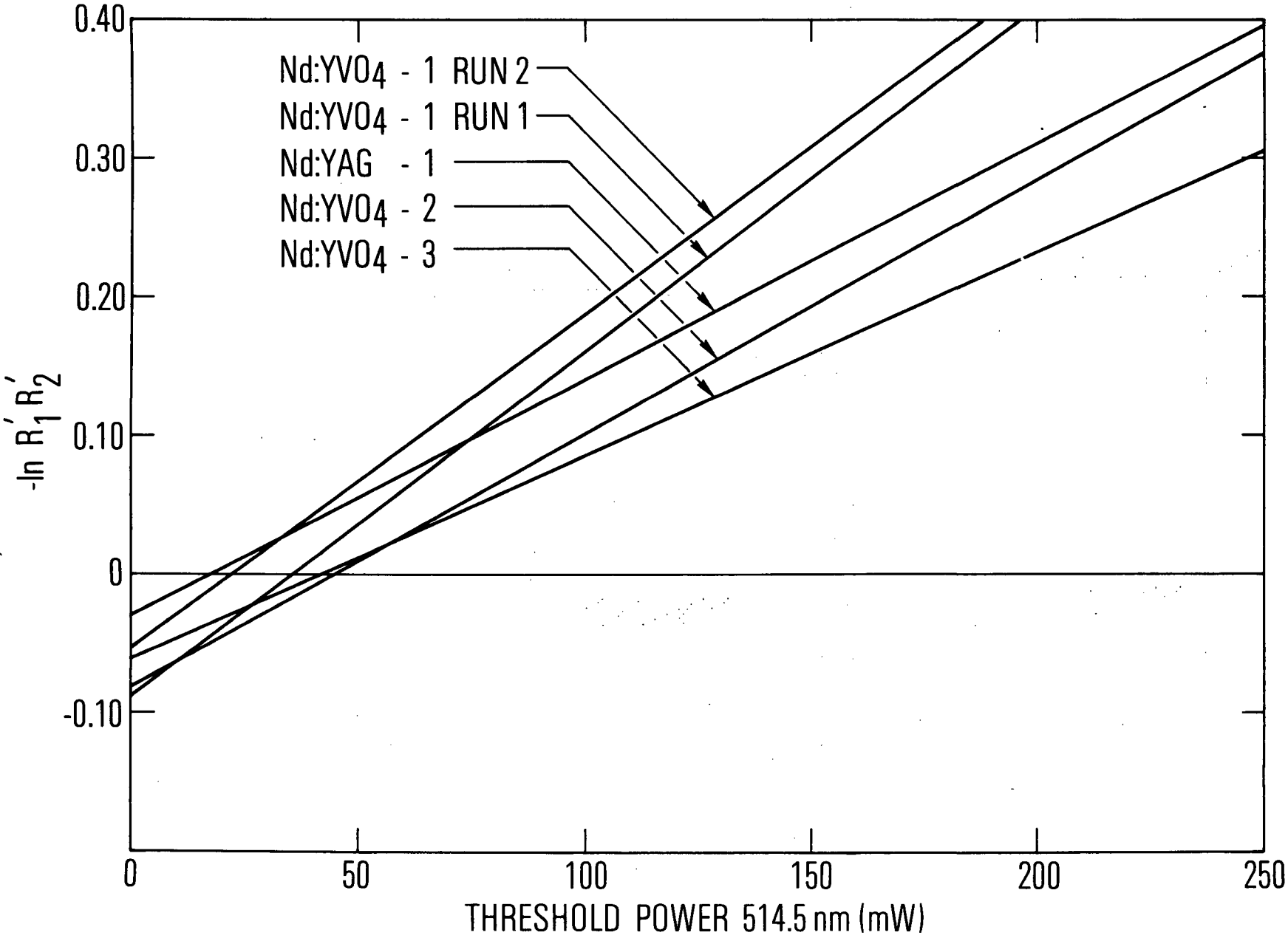

Figure IV-9 Threshold Versus Mirror Reflectivity Plots for Nd:YVO_4 and Nd:YAG Crystals.

$P_T = 0$ according to equation (6). A plot of all crystal data is shown in Fig. IV-9 and the single pass loss coefficients are listed in Table IV-5.

Table IV-5

LOSS COEFFICIENTS FOR Nd:YVO_4 SAMPLES

Crystal	Round Trip Losses, $2L\Delta$ (nepers x 10^{-2})	Crystal Length, L (cm)	Single Pass Loss Coefficient, Δ (cm^{-1} x 10^{-2})
Nd:YVO_4-1 (run 1)	8.73	0.483	9.04
Nd:YVO_4-1 (run 2)	5.16	0.483	5.34
Nd:YVO_4-2	8.18	0.749	5.46
Nd:YVO_4-3	6.15	0.795	3.87
Nd:YAG-1	2.98	1.275	1.17

The difference between run 1 and run 2 of Nd:YVO_4-1 is seen to be only a change in losses which is indicative of non-uniformity of the crystal. The slopes of the two runs are about the same. The lines drawn were determined by making a least squares fit to the data points.

An important parameter determined this quarter is the peak stimulated emission cross section, σ. This was determined from the ratio of the slopes of the P_T vs. $-\text{Ln } R_1' R_2'$ plots for Nd:YVO_4 and Nd:YAG, respectively, using equation (9). In Table IV-6, the associated data and the $\sigma_{(YVO_4)}/\sigma_{(YAG)}$ values for each sample are shown. From these ratios, and accepting the value of 4.6×10^{-19} cm^{-2} for Nd:YAG[7], the value of $\sigma_{(YVO_4)}$ was determined to be 1.24×10^{-18} cm^{-2}.

Table IV-6

Crystal	Slope, M (w^{-1})	Fluorescent Lifetime, τ (μsec)	Boltzman Factor, f_B	$\sigma_{(YVO_4)}/\sigma_{(YAG)}$
Nd:YVO_4-1 (run 1)	2.485	97.5	.5165	2.739
Nd:YVO_4-1 (run 2)	2.407	97.5	.5165	2.653
Nd:YVO_4-2	1.834	74.2	.5165	2.656
Nd:YVO_4-3	1.470	56.9	.5165	2.777
Nd:YAG-1	1.709	240.0	.3953	N/A

Average $\frac{\sigma_{YVO_4}}{\sigma_{YAG}} = 2.706 \pm .053$ $\qquad \sigma_{YVO_4} = 1.2 \times 10^{-18} cm^2$

Using this value of σ_{YVO_4}, the data in Tables IV-4, -6, and equations (12) and (13), a plot of the small signal gain coefficient, g_o, as a function of the population inversion density, n_u/n_o can be obtained. A plot of g_o vs. n_u/n_o is shown for each sample in Figure IV-10.

Finally, the single pass rod gain, LnG_o, may be calculated using equation (14) and the data in Table IV-6. A plot of g_o and LnG_o vs. P_a is shown for each sample in Figure IV-11.

A question often asked about this kind of work is, how well does it agree with the theory. Last quarter the fluorescence lifetime, τ, for the various samples was determined. From equation (7) a fairly simple check of the data can be performed. If the ratio of $\tau_{(1)}/\tau_{(2)}$ between two samples of the same host material is compared with the ratio of their slopes, M, of the P_T vs. - Ln $R_1' R_2'$ plots (see equation (7), it is possible to see if the agreement is good or not. In Table IV-7, the ratio is determined between the samples using the Nd:YVO_4-3 as the reference. The agreement is acceptable within experimental error.

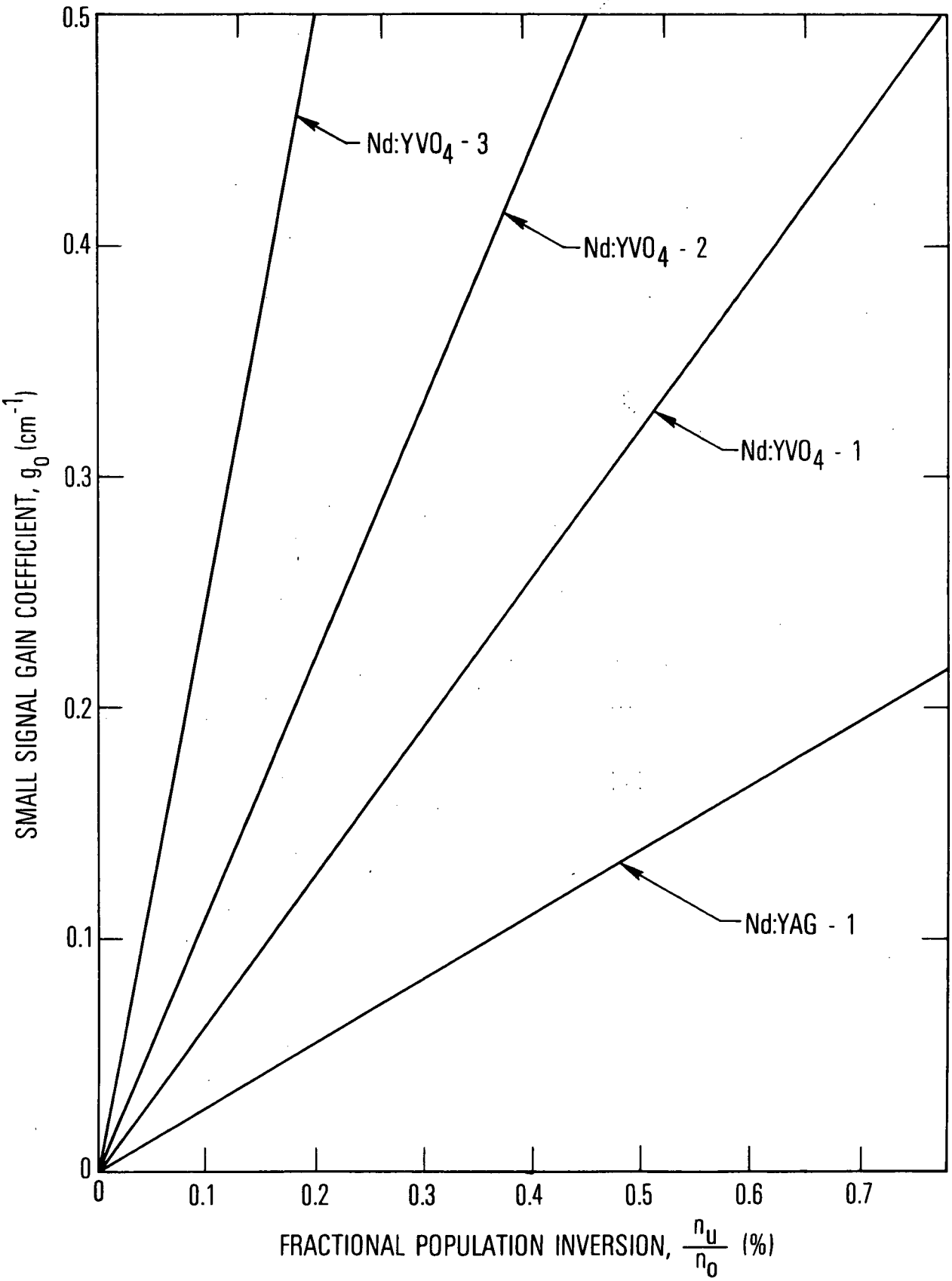

Figure IV-10 Small Signal Gain Versus Fractional Population Inversion in Nd:YVO_4 and Nd:YAG Crystals.

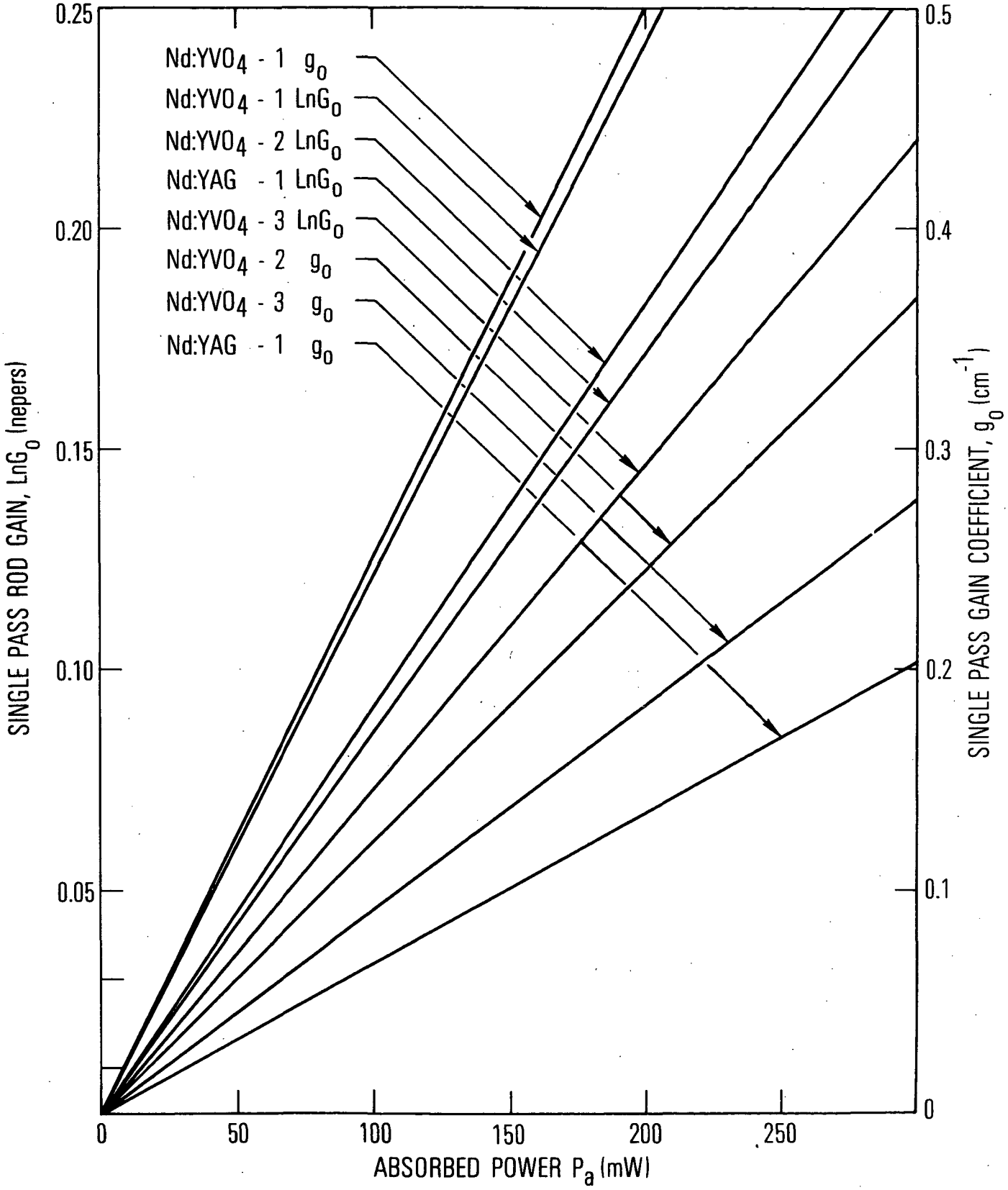

Figure IV-11 Single Pass Laser Gain Versus Absorbed 514.5 nm Pump Power for Nd:YVO_4 and Nd:YAG Crystals.

Table IV-7

Crystal	Fluorescence Lifetime, τ (μsec)	Slope, M (w^{-1})	$\frac{\tau}{\tau_{(YVO_4\text{-}3)}}$	$\frac{M}{M_{(YVO_4\text{-}3)}}$
Nd:YVO_4-3	56.9	1.47	1.00	1.00
Nd:YVO_4-2	74.2	1.83	1.30	1.24
Nd:YVO_4-1 (run 1)[4]	97.5	2.48	1.71	1.69
Nd:YVO_4-1 (run 2)[4]	97.5	2.41	1.71	1.64

A comparison of the laser performance of Nd:YVO_4-2 and Nd:YAG-1 is shown in Figure IV-12. The Nd:YVO_4-2 was chosen, as it is nearest the doping of the YAG at 0.72 at %. The data of Figure IV-8 indicates that the optimum output mirror reflectivity for Nd:YVO_4-2 is 85%, but further work needs to be performed to confirm this. The data taken with this mirror has been used in the comparison to Nd:YAG. The optimum output mirror reflectivity for Nd:YAG was also determined to be 85%. The slope efficiencies for Nd:YVO_4-2 and Nd:YAG using an 85% mirror reflectivity were 28% and 20%, respectively. By assuming a loss coefficient for the Nd:YVO_4-2 sample (heavy solid line) equal to that of the Nd:YAG rod, the expected performance would be that shown by the dashed line in Fig. IV-12. This shows a significant improvement in threshold, a reduction by about a factor of 2.

4. Operation of Faraday Rotation Isolator with the Nd:YVO_4 Laser

Last quarter a Faraday rotator was developed to isolate feedback from the Nd:YVO_4 laser cavity into the Ar^+ ion pump laser. Optimum adjustment of the crystal laser under test proved troublesome because of optical coupling between the pump laser and the test laser. The purpose of the isolator was to remove this difficulty. The isolator performed as desired, but several side effects made its use less desirable. The major problem seemed to be a thermal effect in the ZnSe at high power levels

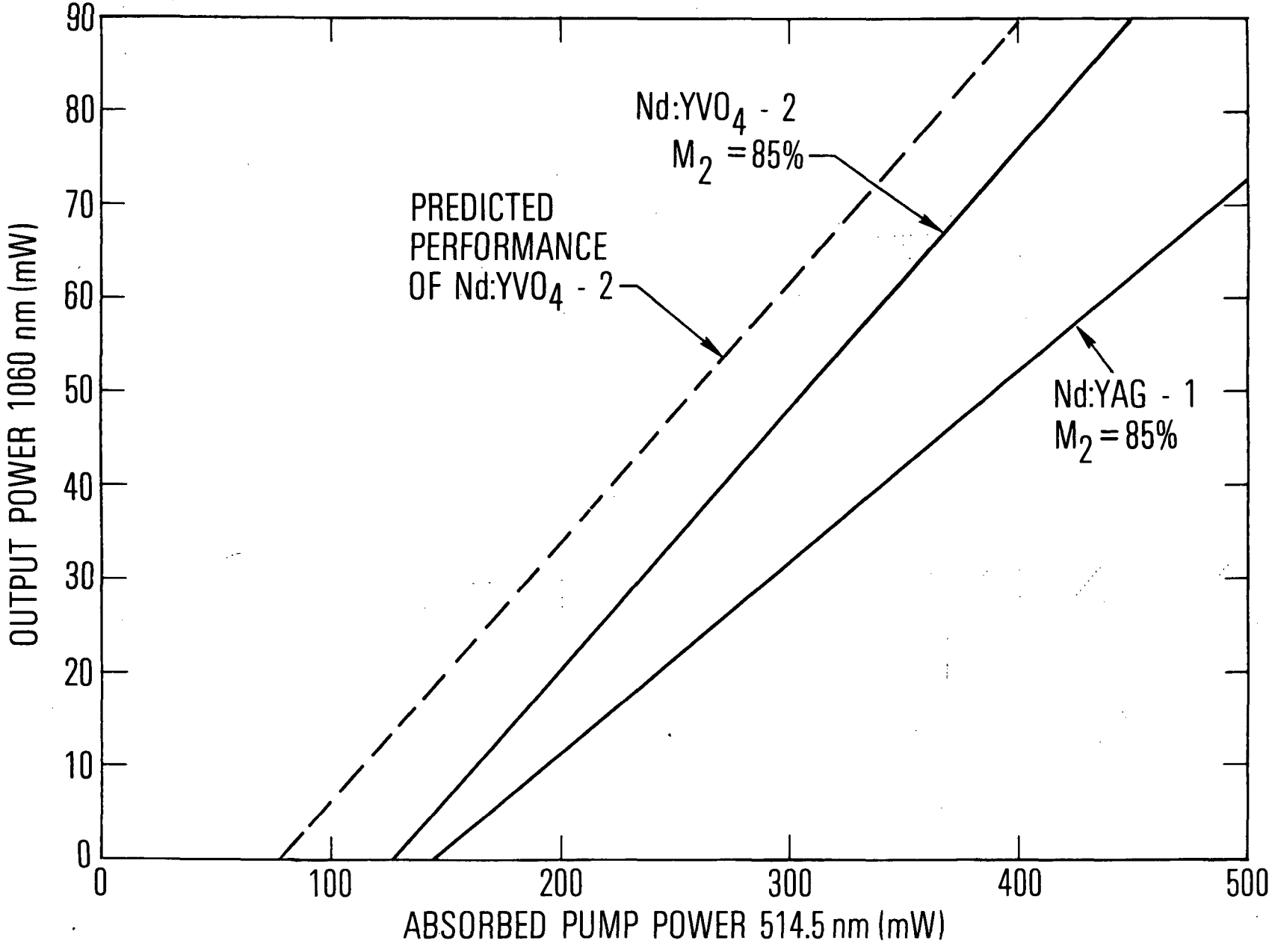

Figure IV-12 Comparative Performance of Nd:YVO_4-2 and Nd:YAG-1 with 85% Output Mirrors.

that led to beam divergence. A second problem was an overall loss of about 50% from the argon laser to the Nd:YVO_4 laser under test. As the output of the argon laser is limited, the range of data points needed to adequately analyze the performance of Nd:YVO_4 could not be obtained. Due to these problems, the isolator was not used in the examination of laser performance.

The laser performance of Nd:YVO_4, using the Nd:YVO_4-2 sample, was evaluated with and without the isolator in place. The characteristics of this crystal were evaluated in the manner described in Section IV-1 through IV-3. The isolator was positioned along the input beam line in the manner shown in Fig. IV-5. The characteristics (of the Nd:YVO_4 laser) measured included the slope efficiencies at various mirror reflectivities, the crystal losses, and the stimulated emission cross section ratio, $\sigma_{YVO_4}/\sigma_{YAG}$. A comparison of this data is shown in Table IV-8.

Table IV-8

EFFECT OF THE FARADAY ROTATION ISOLATOR ON THE Nd:YVO_4-2 PERFORMANCE DATA

	Performance of Nd:YVO_4-2 with Isolator		Performance of Nd:YVO_4-2 without Isolator	
Output Mirror Reflectivity (%)	Slope Efficiency (%)	Threshold Power (mW)	Slope Efficiency (%)	Threshold Power (mW)
99	2.4	48	4.1	43
94	19.4	88	25.9	70
85	24.1	132	28.1	114
78	22.8	162	24.6	162
71	22.5	207	21.7	197
63	18.4	266	15.9	224
Losses, $\Delta = 0.057\ cm^{-1}$ $\frac{\sigma_{YVO_4}}{\sigma_{YAG}} = 2.41$			$\Delta = 0.055\ cm^{-1}$ $\frac{\sigma_{YVO_4}}{\sigma_{YAG}} = 2.66$	

Within limits of experimental uncertainty, the agreement of the losses and cross section ratio are acceptable. The small difference in the loss factor could be due to a slight change in the positioning of the crystal between the two experiments and the different technique used to measure the input power, namely, off a beam splitter instead of measuring the direct beam. (A beam splitter is necessary in measuring the input power without the isolator because optical coupling between the test laser and the pump laser increases the input power. Measuring the input power directly necessitates inserting the detector between the test laser and the pump laser. This results in eliminating the feedback and would therefore give an erroneous reading of the true input power.) The most disturbing differences in the two sets of data are the lower slope efficiencies obtained when using the isolator. This was attributed to a thermal effect in the ZnSe of the rotator causing a defocusing of the input beam at higher power levels. It was observed that at shorter input pulses, the effect was less significant than at longer pulses. With continuous operation, the output at 1060 nm would disappear altogether. Without the rotator, this effect was not observed. In light of the above discussion, the agreement of the losses and cross section ratio, which required measurements at low power levels near threshold, can easily be understood; while the disagreement in slope efficiencies, which required operation at higher power levels, follows.

When the isolator was first considered, output instability was attributed to the feedback. In this quarter we found that most of the instability was due to crystal vibration. Efforts are in progress to minimize vibration effects by utilization of a flotation type of optical bench and by utilization of new mounts for the mirrors and the crystal.

D. Wavelength Measurement*

1. Introduction

It is generally useful and important to know the output wavelength of the laser. We list here a number of applications in which this may be required: design of an amplifier, selection of dye for Q-switching, design of narrow-band transmission filters, and design of dielectric mirrors, etalons, and other equipment. Consequently, we report the determination of the output wavelength of the Nd:YVO_4-1 laser.

2. Method

The experimental arrangement employed was practically identical to that shown in Fig. IV-6. Both cw and chopped-cw were utilized. Some of the essential characteristics were: cw 514.5 nm pump power of 550 mW; 10 pps with a 5 ms pulse duration for chopped operation.

The output wavelength of the Nd:YVO_4-1 laser was determined using a 1/2 m spectrometer with the following characteristics: 590 grooves/mm grating blazed at 1.0 μm; 5 μm slit width; grating scanning rate, 2Å/min; dispersion 0.08Å/mm. Calibration of spectrometer was obtained by use of a cw Nd:YAG laser with operating wavelength of 1064.2 nm.

With reference to the Nd:YAG laser, the output wavelength of our Nd:YVO_4-1 laser was 1064.10 $\pm$ 0.05 nm. This is very close to that of Nd:YAG. In fact, the Nd:YVO_4 amplifiers could be used with Nd:YAG and vice versa.

E. Output Beam Characteristics*

1. Introduction

In many applications, for example, space communications, ranging and tracking, the laser beam characteristics (divergence, mode purity, TEM_{ooq}) are of paramount importance. The output beam characteristics of the Nd:YVO_4 laser pumped with an argon ion laser were studied.

---

*A. W. Tucker, C. L. Fincher, and M. Birnbaum at Electronics Research Laboratory, The Aerospace Corporation

2. Measurements

The experimental arrangement is shown in Fig. IV-13. Observations were made using both the Nd:YVO_4-1 (0.41% atomic percent Nd^{+3}) and the Nd:YVO_4-2 (0.72% atomic percent Nd^{+3}) samples. The Nd:YVO_4 laser was end-pumped by a Spectra Physics model 165 argon ion laser operating cw at 514.5 nm. The input power to the Nd:YVO_4 laser was 540 mW and was focussed into the sample by a double convex lens, L1, of 25 cm focal length. Lowest threshold was obtained when the lens was positioned 27 cm from the center of the sample. The Nd:YVO_4 laser cavity consisted of two planar dielectric coated mirrors, M_1 and M_2, of 99% and 94% reflectivity at 1060 nm, respectively, and separated by 8.25 mm. The cavity length was kept fixed for both the Nd:YVO_4-1 and Nd:YVO_4-2 samples. The Nd:YVO_4-1 sample was 4.83 mm long and the Nd:YVO_4-2 sample was 7.49 mm long. Both samples were cut to put the C-axis normal to the laser cavity. The crystals were pumped along the A-axis, with the C-axis oriented parallel to the polarization of the pump beam. The 1064 nm output was observed to be completely polarized parallel to the C-axis.

The intensity distribution of the 1060 nm output beam was observed with a TV camera and monitor. In order to make quantitative measurements of the beam profile the video signal from the camera was displayed on a dual beam oscilloscope. One beam of the scope was used to display a single horizontal sweep of the video signal from which the horizontal beam intensity distribution was obtained. The second beam was used to display the peak intensity of each horizontal sweep which corresponds to one vertical frame. The vertical beam intensity distribution was obtained from this data.

A 105 mm focal length lens, F_3, was positioned 37.4 cm before the TV camera in order to magnify the beam pattern incident on the ground glass placed at the lens object plane (14.3 cm before the lens). In order to reduce laser speckle effects, the glass was rotated at 3600 RPM to "smooth out" the intensity profile as observed by the TV camera. All beam pattern measurements were referred to the calibration established at this object plane. The

calibration was performed by placing apertures of known diameter at the object plane. Light reflected off the rim of the apertures produced a video signal which was displayed on the oscilloscope. Obviously, no light was reflected from the aperture itself and resulted in the absence of a signal. The signal as observed on the oscilloscope as a result of light reflecting off the rim of the aperture resulted in a dip in the trace. The temporal width of the dip then corresponded to the spatial width of the aperture. The horizontal intensity distribution of the beam was measured on a 5 μsec/div time base and the calibration was 78.4 μm/μsec. The vertical intensity distribution of the beam was measured on the 2 msec/div time base and the calibration was 229.8 μm/msec. A Corning CS 7-56 filter, F_1, was positioned in front of the TV camera to block the 514.5 nm pump beam. In addition, neutral density filters, F_2, were used to reduce the 1060 nm intensity and prevent saturation of the vidicon tube.

Far field measurements were made by setting the ground glass at the focal point of a 50 cm focal length lens, L_2, positioned 67.65 cm from the output mirror, M_2, of the Nd:YVO_4 laser as shown in Fig. IV-13. Near field measurements were made by positioning the ground glass at the image plane of a 15 cm focal length lens focussed on the output mirror, M_2, of the Nd:YVO_4 laser. The image and object distances for near field measurements were chosen to be 100 cm and 17.69 cm, respectively, which provides a magnification of 5.67.

In addition to using the TV camera to monitor spatial characteristics of the output beam, a photomultiplier was used to monitor temporal and amplitude characteristics of the 1060 nm output.

Twenty sets of observations were made using the Nd:YVO_4-2 sample. First the Nd:YVO_4-2 laser was adjusted for maximum output power as observed on the photomultiplifer. This corresponded to 40 mW at 1064nm with 350 mW of absorbed power at 514.5 nm. Next the photomultiplier was removed and the near field and far field patterns of the 1064 nm beam were recorded using the TV camera. The horizontal and vertical profiles for both the near and far field are shown in Fig. IV-14. Similar results were obtained for the Nd:YVO_4-1

sample with maximum output at 1064 nm corresponding to 24 mW with 208 mW of 514.5 nm power absorbed.

From these patterns, beam spot size and beam divergence were calculated and recorded in Table IV-9. Note that measurements of the horizontal width and vertical width are the same within experimental error ($\pm$ 4%) and support the conclusion that the beam is symmetrical about the laser axis. Measurements of the 514.5 nm pump beam at the sample are included in the table for comparison purposes. If the patterns are Gaussian then the ratio of the width at the e^{-2} level to the width at the e^{-1} level is $\sqrt{2}$. The data in Table IV-9 supports the conclusion that the beam is Gaussian within the $\pm$ 4% experimental error and that the laser is operating in the TEM_{oo} mode.

We found consistently that adjustment of the laser for lowest threshold corresponded to TEM_{oo} mode output. These detailed results differ from those obtained by P. Yaney (reported in the 1st quarterly progress report). Yaney's work was performed very early in this study and we believe that they resulted from an artifact in his experimental arrangement.

3. Conclusions

Operation of the Nd:YVO_4 laser at 1064 nm in the arrangement of Fig. IV-13 resulted in TEM_{oo} mode operation. TEM_{oo} mode operation was consistently observed when the Nd:YVO_4 laser was adjusted for minimum threshold.

TABLE IV-9

1060 nm BEAM WIDTH AND DIVERGENCE OF A Nd:YVO_4 LASER LONGITUDINALLY PUMPED BY AN ARGON LASER

SAMPLE	BEAM PATTERN	FULL HORIZONTAL WIDTH AT: e^{-1} level H_1	e^{-2} level H_2	H_2/H_1	FULL VERTICAL WIDTH AT: e^{-1} level V_1	e^{-2} level V_2	V_2/V_1	POWER (mw)
Nd:YVO_4-2	514.5 nm beam at sample	55 μm	79 μm	1.44	47 μm	70 μm	1.49	540
	1060 nm beam near field	102 μm	151 μm	1.48	101 μm	150 μm	1.48	40
	1060 nm beam far field	3.28 mr	4.74 mr	1.44	3.26 mr	4.78 mr	1.47	
Nd:YVO_4-1	1060 nm beam near field	122 μm	175 μm	1.43	119 μm	173 μm	1.45	24
	1060 nm beam far field	2.45 mr	3.57 mr	1.46	2.45 mr	3.53 mr	1.44	

Error is ± 4%

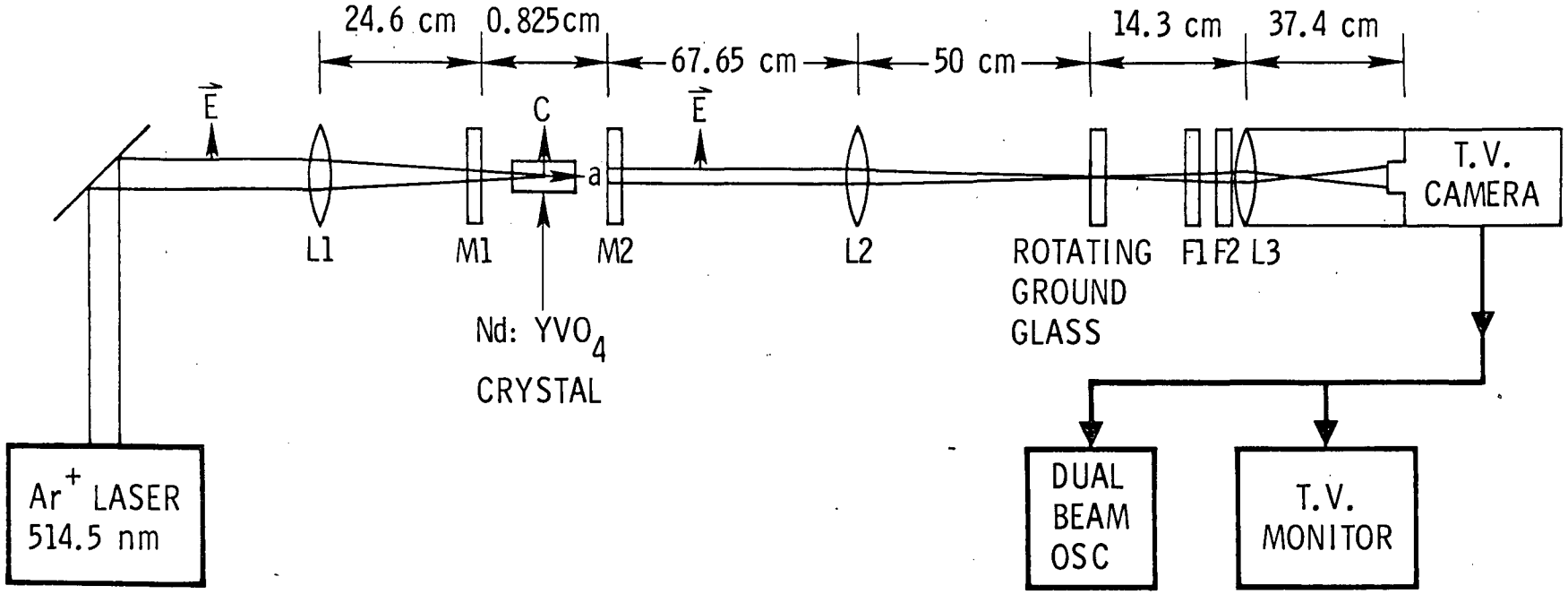

Figure IV-13 Experimental arrangement for determination of output beam parameters of Nd:YVO_4 laser.

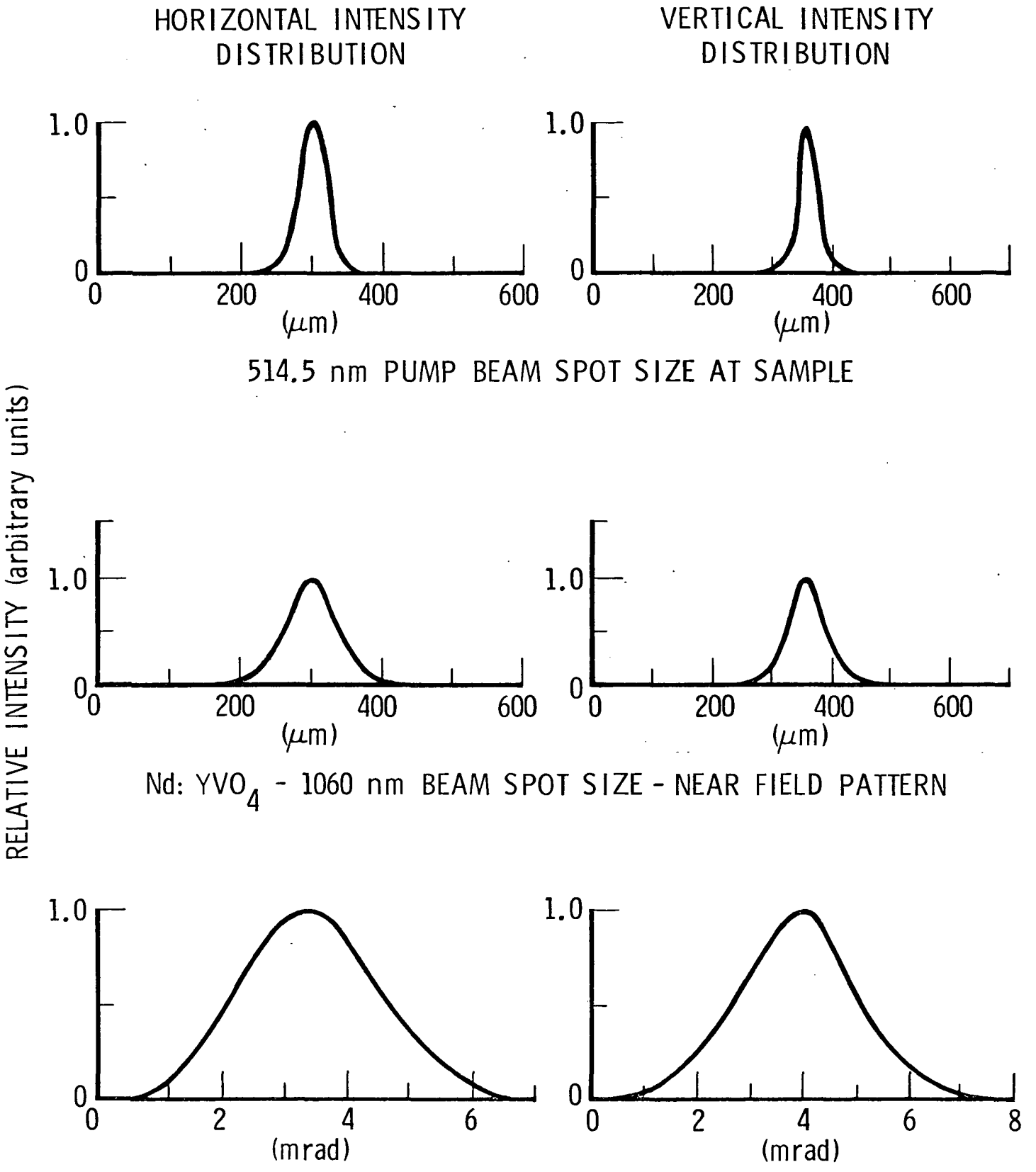

Figure IV-14 Upper - Intensity Distribution of 514.5 nm Pump Laser Beam;
Middle - Near Field of Nd:YVO_4 Laser
Lower - Far Field of Nd:YVO_4 Laser

4. References

1. J. R. O'Connor, "Unusual Crystal-Field Energy Levels and Efficient Laser Properties of YVO_4:Nd," Appl. Phys. Letters Vol. 9, pp. 407-409, December 1, 1966.

2. M. Bass, L. G. DeShazer and U. Ranon, "Evaluation of Nd:YVO_4 and Ho:Er:Tm:YVO_4 as Pulse Pumped-Q-Switched Laser," Report No. ECOM-74-0104-1, July 1974.

3. A. B. Chase, Aerospace Corporation, Section II.

4. D. Findlay and R. A. Clay, Phys. Letters, 20, 277, 1966.

5. M. Birnbaum and J. A. Gelbwachs, J. Appl. Physics, 43, 2335, 1972.

6. J. A. Wunderlich constructed isolator at University of Southern California. See Appendix I.

7. S. Singh, R. G. Smith and L. G. Van Uitert, "Stimulated-emission cross section and fluorescent quantum efficiency of Nd^{3+} in ytrium aluminum garnet at room temperature," Phys. Rev. B 10, 2566-72, 15 September 1974.

V. CONCLUSIONS AND RECOMMENDATIONS

A. Conclusions

The major efforts of this contract were concentrated in the areas of spectroscopy and laser performance. For completeness, in Chapter II, Section A a description of the current state-of-the-art of crystal growth of Nd:YVO_4 is presented which is followed by a description of the physical and crystal characteristics of Nd:YVO_4. In Chapter III a detailed description of relevant spectroscopic properties of Nd:YVO_4 is presented and in Chapter IV the CW laser performance studies of Nd:YVO_4 are presented.

The spectroscopic measurements were utilized to specify the Nd:YVO_4 rod parameters which would result in an efficient laser. The absorption characteristics folded into the lamp spectrum of a quartz-iodine lamp indicated that a 3 mm diam. rod with 0.9 at.% Nd conc. would result in efficient operation.* However, general results are presented (Fig. III-12) which would enable a similar analysis to be readily performed for other lamps.

Detailed measurements of the fluorescent lifetime of Nd:YVO_4 as a function of temperature and Nd concentrations are presented (III-C). These results indicated that (1) the lifetime does not decrease with decreasing temperature, (2) the lifetime for dilute samples (0.5%) is $\sim$ 105 μs, and (3) concentrations in excess of 1% will result in fluorescence lifetime shortening.

In Chapter IV detailed comparisons of laser performance of Nd:YVO_4 and Nd:YAG are presented. The pumping method utilized CW and chopped CW argon ion lasers at 514.5 nm. Although this differs from lamp pumping which will be used in most applications, the comparative performance of the materials determined with laser pumping will closely approximate anticipated results with lamp pumping.

---

* Please refer to Chapter II. Section E for an explanation of the definition of concentration.

A typical comparison of the performance characteristics of Nd:YVO_4 and Nd:YAG is shown in Figure IV-12. Note that the Nd:YVO_4 laser exhibited a lower threshold and higher slope efficiency than the Nd:YAG despite its higher internal crystal losses. For a Nd:YVO_4 laser with internal losses equal to that of Nd:YAG-1, its predicted performance (the dashed line) showed a lower threshold by almost a factor of 2. In the intermediate output power range (above threshold by about a factor of 2 to 3) the output of the vanadate laser is almost twice that of the Nd:YAG laser.

In Table IV-6 measurements of the stimulated emission cross section of Nd:YVO_4 at 1.06μ are summarized. It is 2.70 times that of Nd:YAG or 1.2×10^{-18} cm^2. The output wavelength of the Nd:YVO_4 laser was measured and equals 1064.10 ± 0.05 nm.

A study of the output characteristics beam intensity profile and beam divergence showed that the Nd:YVO_4 laser to operate in the TEM_{oo} mode (lowest order gaussian) with a corresponding beam divergence.

In summary, our measurements have shown that Nd:YVO_4 can substantially outperform Nd:YAG. Development of lasers of this type then, can result in substantial system improvements when utilized in spaceborne high data rate communication systems and other applications which place a high premium on low threshold and high efficiency operation.

B. Recommendations

Attempts to build prototype equipment with Nd:YVO_4 are hampered by a lack of crystals of adequate size and optical quality. Crystal growing is hampered by lack of satisfactory crucible materials. However, other techniques can be used which solve the problem posed by the crucible. It is anticipated that laser quality Nd:YVO_4 will be available in the near future.

A prototype Nd:YVO_4 CW laser suitable for laser communication applications should be developed. This will permit detailed assessment of thermal and other problems which may be encountered in CW operation with lamp pumping at required output levels.

C. Reports and Papers

The following publications and papers resulting from this contract effort are in preparation: (1) Fluorescence Lifetime of the $^4F_{3/2}$ Level in Nd:YVO_4; (2) Stimulated Emission Cross Section of Nd:YVO_4 at 1.06 and 1.34μ; (3) Spectroscopic Measurements and Analysis of Pump Bands in Nd:YVO_4.

It is intended that papers (1) and (2) will be presented at the December meeting of the APS at Stanford University.

VI. APPENDIX I

FARADAY ROTATION ISOLATOR FOR 5145Å LASER LIGHT*

A. Introduction

In operating a Nd:YVO_4 laser oscillator using the laser pumping technique, optical feedback from the oscillator to the pump source can be a serious problem when the pumping power is sufficiently high. For example, 1-3% feedback may be observed in some cases for 1-1.5 watts of argon ion laser input radiation. This feedback problem can affect accurate measurements of laser performance as well as system stability. To minimize such feedback, an isolator has been developed at U.S.C. for use in the Nd:YVO_4 laser performance measurements. The Nd:YVO_4 laser uses an argon ion laser operating at 5145Å as the pump source.

An isolator is a nonreciprocal optical device to insure one-way optical transmission with minimum loss. One of the common methods for obtaining this one way optical transmission is by utilization of the magneto-optic Faraday effect. The Faraday effect is the magnetically induced rotation of the plane of polarization of light incident on and propagating through a medium. The angle of rotation θ is proportional to the length d through the medium and to the magnetic field strength B along the propagation direction, and is described by $\theta = VBd$, where V is the Verdet constant of the medium.[1] The Faraday effect is nonreciprocal since the sense of the rotation is determined by the direction of the magnetic field and not by the propagation direction of the light. The basic isolator consists of two polarizers with a magnet and material causing ~45° rotation placed between them. The acceptance planes of the polarizers are oriented at ~45° to each other so that light passed by the first polarizer will be passed undiminished by the second. However, in the reverse direction, due to the

---

* Work on this chapter was performed by J.A. Wunderlich, U.S.C. Partial support provided by Naval Weapons Center, China Lake, California.

Faraday rotation, light admitted to the isolator by the second polarizer will not be passed by the first.

B. Isolator design

The correct choice of Faraday material is the main consideration in design of Faraday rotation isolators. Materials with a low Verdet constant require high magnetic fields and/or long path lengths to achieve the necessary 45° rotation. To obtain high magnetic fields one must use an elaborately cooled electromagnet. To successfully utilize long path lengths, one requires a material of high optical quality with low absorption coefficient. In our design a short length of ZnSe and low field strength were used due to the high Verdet constant of the material at the wavelength of interest. A permanent magnet provides the isolator field. By suitable design and positioning of external pole pieces, the effective field strength of this magnet may be boosted from a nominal 4505 gauss to the necessary field strength (7019 gauss) for rotation of 42° 21'. To provide this rotation, a sample with thickness of 0.432 cm was utilized. The ZnSe was AR coated for 5145Å radiation normally incident. Figures VI-1 and VI-2 show the essential components of the ZnSe isolator. The polarizers were Nicol (#1) and Glan-Thompson (#2) calcite polarizers. The extinction ratio was less than 0.001 at 5145 Å.

Verdet constant measurements were obtained using three CW visible lasers: HeNe laser (Spectra Physics model 133), argon ion laser (Coherent Radiation model 52), and a rhodamine 6G dye laser (Spectra Physics model 370). The laser beam was passed through a polarizer, air core solenoid, ZnSe sample, analyzer, and focussed onto a magnetically shielded photomultiplier detector. The general procedure of Verdet constant determination consisted of precise measurement of the angle of rotation of laser light incident on a known length of sample material subjected to a known magnetic field strength.[2]

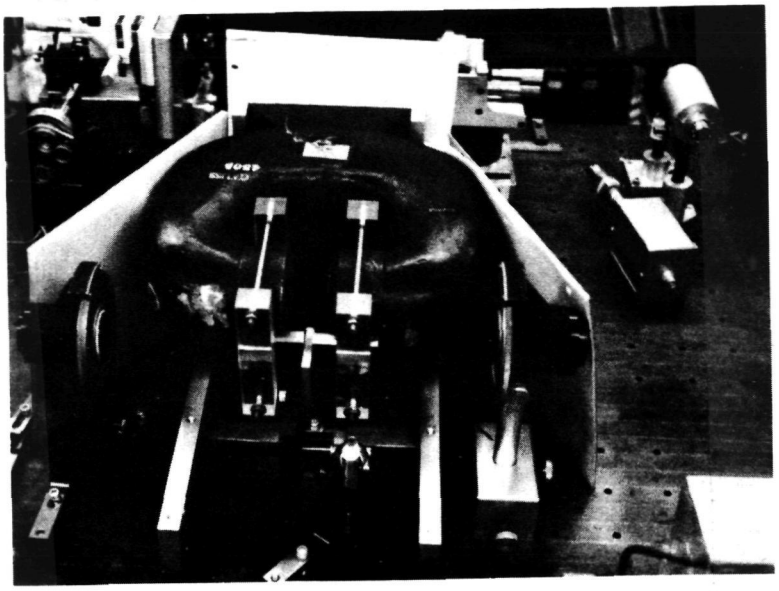

Figure VI-1. Photograph of the Optical Isolator

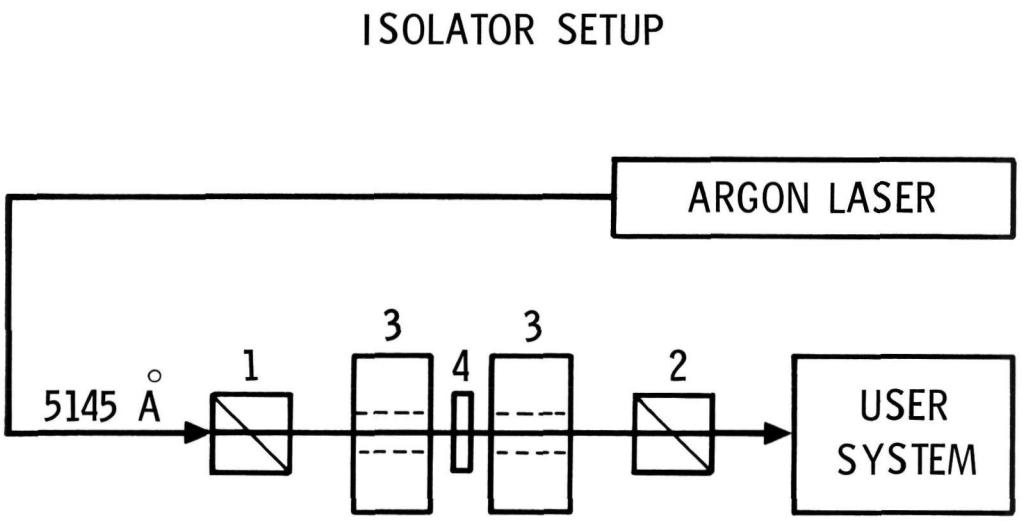

Figure VI-2. Isolator Setup
1) Nicol polarizer; 2) Glan-Thompson polarizer aligned 42°21' to 1;
3) External drilled pole pieces of permanent magnet; 4) ZnSe sample

The characteristics of the isolator were measured by inserting a beamsplitter and mirror in the setup shown in Fig. VI-2. The beamsplitter was inserted prior to the first polarizer and the mirror in back of the second polarizer. Measurements could then be made of the backward transmittance of the isolator from the beamsplitter. The forward and backward transmittances of the isolator are called insertion loss and isolation, respectively, and are normally expressed in decibels. The measurements were made using a RCA 1P28 photomultiplier. The probe beam was the 1.5 watt 5145Å laser output from an argon ion laser.

C. Experimental results

Verdet constant values for ZnSe at several wavelengths are presented in Table VI-1. A graph of V versus λ^{-2} is given in Fig. VI-3.

Table VI-1

λ(Å)	V(min-cm^{-1}-gauss^{-1})
6328	0.410
6072	0.470
5868	0.519
5676	0.611
5145	0.838
5017	0.955
4965	1.038
4880	1.184
4765	1.498

Here the solid line indicates values for the usual fit $V = A + B\lambda^{-2}$ where, in this case, A = -.4510 min-cm^{-1}-gauss^{-1} and B = 0.3403 μm^2-min-cm^{-1}-gauss^{-1}. The dotted line indicates the deviation of the data from this fit as the absorption band is approached. In this region a term of the form $C\lambda^{-4}$ plays an important role in the determination of the Verdet

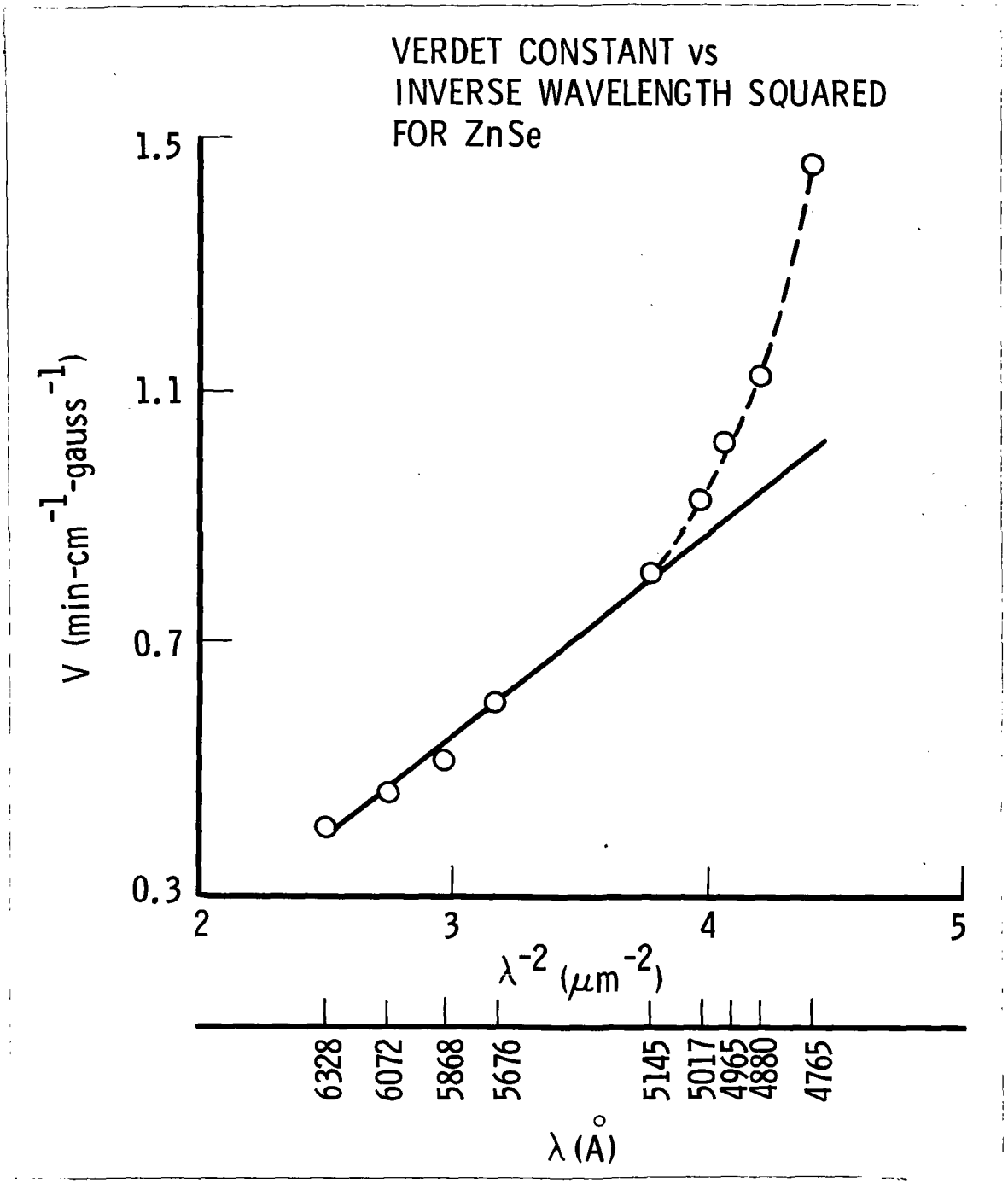

Figure VI-3. Verdet constant versus inverse wavelength squared for ZnSe.

constant. A graph of absorbance (A) versus wavelength for ZnSe is presented in Fig. VI-4. This data was taken using a Cary 17 spectrometer and as such has not been corrected for the reflection component caused by the difference of refractive index between air and the material at each wavelength. The absorption coefficient ( ) may be calculated according to the equation $\alpha = A/L \log_{10} e$ in which L = 0.746 cm and A represents the true absorbance (reflection taken into consideration).

The insertion loss measured -2.06 db for any probe beam diameter up to 0.5 cm, the maximum diameter beam that can be directed through holes in the external pole pieces. The isolation was -25.5 db for probe beam diameters up to 0.5 cm. A figure of merit for isolators is the ratio of forward to backward transmittance which was 23.4 db in this case.

The isolator was found to provide approximately 62 percent transmission or 0.94 watt output for the maximum available input of 1.5 watts despite the high absorption coefficient of ZnSe in the visible region, due to the high Verdet constant of the material which allows short sample thicknesses to be used. Exposure of the isolator to 1.5 W incident radiation at 5145Å for a period of 30 minutes revealed no visible or measurable damage to either the bulk or thin AR coatings.

D. Conclusions and recommendations

A Faraday rotation isolator has been developed to isolate the 5145Å argon ion laser line. Using ZnSe as the rotation material, it is possible, due to the high Verdet constant, to use a thin sample of material and relatively low magnetic field strength to obtain nearly 45° rotation. The result is that even though ZnSe has a high absorption coefficient at visible wavelengths, a low insertion loss and a system both compact and portable can be achieved. The developed isolator weighed approximately 50 lbs.

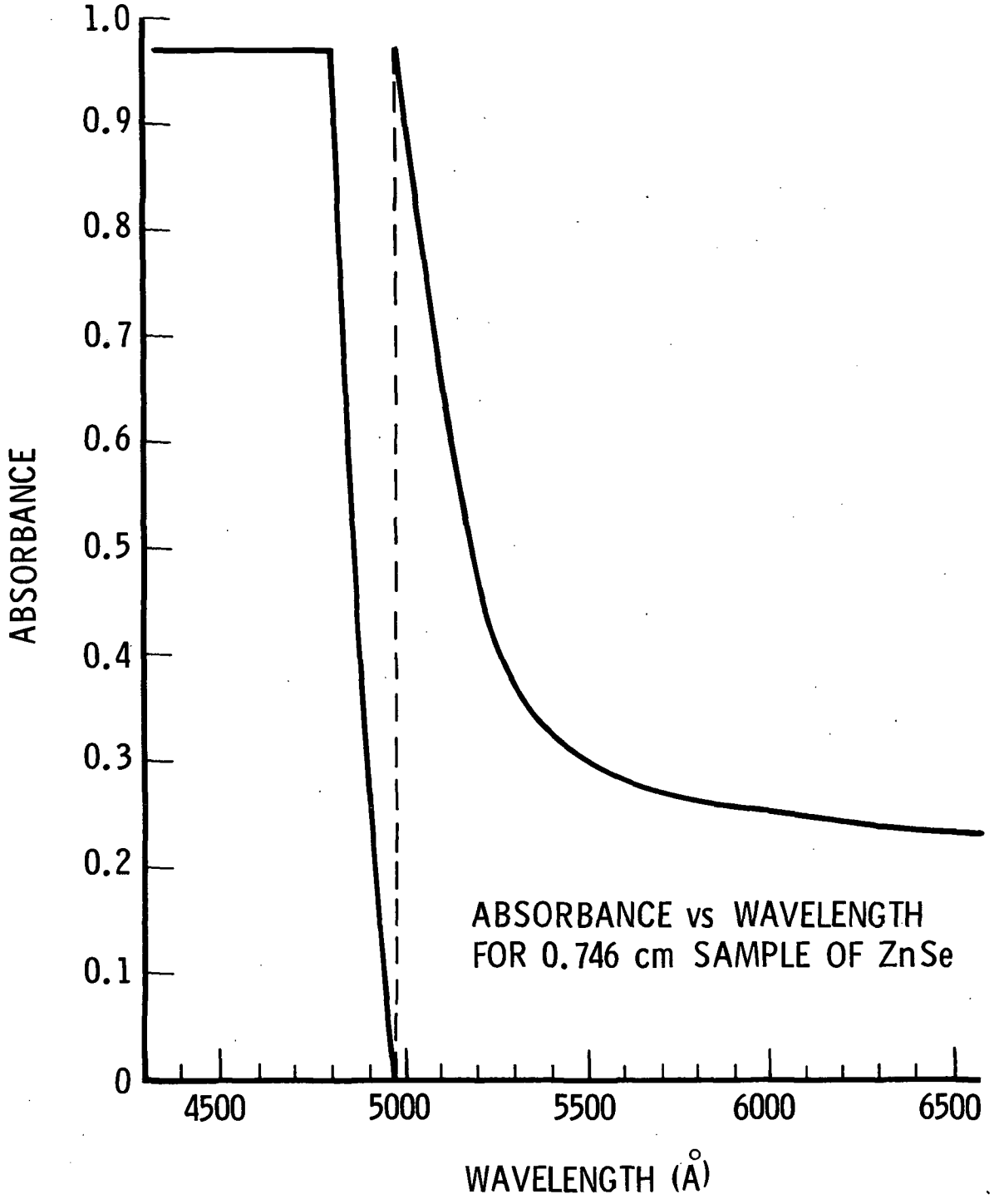

Figure VI-4. Absorbance versus wavelength for a 0.746 cm thick sample of ZnSe.

To further decrease the insertion loss and increase the isolation one must:

1) increase B (thus allowing d and so absorption to be decreased), or

2) increase B and/or d (to achieve nearer 45° rotation), or

3) use ZnSe material with a lower absorption coefficient in the visible wavelength regions.

The isolator external pole pieces consist of two pieces each of one half inch square cross section with a 5 mm diameter hole drilled in its center. These pieces may be positioned at various separations differing from the fixed pole separation of 2.5 cm. Table VI-2 contains data on rotation through 0.216 cm of ZnSe as a function of external pole spacing. As can be seen from Table VI-2, saturation occurs with this configuration at small

Table VI-2

Rotation (deg)	Spacing (cm)
9.5	2.6
17.5	1.3
20.0	1.0
21.0	0.7
20.5	0.4

separations. To avoid saturation, allowing an increase in the effective field strength, a new external pole design should be implemented. A suggested design, which should allow smaller separations (and thus increased field strength before saturation occurs) consists of two pieces each of one inch square cross section with a 5 mm diameter hole drilled in its center. Each piece should be machined at a 30° angle to the pole face leaving a 15 mm diameter region concentric to the hole untouched. An increase in the effective magnetic field strength should result which will allow better isolator performance and the possibility of providing isolation for other laser lines which may be useful as pump sources.

E. References

1. T. M. Lowry, Optical Rotary Power (Dover Publications, New York 1964) Chapters XII and XXXV.

2. H. L. Wang, "Diamagnetic Faraday Effect in the Garnets YAG, YGG, and GGG", Ph. D. Thesis, University of Southern California, June 1975.

Continuous-wave operation of Nd:YVO_4 at 1.06 and 1.34 μ

A. W. Tucker, M. Birnbaum, and C. L. Fincher

Electronics Research Laboratory, The Aerospace Corporation, El Segundo, California 90245

L. G. DeShazer

Center for Laser Studies, University of Southern California, Los Angeles, California 90007
(Received 7 August 1975)

Continuous-wave plane-polarized outputs of 1 W at 1.06 μ and 0.35 W at 1.34 μ were obtained by end pumping small samples of Nd : YVO_4 with an argon-ion laser. Slope efficiencies and material losses were determined. At 1.06 and 1.34 μ, Nd:YVO_4 lasers can substantially outperform Nd:YAG lasers. Self-Q-switched operation of Nd:YVO_4 at both wavelengths was obtained by resonator misalignment.

PACS numbers: 42.60.G

Lasers of high efficiency and low thresholds are required in diverse applications such as communications, ranging, and metrology. The Nd : YAG laser has represented the state-of-the-art in most applications requiring low-threshold and efficient lasers. O'Connor[1] had observed almost ten years ago that Nd : YVO_4 possessed a larger stimulated-emission cross section at 1.06 μ than Nd : YAG and obtained low-threshold laser operation at 90 °K. Recently, detailed spectroscopic measurements quantified O'Connor's observations by showing that the stimulated-emission cross section of A-axis Nd : YVO_4 at 1.0634 μ was 4.6 times greater than that of Nd : YAG at 1.0642 μ.[2]

The superiority of Nd : YVO_4 lasers at 1.06 and 1.34 μ over Nd : YAG is demonstrated here by a comparison of the laser characteristics of small spectroscopic samples of Nd : YVO_4 with a high-optical-quality Nd : YAG laser rod. The comparisons were effected by end pumping with cw and pulsed argon-ion lasers at 514.5 nm, with emphasis on cw performance. Development of Nd : YVO_4 lasers is hindered by the lack of large (3×30 mm) laser-grade crystals. However, difficulties in vanadate crystal growth have been identified and large laser-grade crystals may soon be available.[3]

The equations describing the laser performance can be derived from consideration of the laser-threshold condition

$$R_1'R_2' \exp 2L(n_u\sigma - \Delta) = 1 \tag{1}$$

where R_1' and R_2' are the corrected mirror reflectivities (see explanation which follows), L is the length of the laser sample, n_u is the density of Nd^{3+} ions in the upper state of the laser transition, σ is the peak stimulated-emission cross section, Δ is the total losses per cm (exclusive of transmission losses by the mirrors) which include, for example, diffraction losses, excited-state absorption, and scattering losses. The rod ends were plane parallel and carefully aligned with the plane dielectric-coated end mirrors. In laser operation, the Fabry-Perot condition for maximum reflectivity $R' = (r^{1/2} + R^{1/2})^2[1 + (rR)^{1/2}]^{-2}$ should be a good approximation with r the Fresnel reflectivity of the crystal and R the mirror reflectivity.[4]

In cw operation the upper-level population is related to the pump power according to

$$n_u = \frac{\eta f_B P_a \tau}{h\nu_p V}, \tag{2}$$

where n_u is the population per cm^3 of the upper laser level, η is the quantum efficiency, namely, the fractional number of Nd^{3+} in the $^4F_{3/2}$ level per absorbed photon, f_B is the fractional population in the upper laser sublevel of the $^4F_{3/2}$ state, P_a is the pump power absorbed by the laser crystal, τ is the fluorescence lifetime of the $^4F_{3/2}$ level, $h\nu_p$ is the energy per pump photon, and V is the volume pumped. Substitution of Eq. (2) into Eq. (1) yields

$$\frac{\eta f_B P_a \tau}{h\nu_p V} 2L\sigma = 2L\Delta - \ln R_1'R_2'. \tag{3}$$

The advantages of our method, namely, the accessibility of the quantities in Eq. (3) to direct measurement have been described earlier.[5] A critical evaluation of the measurement techniques will be treated in a subsequent publication.

One of the more difficult quantities to measure in a four-level laser system such as Nd : YVO_4 is the loss factor Δ. This can be determined by measurement of

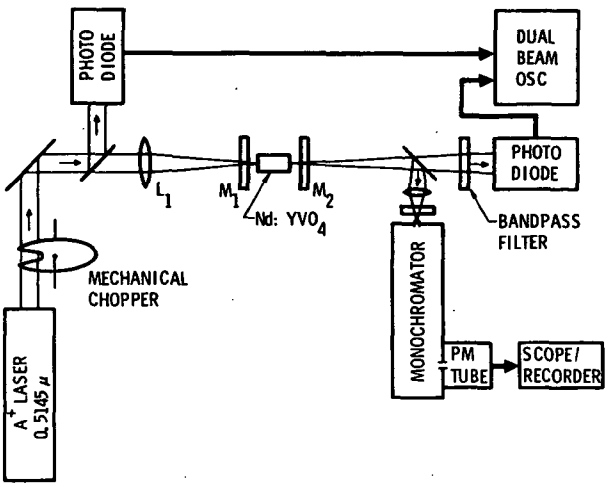

FIG. 1. Experimental arrangement.

TABLE I. Partial list of the parameters of Nd:YVO_4 (1%) and Nd:YAG (1%) crystals used in the paper. Entries above the broken line are taken from Ref. 2. The other values were obtained in this study.

	Nd:YVO_4 (*A* axis)	Nd:YAG
λ (μm)	1.0634	1.0643
τ (μs)	92	240
$\Delta\nu$ (cm^{-1})	7	6
σ (cm^{-2})	30×10^{-19}	6.5×10^{-19}
L (cm)	0.48	1.275
V (cm^3)	1.27×10^{-5}	3.86×10^{-5}
Δ (cm^{-1})	0.16	0.018

the laser threshold as a function of the reflectivity of the output mirrors.[5]

The experimental arrangement utilized for these measurements is shown in Fig. 1. By chopping the cw argon-ion laser beam, pump pulses of several millisecond duration were provided. Since this is long compared to the cavity and crystal response times, the results are directly applicable to cw performance of the lasers. Chopping reduces the heat load in the crystal and also prevents damage to the dielectric coatings on the mirrors. The Nd:YAG rod was antireflection coated at 1.06 μ, while the Nd:YVO_4 sample was uncoated. The resonator consisted of two plane-parallel mirrors; one a high (99%) reflector and the other a partial reflector of 99, 95.6, 84, 72.6, 67.6, and 53% reflectivity. A plot of the absorbed power vs $-\ln R_1' R_2'$ was accurately linear. The intercepts of the ordinate axis at $P_a = 0$ provided the loss coefficients, $\Delta = 0.16$ cm^{-1} for Nd:YVO_4 (1% concentration) and 0.018 cm^{-1} for Nd:YAG (1% concentration). The large losses for Nd:YVO_4 were attributed to scattering by the iridium platelets in the crystal which were introduced during the growth process.[3] A partial list of the parameters of Nd:YVO_4 (1%) and Nd:YAG (1%) crystals used in this paper is given in Table I.

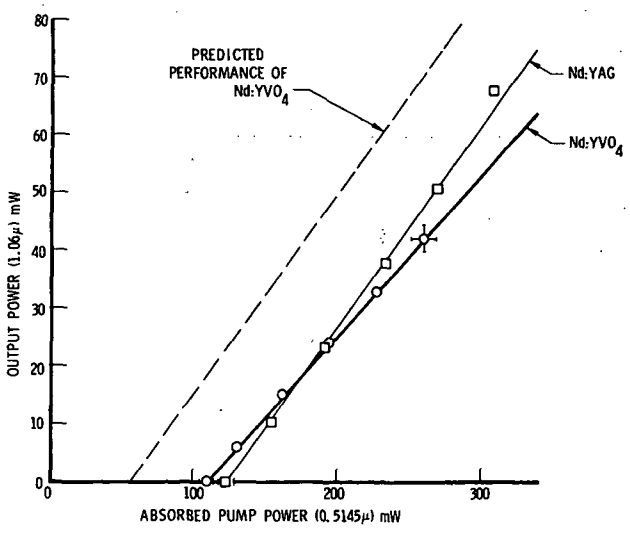

FIG. 2. Output power of Nd:YVO_4 (1%) and output power of Nd:YAG vs absorbed 0.5145-μ input power.

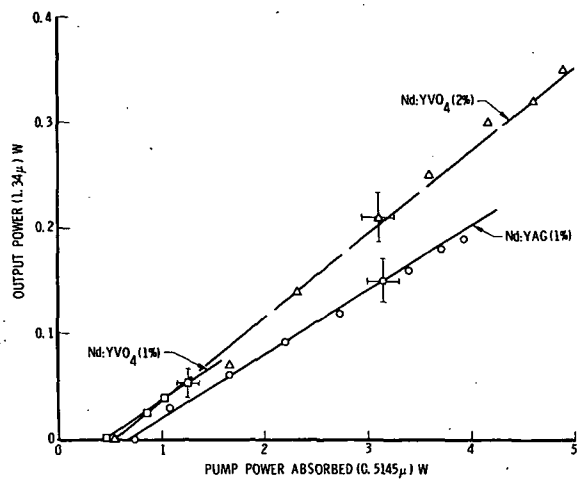

FIG. 3. Output power of Nd:YVO_4 (1%), Nd:YVO_4 (2%), and Nd:YAG (1%) vs absorbed 0.5145-μ input power.

Comparison of the laser performance of Nd:YVO_4 and Nd:YAG with optimum output mirrors of reflectivity of 67.6 and 84%, respectively, is shown in Fig. 2. The dashed line in Fig. 2 is obtained by assuming a loss coefficient for the Nd:YVO_4 sample (heavy solid line) equal to that of the Nd:YAG rod and is illustrative of the superior performance of Nd:YVO_4 to be expected with low-loss material. The slope efficiency of Nd:YVO_4 at 1.06 μ (Fig. 2) for optimum coupling was 20%. Some advantages of investigation of laser properties by laser end pumping are evident by the well-controlled performance and the exact linearity of the graphs of Figs. 2 and 3. When the laser is operated close to threshold, the output power of the laser is given by[6] $P = P_s[(W/W_{th}) - 1]$, where P is output power, P_s is a constant which depends upon the material parameters, W is the pump power absorbed, and W_{th} is the pump power absorbed at threshold. A difficulty was encountered in that optical feedback produced by reflection of pump light back into the argon-ion laser made optimum adjustment of the apparatus critical. A Faraday rotator is currently under construction which will isolate the argon-ion laser from the test laser and should circumvent this difficulty in future experiments.

There has been considerable interest in the development of eye-safe lasers, and this consideration prompted our investigation of the performance of Nd:YVO_4 at 1.34 μ. Continuous-wave operation of Nd:YVO_4 at 1.34 μ was readily achieved. A comparison of the cw operation of Nd:YVO_4 (1 and 2% samples) and Nd:YAG (1%) is shown in Fig. 3. The samples used in Fig. 3 were the same as in Fig. 1, except for the 2% Nd:YVO_4 sample.

The experimental arrangement was similar to that of Fig. 1, except that a 10 W argon-ion laser was used to provide pump power at 0.514 μ. The resonator consisted of a pair of plane-parallel mirrors both of 99% reflectivity at 1.34 μ which were specially designed for low reflectivity (less than 10%) at 1.06 μ, thereby suppressing oscillation at this wavelength. The superiority of the Nd:YVO_4 samples is evident despite their greater

losses. The slope efficiency of the 2% Nd : YVO_4 at 1.34 μ was 7%.

Work is in progress to determine the loss coefficient at 1.34 μ and to measure the stimulated-emission cross sections of Nd : YVO_4 and Nd : YAG at 1.34 μ. A preliminary estimate of the stimulated-emission cross section of Nd : YVO_4 (1%) at 1.34 μ (assuming a Δ of 0.16 cm^{-1}) and using the data of Fig. 3, shows that it is considerably larger than that of Nd:YAG.

In adjustment of the mirrors of the Nd : YVO_4 lasers, in the quasi-cw mode of operation at 1.06 μ, pulsed outputs, in several instances, were observed. The YVO_4 sample was misaligned with respect to the resonator axis by about 25 arc min and self-giant pulsing at 1.06 μ was readily obtained. Pulsewidths of 40 ns were observed with peak powers over 1000 times greater than the cw output of the laser. Self-giant pulsing was observed at 1.34 μ, but only preliminary observations were obtained. Self-Q-switched operation of Nd : YAG could not be achieved under the same conditions, but had been observed earlier by cooling the Nd:YAG.[7] The ease of self-Q-switching the Nd:YVO_4 evidently stems from the higher stimulated-emission cross sections.

[1]J.R. O'Connor, Appl. Phys. Lett. 9, 407 (1966).
[2]M. Bass, L.G. DeShazer, and U. Ranon, Report No. ECOM-74-0104-1, 1974 (unpublished).
[3]A.M. Chase (private communication).
[4]D. Findlay and R.A. Clay, Phys. Lett. 20, 277 (1966).
[5]M. Birnbaum and J.A. Gelbwachs, J. Appl. Phys. 43, 2335 (1972).
[6]G. Birnbaum, *Optical Masers* (Academic, New York, 1964), p. 90.
[7]M. Birnbaum and C.L. Fincher, Proc. IEEE 57, 804 (1969).

VI. APPENDIX III

BIBLIOGRAPHY OF YVO_4 AND Nd:YVO_4

A. Crystal Structure and Characteristics

1. E. Broch, "The crystal structure of yttrium vanadate," Z. Physik. Chem. 20 B, 345-350 (1933).
2. R.W.G. Wyckoff, Crystal Structures (Interscience, New York, 1963).
3. G.F. Koster, J.O. Dimmock, R.G. Wheeler, and H. Statz, Properties of the Thirty-Two Point Groups (M.I.T. Press, Cambridge, Mass., 1963).
4. E.M. Levin, "The system Y_2O_3 - V_2O_5," J. Am. Ceramic Soc. 50, 381-388 (1967).
5. H.G. Kahle, H.C. Schopper, W. Urban and W. Wuchner, "Temperature effects on zircon structure lattice parameters and zero-field resonance for substituted Gd^{3+}," Phys. Stat. Solidi 38, 815-819 (1970).
6. D.S. Bondreaux and T.S. LaFrance, "Energy transfer from the excited VO_4^{3-} ion in dielectric crystals," J. Phys. Chem. Solids 35, 897-899 (1974).
7. M. Gupta, and D. E. Ellis, "Cluster model for lattice distortion effects on electronic structure: VO and VO_2," Phys. Rev. B, 13, 3405-3418 (1976).

B. Physical, Optical and Laser Properties

1. J.R. O'Connor, "Unusual crystal-field energy levels and efficient laser properties of YVO_4:Nd," Appl. Phys. Lett. 9, 407-409 (1966).
2. J.R. O'Connor, "Optical and laser properties of Nd^{3+}- and Eu^{3+}-doped YVO_4," Trans. Met. Soc. AIME 239, 362-365 (1967).
3. Kh.S. Bagdasarov, A.A. Kaminskii, V.S. Krylov, and V.I. Popov, "Room temperature induced emission of tetragonal yttrium orthovanadate crystals containing tripositive neodymium ions," Phys. Stat. Solidi 27, K1 (1968).
4. Kh.S. Bagdasarov, G.A. Bogomolova, A.A. Kaminskii and V.I. Popov, "Absorption, luminescence and stimulated emission of YVO_4-Nd^{3+} crystals," Soviet Phys. Dokl. 13, 516-518 (1968).
5. H.E. Rast, H.H. Caspers, S.A. Miller, "Infrared spectral emittance and optical properties of yttrium vanadate," Phys. Rev. 169, 705-709 (1968).
6. T.S. Davis and R.K. Datta, "High-temperature absorption of YVO_4 and YVO_4:Eu," Trans. Met. Soc. AIME 242, 714-716 (1968).

7. A.A. Kaminskii, G.A. Bogomolova and L. Li, "Absorption, luminescence, induced radiation, and crystal splitting of the levels of ions of Nd^{3+} in the crystal YVO_4," Inorganic Materials 5, 573-586 (1969). [English translation of Izv. Akad. Nauk SSSR, Neorg. Mater. 5 (4) 673-690 1969.]

8. J.D. Kingsley, G.W. Ludwig, "Optical constants of YVO_4 between 2 and 25 eV," J. Appl. Phys. 41, 370-375 (1970).

9. Kh. S. Bagdasarov, S.E. Salibekov, V.S. Krylov, V.I. Popov, and N.I. Timoleeva, "Thermophysical propteries of neodymium-doped yttrium orthovanadate crystals," Inorganic Materials 6, 1356-1357 (1970).

C. Spectroscopic Studies

1. N. Karayianis, C.A. Morrison and D.E. Wortman, "Analysis of the ground term energy levels for triply ionized neodymium in yttrium orthovanadate," J. Chem. Phys. 62, 4125-4129 (1975).

2. P.P. Yaney and L.G. DeShazer, "Spectroscopic studies and analysis of the $^4I_{9/2}$, $^4I_{11/2}$, $^4F_{3/2}$, and $^2P_{1/2}$ states of Nd:YVO_4," to be published.

D. Laser Performance Testing

1. L.G. DeShazer, M. Bass, U. Ranon, J.K. Guha, E.D. Reed and J.W. Strozyk, "Laser performance of Nd^{3+} and Ho^{3+} in YVO_4, and Nd^{3+} in Gadolinium Gallium Garnet (GGG)," IEEE J. Quantum Electron. QE-10, 7-8 (1974).

2. M. Bass, "Electrooptic Q switching of the Nd:YVO_4 laser without an intracavity polarizer," IEEE J. Quantum Electron., QE-11, 938-939 (1975).

3. A.W. Tucker, M. Birnbaum, C.L. Fincher and L.G. DeShazer, "Continuous-wave operation of Nd:YVO_4 at 1.06 and 1.34 μ," J. Appl. Phys. 47, 232-234 (1976).

E. Other Related Properties

1. U. Ranon, "Paramagnetic resonance of Nd^{3+}, Dy^{3+}, Er^{3+} and Yb^{3+} in YVO_4," Phys. Lett. A28, 228-229 (1968).

2. J. Rosenthal and R.F. Riley, "Electron paramagnetic resonance of Gd^{3+} in zircon structures. II. YVO_4, YPO_4, $YAsO_4$," Phys. Rev. 177, 625-628 (1969).

3. A. Chaves and S.P.S. Porto, "Raman scattering of YVO_4," Solid State Communications 10, 1075-1077 (1972).

4. E.D. Reed, Jr. and H.W. Moos, "Multiphonon relaxation of excited states of rare-earth ions in YVO_4, $YAsO_4$, and YPO_4," Phys. Rev. B 8, 980-987 (1973).

5. K.M. Leung and L.G. DeShazer, "Surface defects on crystals of TiO_2 and YVO_4 studied by laser-induced damage effects," in Laser Induced Damage in Optical Materials: 1974, edited by A.J. Glass and A.H. Guenther, NBS Special Publication 414, 193-199 (1974).

F. Technical Reports

1. J.R. O'Connor, "Unusual Crystal-Field Energy Levels and Efficient Laser Properties of YVO_4:Nd," Final Technical Report JA-2857, U.S. Air Force E.S.D. No. AF 19(628)-5167 (Nov. 1966).

2. R.J. Pressley, P.V. Goedertier, and H. Weakleim, "MBT 70 Laser Materials Research and Exploratory Development," RCA Lab., Princeton, N.J., Final Technical Report (Oct. 1969).

3. H.G. McKnight and L.R Rothrock, "Research and Development Work for the Growth of Single Crystal Yttrium Orthovanadate," Final Technical Report ECOM 0022F, U.S. Army ECOM Contract No. DAAB07-72-C-0022 (April 1973).

4. M. Bass, L.G. DeShazer and U. Ranon, "Evaluation of Nd:YVO_4 and Ho:Er:Tm:YVO_4 as Pulse Pumped Q-Switched Lasers," U.S. Army Electronics Command, Fort Monmouth, N.J., Semi-Annual Report ECOM-74-0104-1 (July 1974).

5. M. Bass, L.G. DeShazer, and P.P. Yaney, "Evaluation of Nd:YVO_4 and Ho:Er:Tm:YVO_4 as Pulse Pumped Q-Switched Lasers," U.S. Army Electronics Command, Fort Monmouth, N.J., Final Report ECOM-74-0104-F (Jan. 1976).